A TRIDENT SCHOLAR PROJECT REPORT

"TIME DEPENDENT SHEAR STRESS BENEATH A SHOALING WAVE"

UNITED STATES NAVAL ACADEMY
ANNAPOLIS, MARYLAND

1972

UNCLASSIFIED
Security Classification

DOCUMENT CONTROL DATA - R & D

(Security classification of title, body of abstract and indexing annotation must be entered when the overall report is classified)

1. ORIGINATING ACTIVITY (Corporate author) U.S. Naval Academy, Annapolis.	2a. REPORT SECURITY CLASSIFICATION UNCLASSIFIED
	2b. GROUP

3. REPORT TITLE

TIME DEPENDENT SHEAR STRESS BENEATH A SHOALING WAVE.

4. DESCRIPTIVE NOTES (Type of report and inclusive dates)
Research report.

5. AUTHOR(S) (First name, middle initial, last name)

John Fisher

6. REPORT DATE May 19, 1972	7a. TOTAL NO. OF PAGES 100 p.	7b. NO. OF REFS 25.

8a. CONTRACT OR GRANT NO.	9a. ORIGINATOR'S REPORT NUMBER(S) U.S. Naval Academy - Trident Scholar project report. (U.S.N.A. - TSPR no 26)
b. PROJECT NO.	
c.	9b. OTHER REPORT NO(S) (Any other numbers that may be assigned this report)
d.	

10. DISTRIBUTION STATEMENT

This document has been approved for public release; its distribution is UNLIMITED.

11. SUPPLEMENTARY NOTES	12. SPONSORING MILITARY ACTIVITY U.S. Naval Academy, Annapolis.

13. ABSTRACT

The celerity of a shoaling wave was measured and plotted as a function of the parameter d/L_o and compared to linear wave theory. A noticeably higher celerity was measured in the free stream than was measured by hot film shear sensors in the boundary layer.

Hot film shear sensors were also used to determine the phase relationship between shear stress and free stream particle velocity. Data results indicate that the maximum shear stress in an oscillatory flow field leads the maximum particle velocity by approximately $30^o - 35^o$ and that this has increased with distance from the bottom. The phase difference was also found to be dependent upon the length of the incident wave.

It is hypothesised the boundary layer growth and particle velocity increase in an alternately accelerating and decelerating flow field are related such that the maximum velocity gradient du/dy will occur $\approx 30^o$ prior to the maximum particle velocity.

DD FORM 1 NOV 65 1473

UNCLASSIFIED
Security Classification

U.S.N.A. - TSPR no. 26.

"Time Dependent Shear Stress
Beneath A Shoaling Wave"

A Trident Scholar Project Report

by

Midshipman John Fisher

First Class

U. S. Naval Academy

Annapolis, Maryland

Michael E. McCormick

Dr. M. E. McCormick, Naval Systems Engineering

Bruce Johnson

Dr. Bruce Johnson, Naval Systems Engineering

Accepted for Trident Scholar Committee

V V Utgoff

Chairman

19 May 1972

Date

ib

ABSTRACT

The celerity of a shoaling wave was measured and plotted as a function of the parameter d/L_o and compared to linear wave theory. A noticeably higher celerity was measured in the free stream than was measured by hot film shear sensors in the boundary layer.

Hot film shear sensors were also used to determine the phase relationship between shear stress and free stream particle velocity. Data results indicate that the maximum shear stress in an oscillatory flow field leads the maximum particle velocity by approximately 30°-35° and that this has increased with distance from the bottom. The phase difference was also found to be dependent upon the length of the incident wave.

It is hypothesized that the boundary layer growth and particle velocity increase in an alternately accelerating and decelerating flow field are related such that the maximum velocity gradient du/dy will occur ≈ 30° prior to the maximum particle velocity.

ACKNOWLEDGEMENT

Certainly there are no words to express so great a debt as is owed to so many people for their aid in the completion of this project. Nothing would have been possible without the untiring encouragement and guidance of the project advisors, Dr. M. E. McCormick and Dr. Bruce Johnson, who gave so freely of their time and expertise. The author also wishes to recognize the sizeable contribution of Mr. Vernon Leitch, Mr. Bob Popp and Mr. Ted Polaski in the design and construction of the experimental apparatus. Special thanks are extended to Mr. Joe Enzinger and the Technical Support Department for their patient help in the continual process of placing and removing the large and bulky beach sections. And, finally, a quiet word of appreciation to Miss Lisa Schmuhl for her aid in acquiring the data results and her unending encouragement in times of lesser successes. To all those mentioned, and the vast numbers regrettably omitted, the author expresses his sincere gratitude and appreciation.

TABLE OF CONTENTS

FIGURES

TABLE OF SYMBOLS

c = celerity

c_o = deep water celerity

d = water depth (from SWL)

d_p = probe immersion depth (from SWL)

f = frequency

H = wave height

H_o = deep water wave height

l = computed distance

k = wave number = $2\pi/L$

L = wave length

L_o = deep water wave length

m = beach slope

t = measured time increment

T_o = wave period

U = particle velocity

z = vertical distance from beach surface

δ = boundary layer thickness

ε = non-dimensional parameter = $(H/L)\ 1/\sinh kd$

ξ = wave position = $k\ x$

η = free surface

θ = phase difference between sensors

ϕ = orientation angle of hot film sensor to flow

ρ = density

τ = ωt

τ_w = shear stress

ν = kinematic viscosity

INTRODUCTION

Within the last four years a large amount of basic research, both theoretical and experimental, has focused on the velocity field of water waves traveling over an uneven bottom--primarily at steadily decreasing depth. Simultaneously, experimental hydrodynamics research has enjoyed a significant boom with the introduction of flush-mounted hot film shear stress sensors and wide-spread use hot film cylindrical sensors for particle velocity studies. To date, however, only Iwagaki and Sakai (1970) have made a systematic investigation of water wave particle velocity profiles using hot film velocity probes, and a search of current literature reveals no documented research employing hot film shear stress sensors in wave studies.

The validity of hot film flush mounts as sensors of the true wall shearing stress has been established theoretically by Liepmann and Skinner (1965) and Ludweig (1950) among others, and experimentally in water by Johnson and Barchai (1968), Mies (1967), Geremia (1970), and in air by Liepmann and Skinner (1965) and Bellhouse and Shultz (1966). Their use has been limited, however, to turbulant boundary layer and steady flow laminar boundary layer studies. There is no documented research involving hot film shear stress sensors in oscillatory systems, specifically in wave studies. The utility of such sensors in shoaling wave studies is questionable, particularly in the near breaker zone where bubble entrainment and mixing by circulation cells creates the very real problem of two phase flow. Such flows have a decidedly detrimental effect on the sensor output signal, as will be later shown.

In light of the above observations, the primary objectives of this project have been twofold:

(1) To evaluate the utility of hot film sensors in near breaker zone wave studies; and

(2) To determine the phase relationship between the bottom wall shear stress and the particle velocity profiles as a function of location in the water column and wave length.

PRELIMINARY DISCUSSION

In spite of the quickened interest in breaking waves and a proliferation of water wave theories, the shape of the shoaling wave front remains unaddressed. Several experiments have investigated the particle velocity amplitude variation with depth, however, no attempt has been successful in determining the phase change with incursion depth.

In speaking of breaking waves, it becomes necessary to limit the area of discussion by definition. Only shoaling waves, as opposed to deep water breaking waves, were considered in this study. Shoaling beach waves may be further divided into three distinct forms, depending on wave geometry and beach characteristics. Wiegel (1964) categorized them according to the following characteristics:

(1) Spilling Wave: Characterized by white water at the crest, breaks gradually and the crest appears to slide down the face of the wave. Occurs of $H_o/L_o > .06$ on all beaches and $.06 > H_o/L_o > .03$ on flatter beaches.

(2) Plunging Waves: Characterized by curling over of the crest and rapid descent of the top. Thrown spray usually accompanies this process. Occurs for $.06 > H_o/L_o > .03$ on steeper beaches, $.03 > H_o/L_o > .009$ for all beaches, and $.009 > H_o/L_o$ on flatter beaches.

(3) Surging Waves: Characterized by peaking as if to plunge but instead the base surges up the face of the beach. The wave appears to break upside down and the crest seems to disappear in the surging base. Occurs on steeper beaches for $.009 > H_o/L_o$.

This project will limit itself to plunging waves only. Galvin (1969) established plunging wave criteria by laboratory experiment using the deep water wave height-to-length ratio and beach slope as parameters. His results indicate that for:

$$H_o/L_o m^2 \quad .09 \text{ to } 4.8 \quad \text{or}$$
$$H_b/gT^2 \quad .0036 \text{ to } .068 \qquad \ldots\ldots\ldots\ldots \qquad (1)$$

where,

m = beach slope

H_b = wave height at break point

H_o = deep water wave height

the wave will plunge.

The most common tools used in velocity profile studies are hot film velocity sensors and hydrogen bubble injection. The most recent study, employing both methods, was the investigation of Iwagaki and Sakai (1970). The study was an experimental investigation into the vertical distribution of horizontal particle velocity for a shoaling, finite amplitude wave. In the hot film portion of the study, only particle velocity at a uniform point of absolute phase (the wave crest) and the probe depth were recorded. Since this phase was not time referenced to any constantly occuring event, no time comparison between points of different depths is possible. Thus, while the absolute phase of the wave is recorded, the phase of any depth relative to the phase at any other depth at any single instant of time is not recorded and the vertical phase profile cannot be calculated.

Hot film sensor can be adapted to celerity studies by placing two or more probes along a longitudinal line parallel to tank bottom. Two probes separated longitudinally by some Δl, and at the same depth, will measure some specific wave event, such as a crest, sequentially, separated by a time Δt. This time will be dependent upon the celerity, which may be calculated by the simple speed-time-distance relation:

$$c = \frac{\Delta l}{\Delta t} \qquad \ldots\ldots\ldots\ldots\ldots\ldots\ldots \qquad (2)$$

By varying the depth of the two probes the celerity amplitude profile can be plotted as a function of depth.

Velocity sensors could also be used to determine the vertical distribution of phase by holding one probe in a constant position and varying the depth of a second probe directly below the first. This method was rejected because of the anticipated size of the time variations over the entire vertical range. From top to bottom only a 10°-15° change was expected, which represents a time variation of only 20-30 msec. This was considered to be too small for accurate determination utilizing the correlation techniques available.

Iwagaki also used hydrogen bubbles injected along a vertical axis and subsequently photographed after some Δt to calculate the horizontal particle velocity. Vertical distribution of the bubble generating surfaces allowed simultaneous determination of the entire vertical velocity profile. Error was estimated at less than 3%. This method was considered as a possible means of physically observing and photographing the wave front; however, it was rejected as being unworkable.

Consider the arbitrarily assumed linear nonvertical wave front in Fig.(2). At some injection time t=0 the particle velocities can be represented by the vector quantities shown. Since wave period remains approximately constant throughout the vertical distribution over any short longitudinal distance, injected hydrogen bubbles will return to their original relative orientation at injection after each wave period. There will be small variations caused by varying mass transport rates over the vertical distribution of the velocity field; however, they can be neglected for this example since they are not a mechanism of the wave action per se.

During the wave cycle, the bubbles will follow widely different path lines unless the injection profile is coincidental with the wave front. At time $t = \pi/2$ the bubbles injected along A-A' at $t=0$ will have the approximate path lines to the position shown at $\pi/2$. The orbital centers were determined by the intersection of a line normal to the velocity vector at $t=0$ with a line of constant velocity. Corrections were made for the decreasing vertical velocity with depth. The indicated wave front (celerity profile) has been determined by connecting the bubble positions at $\pi/2$. Similarly, the wave front has been determined at $t = \pi$, $3\pi/2$ and 2π. Assuming a zero or approximately constant (over the vertical distance) net mass transport, the bubbles will never approach the true celerity profile of the wave crest since the orbital center of each bubble is cocked in the opposite direction at the time of injection.

The problem of determining the time-dependent celerity profile required a fixed phase event for reference and a fixed position reference. The wave crest was used as the reference and a flush-mounted shear stress sensor was used for a reference-time history of the wave over a fixed point.

The process of determining the celerity profile using a shear stress sensor is a simple concept. A shear sensor is mounted flush to the beach at some fixed point. Immediately above it, or displaced slightly to either side to prevent thermal interference, a horizontal velocity probe records the time-history of the particle velocity. Assuming the shear stress is exactly in phase with the particle velocity, any phase difference between the shear record and the particle velocity record will be the result of a deviation from the vertical line through the two probes. By varying the depth of the velocity probe the phase deviation at the crest at several points along the vertical axis may be determined. Knowing the wave celerity, from the c/L_o -vs- d/L_o curves and the deep water celerity from Fig.(16), the time lag can be converted to distance using Equation (2).

The assumption that the particle velocity and shear stress will be in phase is by no means an obvious one, nor is it undisputed. Lamb (1963) derived the equation for the particle velocity in an oscillatory fluid as:

$$U_o = \sin(\xi-\tau) - e^{-\zeta/\sqrt{2}} \sin(\xi-\tau+\frac{1}{\sqrt{2}}\zeta) + \frac{2}{\pi}\int_0^\infty \exp\,[(\xi-\tau)\sigma^2]\ \frac{\sigma\sin\zeta\sigma}{1+\sigma^4}\ d\sigma \qquad \text{.............. (3)}$$

For sufficiently large τ the third term disappears. Since the shear stress is related to the particle velocity by the relation:

$$\tau_w = \mu(\frac{du}{d\zeta})\ \zeta=o \qquad \text{................ (4)}$$

the time-dependent shear stress may be derived from (3) as:

$$\frac{\tau w}{A} = \frac{1}{\sqrt{2}}\ e^{-\zeta/\sqrt{2}}\ \sin(\xi-\tau+\zeta/\sqrt{2}) - \cos(\xi-\tau+\zeta/\sqrt{2}) = \frac{1}{\sqrt{2}}\sin(\xi-\tau)-\cos(\xi-\tau) \qquad \text{........ (5)}$$

Letting $\xi=0$ in (3) and (5) and plotting $\frac{\tau w}{A}$ as a function of $-\tau$, the phase relationship between the particle velocity (from (3) $U_o = \sin(\xi-\tau)$) and the shear stress ($\tau w/A = \sin(\xi-\tau)-\cos(\xi-\tau)$) can be readily seen in

Fig.(3). For this simplified case, where the third term has gone to zero, the shear stress will lead the velocity by $\pi/4$.

Iwagaki et. al.(1967) performed the integration of (3) and arrived at the relation for shear stress

$$\frac{\tau_w}{\rho u_o^2} Re^{1/2} = \sin(\xi-\tau-\pi/4) + \varepsilon \left[\frac{1}{2\sqrt{2}} + \left(\frac{11}{18} - \frac{5\sqrt{2}}{18} \right) \sin 2(\xi-\tau) + (11/18 - 4\sqrt{2}/18) \cos 2(\xi-\tau) \right] + O(\varepsilon) \quad \text{.............} \quad (6)$$

where

$$\varepsilon = \frac{\pi(H/L)}{\sinh kd}$$

$$Re = \frac{U_o^2 T}{\nu} \frac{1}{2\pi}$$

This relation was programmed in BASIC on the Naval Academy's GE-635 and plotted in Fig.(4). The conditions of the experiment were used to calculate the parameter ε, i.e., a constant depth and varying wavelengths within the limits of the wave generator. Two things should be noted from this figure:

(1) The shear stress definitely leads the free surface; and,

(2) The phase lead will increase for an increase in wavelength, both at the trough and the crest.

The reason for this indicated phase lead is not entirely clear. It does point out, however, the necessity of investigating the laminar boundary layer beneath the wave as an integral factor in the time dependency of the shear stress. Unfortunately, the boundary layer thickness has not been clearly formulated as a time-dependent function.

The most noted authority, Schlichting (1960) formulated the approximate boundary layer thickness over an oscillatory plate as a constant δ where,

$$\delta \approx \sqrt{T_0 \nu / 2\pi} \qquad \ldots\ldots\ldots\ldots\ldots\ldots \qquad (7)$$

Using wave periods of .765 sec, 1.09 sec., 1.33 sec. (corresponding to L_0 = 3', 6' and 9'. See Appendix C for linear wave theory conversion), theoretical boundary layer thicknesses of 1.16×10^{-3} feet, 1.38×10^{-3} feet and 1.53×10^{-3} feet, respectively, were calculated. These are constants, however, and offer no insight into how the boundary layer thickness fluctuates.

According to steady flow boundary layer theory the boundary layer thickness will vary inversly proportionally to the free stream velocity generating it. That is, $\delta \propto 1/Re \propto 1/U_0$. In the case of a shoaling wave, however, the fluid is in a state of continual acceleration, alternately positive and negative. The effect of this acceleration apparently has not been accounted for in the Schlichting approach.

Recent experimental work done by Teleki and Anderson (1970) suggests that the boundary layer is of a much greater thickness--on the order of 3 to 8 times as large as that predicted by Schlichting. They also noted that the boundary layer appeared to be thicker for a crest than a trough, despite a higher measured particle velocity. Several explanations are possible, two of which are pertenent to this paper. The investigators were using a full round Preston tube 5.2×10^{-3} feet in diameter as a measurement device for shear stress. The theoretical boundary layer is on the order of 1/3 this size and the experimental results on the same order of magnitude as this size. It is anticipated, therefore, that significant flow distortion occurred. A greater distortion would occur for the higher velocity, thus giving a possible higher value of δ for the higher velocity of the wave crest.

In the same experiment, Teleki and Anderson plotted the vertical distribution of horizontal particle velocity in the vicinity of the wall. A bulge of approximately 10% in the horizontal velocity profile was observed at a distance from the wall of approximately 2-4 times the boundary layer thickness.

INSTRUMENTATION

Velocity measurements were made using TSI model 1210 and 1211 cylindrical hot film sensors with a .002" sensor diameter. Shear measurements were made with TSI model 1237 flush-mounted sensors. The sensors were connected to a TSI model 1050 two-channel constant temperature anemometer (See Appendix A) coupled to an isolated TSI model 1050-6 power supply. The TSI 1210 velocity probes were aligned parallel to the longitudinal axis of the tank. Thus, assuming a zero or slowly changing transverse current, the maximum velocity sensitivity would occur for pure vertical flows. Similarly, the TSI 1211 probes were aligned vertically with the supports transverse to the tow tank. Assuming a near zero transverse flow, the maximum output would represent a purely horizontal flow. Two dimensionality of the incident wave was assumed throughout the experiments.

The output of the anemometer was monitored on a Hewlett-Packard (H/P) model 181A dual trace variable persistance oscilloscope. A simple switching box allowed quick monitoring of all signals. A visual record of the anemometer output was made on a Clevite mk 280 two-channel strip chart recorder. A 0-10 volt positive D.C. zero suppression permitted sensitivities on the order of 125-315 mv/cm. A H/P model 3960 4-channel frequency modulated instrument tape recorder was used to record all signals for later analysis.

Signal analysis was performed in the Naval Acadmey's data acquisition laboratory using the existing time series analysis equipment. The recorded outputs were passed through a Rockland model 1022F dual Hi/Lo filter set to high pass above .05Hz, thus blocking the D.C. signal. The signals were then passed through a Krohn-Hite model 3202R low pass filter set at 40 Hz to filter out extraneous random noise and tank vibration. The filtered waveforms were monitored on a H/P 1201B variable persistance dual beam oscilloscope and patched into a Time Data/100 time series analyzer.

The Time/Data is a two-channel, high-speed, real-time, all digital, hard-wired program processor with pushbutton selection of the basic time series algorithms. The cross correlation algorithm was the only one of concern in this project. For cross correlation, the T/D 100 employs a 2002 word input frame with 8 bit resolution and outputs 1001 positive lags and 1001 negative lags with 18 bit resolution. A/D aperature time is 1 μsec and processing time 5 sec. (See Appendix B)

The T/D 100 was coupled to a PC102 display coupler which linked it to a H/P 7004B X-Y recorder for automatic plotting. A Tektronix C-27 oscilloscope camera was also attached to the T/D 100 output oscilloscope to record selected sample outputs.

TOWING TANK AND BEACH

Waves were generated and measures in the Naval Academy's ship model towing tank. Though designed primarily for testing of ship models, it is equipped with a pneumatic wavemaker designed for model seakeeping tests. The tank measures 85' in length, 41-3/4 inches in depth, and approximately 70" in width. The width varied from 69.5" to 71.5" depending on where the measurement was made. While this variation could be neglected as far as its effect on the waves, it posed a very real problem when designing a beach to fit snugly against the tank walls, yet which could be installed and removed with only a minimum of difficulty. The tank is of steel construction bolted to studs imbedded in the concrete floor slab.

The wavemaker is of pneumatic design employing a 60 cycle motor rated at 3/4 HP at 1725 rpm coupled to an air blower. Frequency is regulated by a Bodin Type ASH502 DC motor control modified later in the experiment to accept a ten turn potentiometer for better frequency resolution and more steady operation. The standard model was found to experience significant drift even after several hours warm-up time, apparently as a result of thermally caused resistance changes.
The control acted as a rheostat to a DC motor coupled through a cam on the rotor to flapper valves on the air blower outlet pipes, thus modulating air flow to the wave generator air chamber.

A simple check made to determine wave amplitude variation with wave length indicated that wave height was independent of generated wave length. Thus, the wave generator efficiency varied with wave period and a constant setting could be set on the blower motor for a constant wave height regardless of wave length. The wave height chosen as best suited for these experiments was 1.88". The wave period was monitored on a Beckman 6144 EPUT and timer. Wave frequency was monitored on a H/P 5214L preset counter set to a 10 second period, and recorded on a H/P 562A digital recorder. Input to both the Beckman and preset counter was from a photocell modulated by a 10 slit disk attached to the D.C. motor rotor.

Wave frequency and period for a given wavelength was determined by a computer program employing linear wave theory. The program was run for the specific depth of the USNA tow tank (42") and is tabulated in Fig.(5).

The waves were allowed to propagate the entire length of the tank and shoaled on a semi-rigid, variable slope beach. The slope (m) of the beach was determined using Galvin's (1969) criteria for plunging waves:

$$.09 < \frac{H_o}{L_o m^2} < 4.8 \qquad \text{.................} \qquad (1)$$

A median value of 2.6 was selected to allow maximum variation of L_o on either side of the design wave. Using a design wave height of 2" and design wavelength of 6.5', the beach slope was calculated to be m = .12 or approximately 7°.

The initial beach constructed was 192" x 69" and constructed of 1/2" exterior grade plywood reinforced by 2"x8" sections along butt joined seams on the underside. Three coats of Rust-O-Leum were applied to inhibit warping. The beach was installed resting on the existing permanent, variable slope stainless steel beach with the upper edge of the plywood beach protruding from the water on clamped to this base. The beach extended to 18" below the still water level and was restrained by the devices shown in Fig.(6). The large net positive bouyancy and relatively small force of the plunging waves posed a restraint problem apparently of hold-down alone. The beach motion due to wave action was assumed to be negligible. As is discussed in the error analysis, this was not the case.

After approximately 8 weeks of intermittent immersion the beach had warped considerably and was not acceptable as a primary measurement platform. Data taken was also found to be probably affected by the shallowness of the beach, and a second beach section was constructed.

The second beach was 96" x 69" and constructed of 3/4" marine grade plywood coated with a primer and 3 finish coats of Rust-O-Leum. Transverse support was supplied by 3 lengths of 2" x 1/4" aluminum angle bolted to the underside of the beach. A slot 81" long and 2" wide, with 1" wide and 3/8" deep rabbits on each side was cut down the length of the beach. Plexiglass strips 1/2" thick were machined to fill this slot and were screwed in place, flush to the beach surface. Two TSI model 1237 shear stress sensors were mounted on 2" centers along the longitudinal axis of a 3" long plexiglass block. Modeling clay was used as filler between strips to smooth any incongrueties in the region of the probes.

The second beach was installed, using a system similar to that of the first beach, and butt joined to the first beach, which was pushed to the tank bottom. Due to certain configurations of gear in the tank, the maximum depth the first beach could be fixed at was 33". Both beaches were set at a slope of .12. Continuity of the beach surface at the butt joint was preserved by fixing a 4" wide strip of 1/16" aluminum sheet to the upper beach, and bending it downward at a 10° angle. The first beach was allowed to rise until the aluminum made a snug fit over its entire width.

Dye injection tests on 4 April 1972 demonstrated the existence of circulation cells in both a transverse direction across the top of the beach from one side of the tank to the other and back again underneath the beach, and around the perimeter of the beach surface. The transverse circulation was apparently due to the gaps left between the tank walls and the beach edges and was corrected by filling those gaps with foam rubber. The circumferential circulation was ascribed to a transversely non-horizontal condition, and hence an uneven wave break. When the wave began to break sooner on one side than the other, it canted the wave break line and set up a net positive particle velocity toward the far side. This mass transport at the break point was countered by a flow in the opposite direction at a point approximately 4'-5' from the break point. This effect could be limited by leveling the beach as much as possible, but could not be eliminated. The velocities were found to be of a relatively small order at magnitude and their effects were neglected.

EXPERIMENTAL PROCEDURE

A. Celerity Investigation

An investigation of the varying wave celerity of a shoaling wave was made using two methods--constant wavelength, varying depth and constant depth, varying wavelength. Two particle velocity probes were mounted a measured distance apart (usually around 15") along the longitudinal axis of the tank. Probe immersion was the same for both probes, around 3.5" below SWL. Waves of 6.5' length were generated and allowed to travel the length of the tank and break on the beach. All measurements using this method used only the single 192" beach on a slope of .12. The probes were suspended from 2"x1/4" aluminum angles running transverse across the tank. Because of vibrations from the wave generator transmitted to the probes through the steel walls of the tank, the aluminum angles were placed on cedar blocks isolated from the tank by foam rubber pads.

The two anemometer outputs were recorded on the mk 280 strip chart recorder and cross correlated on line on the T/D 100. The time lag was averaged over 10-12 cycles to obtain a mean time lag. Celerity was calculable using the relation $c = \Delta l/\Delta t$ where Δl = probe separation distance. The parameter d/L_0 was calculated using the mean depth of the two probes.

The second method made use of the fixed position shear stress sensors. Wavelength was incremented from 2.0' to 10.0' at .5' increment and the outputs cross correlated on line. Once again celerity was calculated using the probe separation distance.

B. Velocity Profile

To accurately determine the velocity profile of a wave, it is necessary to establish a fixed frame of reference, both in time and position. The wave crest was chosen as the time reference and the flush-mounted shear sensor used as position reference. Two flush-mounted films were imbedded in plexiglass on a 2" center and bolted to the 8' beach section. Directly above the forward shear stress sensor a horizontal particle velocity probe (TSI 1211) was mounted on a vertical traversing device. A straight edge was leveled and used to ensure vertical alignment of the two sensors. The signals from all three sensors were recorded on the mk 260 strip chart recorder, monitored on a dual trace variable persistance oscilloscope, and recorded on an FM tape recorder.

Cross correlation of the two shear stress sensors yielded a time lag from which celerity was computed and compared to the previously determined curves. Cross correlation of velocity probe against the shear sensor directly below also yielded a time variation, Δt, which was converted to a phase variation.

The immersion depth of the velocity was varied to traverse the entire distance from just below the wave trough to the beach bottom. The time variation was measured at each point and used to calculate phase and position parameters.

RESULTS

Initial celerity studies to determine the c/c_0 -vs- d/L_0 curve for the 16' beach were carried out 21 February 1972 and 11-12 March 1972. The second beach was added 1 April 1972 and further celerity studies and initial shear stress investigations were made over the weekends of 8-9 April 1972, 15-16 April 1972 and 29-30 April 1972. Analysis for time variation was carried out on the T/D 100 while monitoring the filtered output signals on a dual trace oscilloscope. Data sections which exhibited irregularities and non-periodic incongrueties not associated with wave phenomen were edited from the analysis. Data marked by such irregularities as sudden shocks to a sensor, cocked waveforms from misaligned probes, and bubble entrainment and shedding were excluded from the analysis. A minimum of at least 10 samples, usually at a 5 msec. sampling rate, were obtained from each run and the average of the resultant valves at the time of the first correlation peak were calculated.

Results from the initial celerity investigation are plotted in Fig. (15). The rise in celerity at a d/L_0 of $\approx .18$ was assumed to be a result of the principal of conservation of energy, this being the region of minimum wave height. The loss of potential energy of the decreased wave height would be balanced by a kinetic energy increase in the form of higher celerity. When the beach was extended to the bottom of the tank by the addition of the second beach section, however, this rise disappeared. The most probable explanation is that the first beach, extending to a depth of only 18", was too shallow and acted as a shelf cutting off the entire lower half of the wave. The upper half was suddenly without a significant portion of its energy and slowed down. It was, however, still essentially a deep water wave, though now in shallow water, and sped up to the shallow water velocity. From then on it followed the normal celerity curve for a shoaling wave. Thus, in actuality, the observed rise was not a rise at all, but merely a return to normal celerity from an unnatural drop in celerity caused by the shelving effect of the beach. This hypothesis is confirmed by comparison of the c/c_0 -vs- d/L_0 waves plotted from data taken 21 February 1972 and 11-12 March 1972 with linear wave theory.

It should be noted that the comparison of this data with data taken 8 April 1972 (Fig.(16)) will show significantly higher celerities. This can be accounted for as the effect of beach friction present only on 8 April 1972, and due to the extension of the beach several feet in front of the measurement point. The c/c_0 -vs- d/L_0 curve plotted from data taken 8 April 1972 was accepted as the standard curve for the beach on a slope of .12.

A comparison was also made between the celerity measured beneath the boundary layer by the shear sensors and the celerity measured in the free flow measured by two colinear negative probes. The two celerity curves are plotted in Fig.(17) with the linear theory presented as a reference.

No explanation is offered for the higher celerity in the free stream than in the boundary, particularly in light of the higher particle velocities measured in the boundary layer by Telaki and Anderson (1970) and Jonsson (1963). There is also an unexplained anomaly in both data curves at d/L_0. It may be only a coincidence of normal experimental data scatter, however, the close correlation between the two lines suggests this is an area worthy of further investigation. These data were taken at a constant position (constant depth) for varying wavelength, hence beach anomalies should not seriously affect only a single range of wavelengths.

Phase relation data was taken 8, 15 and 29 April 1972 and reduced on the T/D 100 in the same manner as the celerity data. Time variation was converted to phase by the relation:

$$\theta = (\Delta t)(fo)(360°) \qquad \text{...........} \qquad (8)$$

where fo is the wave frequency recorded on the H/P 561 digital recorder. This phase was plotted in Figs.(18-20) as a function of vertical probe distance (z) from the shear sensor ($z = d - dp$ where dp = probe immersion depth at SWL) the trend appears to predict a divergent velocity-shear stress phase shift as z approaches the free surface, and as wavelength increases. The increasing value of the velocity gradient between $z = .5"$ and the free surface for increasingly longer waves tends to suggest a depth dependency in the curvature phenomena observed in these intermediate water waves.

This gradient is more readily seen when phase is converted to a distance displacement by the relation $l = c\Delta t$. The resultant curves for the three wavelengths investigated are presented in Fig.(21). The values of c were taken from the c/c_0 -vs- d/L_0 curve of 15 April 1972.

Fig.(21) may be interpreted as a plot of the locus of points in phase with the shear sensor at that point in time when the free surface wave crest is felt by the shear sensor. No other relationship between the shear sensor and the celerity profile may be implied since the phase relationship between the physical occurace of the maximum particle velocity and the maximum shear stress. The lines in Fig. (21) are simply in the shape of the advancing wave front, as measured between the free surface and some distance outside the boundary layer.

DISCUSSION

The interpretation of the data presented in Figs.(18-20) is subject to several possible explanations, only two of which will be presented here. An attempt has been made to explain the phenomena observed and reconcile it with accepted boundary layer theory and documented observations. The state of oscillatory boundary layer theory being what it is, however, it was not held as law and has been challenged somewhat by these explanations.

Assuming the velocity profile data from Teleki and Anderson (1970) to be correct, an amplitude bulge exists in the particle velocity at the base of the wave. This bulge appears to be in the vicinity of the laminar boundary layer. A similar bulge in the profile was observed by McCormick, Johnson, and Lee (1972) for the steady flow case. As the fluid progresses up an inclined beach, it is being channeled as a result of squeezing from the bottom. Water is basically incompressible, hence the excess fluid from this channeling effect is forced forward through the boundary layer closest to the squeezing wall at a higher velocity than the free stream velocity.

The phase results indicate that a physical bulge, as well as a velocity amplitude bulge, is present for the shoaling case. This is a necessity if the velocity bulge is accepted, since the mass flow rate will be increased for a higher particle velocity.

Applying this theory of a water bulge preceeding the wave to these results, it is apparent that the bulge would have to lead the wave front by approximately 30° to account for the shear stress lead. This is assuming, of course, that the maximum shear stress occurs for the maximum particle velocity in an oscillatory flow. It is also apparent that the size of this bulge is dependent on the parameter d/L_0. An artist's conception of the wave front predicted by this theory is presented in

Fig.(21). This plot may be interpreted as representing the locus of points experiencing their respective maximum forward particle velocity simultaneously. Note that for the 9.0' wave this is very nearly the π/4 phase difference between shear stress and the free surface predicted by Iwagaki (1966) and Jonsson (1965).

The theorized high velocity water bulge is predicted to oscillate with the same frequency as the rest of the water column, but approximately 30° out of phase. Thus it would lead the trough by 30° as well as leading the crest. This constant phase lead at all points of oscillation is consistant with the observed results taken from strip chart recordings. The driving force of the boundary layer bulge would come from the compression of the fluid caused bythe succeeding wave. Thus, the bulge would be expected to grow as it progressed up the beach, i.e., as the parameter d/L_0 decreased. Again, this is borne out by the data as phase lead increases for the longer wavelength at the same depth.

The bulge theory appears to explain most of the observed phenomena including a greater inshore mass transport rate of dye injected at the beach surface that is the free flow. However, the concept of a physical intrusion of a small water layer, on the order of a few hundredths of a foot thick, sandwiches between the boundary layer and the free flow, oscillating out of phase with both of them and subject to the requisite shear stresses on both sides, and yet continuing to grow in length to the point where it is 30° ahead of the wave front, stretches credibility to the breaking point. As a more plausible explanation for the observed shear stress lead, the nature of the time-dependent boundary layer thickness must be determined.

The fluctuating boundary layer is a significant area of interest in any shear stress investigation involving fluctuating flow since

$$\tau_w = \mu \frac{du}{dy}$$

and both velocity and the boundary layer thickness are time dependent. A possible explanation for the observed 30° phase lead is that the boundary layer thickness is not fluctuating in phase with the particle velocity causing it. The breaking wave case may be defined essentially as an alternating accelerating and decelerating flow over an inclined flat plate. Flow visualization studies by M.I.T. (National Committee for Fluid Mechanics Film) indicates that for a sudden flow acceleration in a channel the boundary layer grows out from the wall, thickening as the fluid accelerates. Any further increase would result in a thinning of the boundary layer, as per accepted steady state boundary layer theory. The maximum shear stress will be registered not for the maximum velocity, but for the maximum velocity gradient. It is the opinion of the author that this gradient reaches a maximum at some point of phase leading the free stream velocity the magnitude of such phase lead being dependent upon the magnitude of the maximum horizontal particle velocity in the free stream, and hence upon the wavelength. This hypothesis explains the large initial value of the phase lead as being a result of the phase relationship between shear stress and free stream velocity, and the increasing phase lead with increasing z as being an indication of the wave front curvature.

This hypothesis is strongly supported by the results of Jonsson (1963). In a study of the vertical distribution of horizontal particle velocity in an oscillating water tunnel, Jonsson determined particle velocity versus depth for the entire wave period in 15° increments. His results show the velocity gradient is greater for 135° than 180° (the trough was used as 0° phase reference. This 45° is very similar to the results obtained in this study.

T/D 100

While on line analysis of the anemometer output signals would seem to be a desirable feature as a time saver, it was found in truth to require an excessive amount of run time to generate a sufficient number of correlations. The computer, as linked, had a minimum recycle time of approximately 20 seconds: 5 seconds data acquisition, 5 seconds processing, 5 seconds correlation output, 5 seconds for the x-y plot, manual reset of the PC102, and restart of the algorithm. Thus, from any 20 second real-time run, only 5 seconds of data could be analyzed, representing a maximum data utilization efficiency of 25%. Because the water surface deteriorated with time from wave reflection effects, the excessive time required to obtain a correlation series reflected an unacceptable inefficiency. It is therefore recommended that on line analysis not be attempted except as a preliminary check on results for correct system operation. The H/P 3960 FM tape recorder proverb invaluable in recording signals for later playback analysis. Shorter real time runs were thus possible by repeated replays of the recording to obtain the necessary number of correlations. It is highly unlikely that any two correlations reflected identical data samples, thus the possibility of undue biasing from repeatedly analyzed data was minimal.

Throughout this project a qualitative evaluation has been made of the performance of the hot film sensors. The observations included are based on 6 months of use.

Probe Evaluation

The utility of hot film velocity sensors was found to be without serious drawbacks. The probes provided an accurate wave record as long as they were immersed at least .5" below the minimum wave trough water level. A wave gage, therefore, is required to record the free surface time history.

Probe orientation was found to be a critical factor in eliminating distortion, particularly in the case of longitudinally oriented vertical velocity probes (TSI 1210). A very small angular shift off the longitudinal axis was sufficient to impart a horizontal velocity component

normal to the film surface, thus significantly distorting the vertical velocity record. Examples are shown in Fig.(30-31).

Angular orientation of the flush-mount sensor face was found to be far less critical than for the velocity probes, primarily because there was essentially only two-dimensional flow. Huang and Dlysy (1969) found the directional response of the shear probe to be proportional to the cosine of ϕ up to a ϕ of 50 degrees where ϕ is defined as:

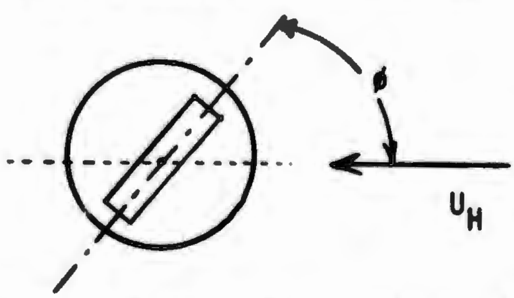

In order to define as small a point as possible as the reference origin, a ϕ of 90° was used on both shear sensors, thus reducing the longitudinal length of measurement to be the width of the heated element.

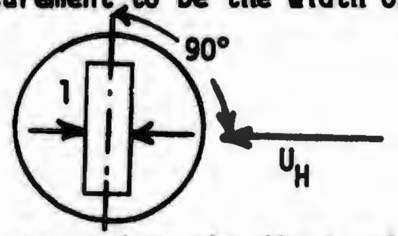

The center of this element was used as the fixed reference point.

An initial attempt to confirm the angular relation of Huang and Dlysy was abandoned after a problem of air bubble entrainment was encountered. Air bubbles were included in the breaker zone and mixed through the shoaling region by the circulation cells previously discussed. The heated element of the shear sensor seemed to attract these bubbles, severely altering the heat transfer characteristics and changing magnitude of the output. Fouling seemed to be dependent on both time and bubble concetration. It was necessary to clean the probe faces immediately prior to the beginning of each data run. This was accomplished by lightly brushing the bubbles clear with the fingertips. The effects of bubble entrainment were sufficient to indicate that calibration of the shear sensor would be uncertain if not impossible. In the shoaling region an example of the results of air bubble entrainment and the effects of brushing away the bubble is shown in Figs.(25-26).

It was noted that for both the velocity probes and the shear sensors the signal output never crossed through the zero flow value. Since the frequency response of both types of sensors is on the order of at least 1000 Hz it can be inferred that the lack of a zero flow signal represents the continuous presence of a flow, rather than a lack of proper sensor frequency response. However, the nature of oscillatory flow dictates that the flow must stop in order to reverse itself at each horizontal extremety at the oscillation. Thus it would appear that the flush-mounted hot film is sensitive to velocity gradients at end near wall and that the minimums of each are out of phase.

The flush mounts were also found to exhibit a much shorter lifetime. Though considerably less prone to breakage than the velocity probes, two of the three specially modified TSI 1237 sensors flooded after less than 36 hours constant immersion. The flooding process was indicated by severe fluctuations in the output voltage and an inability to adjust the reference voltage to a steady value. After approximately 3-4 minutes the probe would short and burn out. It was found that sensor life could possibly be prolonged by switching the anemometer to standby at the first indication of trouble, disconnecting the probe cable entirely from the anemometer and removing the probe from the water to dry. In any case, it is recommended that all probes be removed and dried following each day's run. Easy accessibility and sensor removal should therefore be incorporated into the beach design.

Conclusions & Recommendations

This project was one of an exploratory nature, and several questions have come to light, questions on which more attention should be focused. The most important of these is the phase relationship of the fluctuating boundary layer thickness and the free stream velocity. This must be developed to determine a meaningful measure of the boundary layer while in a state of constant flux.

A closer investigation into the observed water bulge near the boundary layer is also warranted. While this bulge might be unacceptable as the sole explanation for the shear stress lead, it is nonetheless of significance from the standpoint of its possible effect on mass transport at the beach surface. The bulge size and velocity should be determined for several wavelengths at several points along the full length of the shoaling beach.

A more definitive investigation of the depth dependency of the wave front also needs to be carried out. As presented, only wavelength was varied in changing the parameter d/L_0, hence celerity and particle velocity was likewise varied. To obtain a more accurate concept of the relationship between the wave front profile, the free surface profile and the beach slope, further tests have to test new variables.

It is recommended, however, that no further wave investigations of this nature be conducted in the current tow tank configuration. Problems of tank scheduling, the transient nature of any beach, poor wave gage instrumentation and a poorly designed wave generator doom to failure almost any serious investigation into the finer areas of wave research. Fortunately, the new Engineering Studies Complex will provide much needed facilities in which these investigations may be carried out.

ERROR ANALYSIS

There are several factors acting as possible sources of error, some of them capable of exerting significant impact on the test results.

In the early test runs from which c/co was calculated in Fig (15), the frequency regulation of the wave generator was very poor and variations of ± 3-4% were recorded during single runs. As may be ascertained from Fig. (5), an increase of .03HZ from a reference 6.0' wave (approximately .924 HZ) increases the wavelength .4' (6.7%) and increases the celerity .18 FPS (3.3%). After the installation of a ten turn potentiometer on the frequency control unit, the frequency was steadied to well within 1% and any variation was to all extent nullified by taking a cross correlation sample input span of 4-6 wave periods. Frequency variation was not considered to be a significant source of error in all runs made after 1 April 1972.

A more noticeable defect in the experimental apparatus was a slight "breathing" motion of the non-rigid beach. Under excitation of the incident waves, the upper beach section pivoted about the upper end clamped to the permanently installed stainless steel supporting beach, and the lower section pivoted about the lowest point of negative support. Movement was most evidenced at the two section interface where each section traversed a vertical distance of approximately .25". To minimize flow field distortion beyond the joint, foam rubber padding was squeezed between the two overlapping sections, thus preventing flow through the "solid" bottom boundary. The possible effects on the shear stress sensors was assumed to be negligible, although the boundary layer may have been affected. This is one possible reason for the inconsistancies between successive weeks' runs. It would be impossible to quantitize this effect, however, hence it has been neglected.

Possible longitudinal misalignment of the velocity probe above the shear stress sensor offers a third possible source of error. Since any offset would be constant error, while the wave period and celerity vary for variations in wavelength, any misalignment would result in a non-constant, non-linear error. For example, a negative .5" error (shear sensor oriented .5" behind the velocity probe) would lower the calculated phase lead of the shear sensor 7°, 4°, and 3.3°, for 3', 6' and 9' deep water wavelengths, respectively. The method of calculation was:

$$A\theta = \left[1 - \frac{(L/L_o)\, L_o - (.5/12)}{(L/L_o)\, L_o} \right] \times 360°$$

where $L/L_o = c/c_o$ and is taken from Fig. ( ).

The net results of .5" position errors, both positive and negative are shown in Figs. (33) and (34). As is evident, a negative shear sensor displacement tends to lower disperse the three wavelength curves while a positive displacement collapses the curves at a higher phase difference. The actual magnitude of error was probably within $\pm$ .13".

Probably the most significant source of error was in the vertical alignment of the flush mount shear sensors. As has been noted using Schlichting's approach (Eq.7), the thickness of the laminar boundary layer is on the order of .0015 feet. Even accepting the experimental results of Teleki and Anderson (1970) the boundary layer thickness is still on the order of only .012 feet. In real terms, a positive misalignment of .00063', less than 1/128" would place the probe face over 40% of the way through the Schlichting boundary layer and through 5% of the Teleki and Anderson boundary layer. While the flow might not be significantly disturbed, there would be an unmeasurable net change in the point of measurement of the shear wave. Trends in phase difference with changing depth would remain approximately constant for very small differences in vertical probe alignment. However, the absolute value of the phase difference would vary significantly for small vertical shifts because of the apparent steep phase gradient within the boundary layer. It is the opinion of the investigator that such a misalignment is responsible for the similar trends and constant phase difference between runs taken of 8 April 1972 and 29 April 1972. It is also the investigator's opinion that the shear sensors were vertically misaligned on 15 April 1972 to such a magnitude that they either disturbed the fluid flow or were outside the laminar boundary layer. An intrusion of 1/64" above the beach surface would be sufficient to create either situation.

There also exists possible human bias error in the visual analysis of the cross correlations. The correlation peaks were individually established by eyeball and the total averaged for each run. Realistically speaking, errors on the order of 10% for the 3' waves and 5-8% for the 9' and 6' waves were quite possible. Consistancy of results indicate, however, that this error was, in all probability, a constant one.

During the course of running the shorter wavelength, a standing wave was eventually set up in the tank. For the 2' and 3' waves, the time required was in the order of 2-3 minutes. Since it was usually necessary to take data for some time past the initial establishment of the standing wave, its effect on the cross correlation was of some interest. After comparing numerous correlations, it was determined that the standing wave would visibly alter the shape of the cross correlation, but not the time to the first correlating peak. This being the case, no further concern was in order over the existance of the standing wave, except as it modulated the sensor output amplitudes.

FIGURE (1)

Shoaling wave characteristics

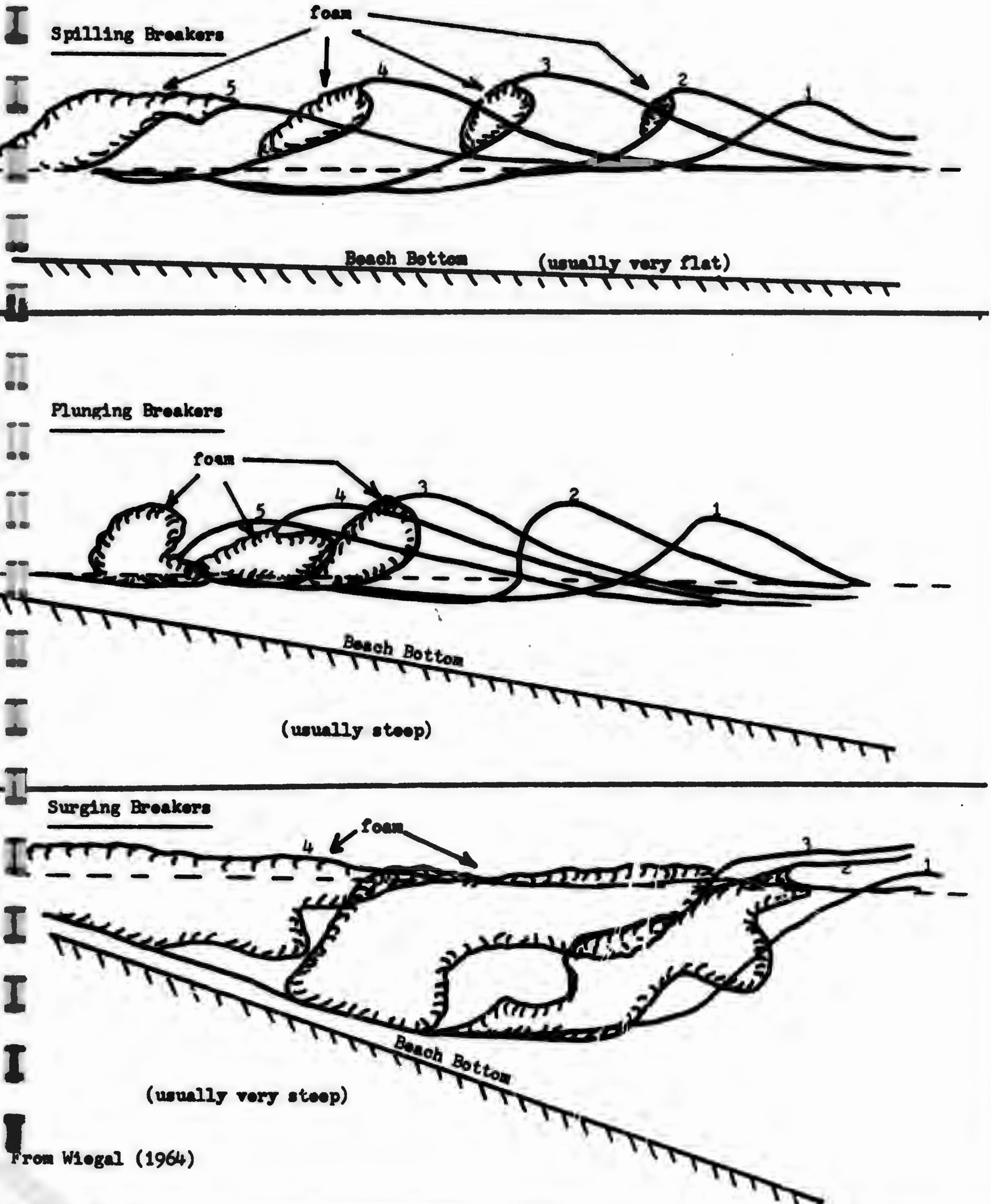

From Wiegal (1964)

FIGURE (2)

Hydrogen bubble injection problem

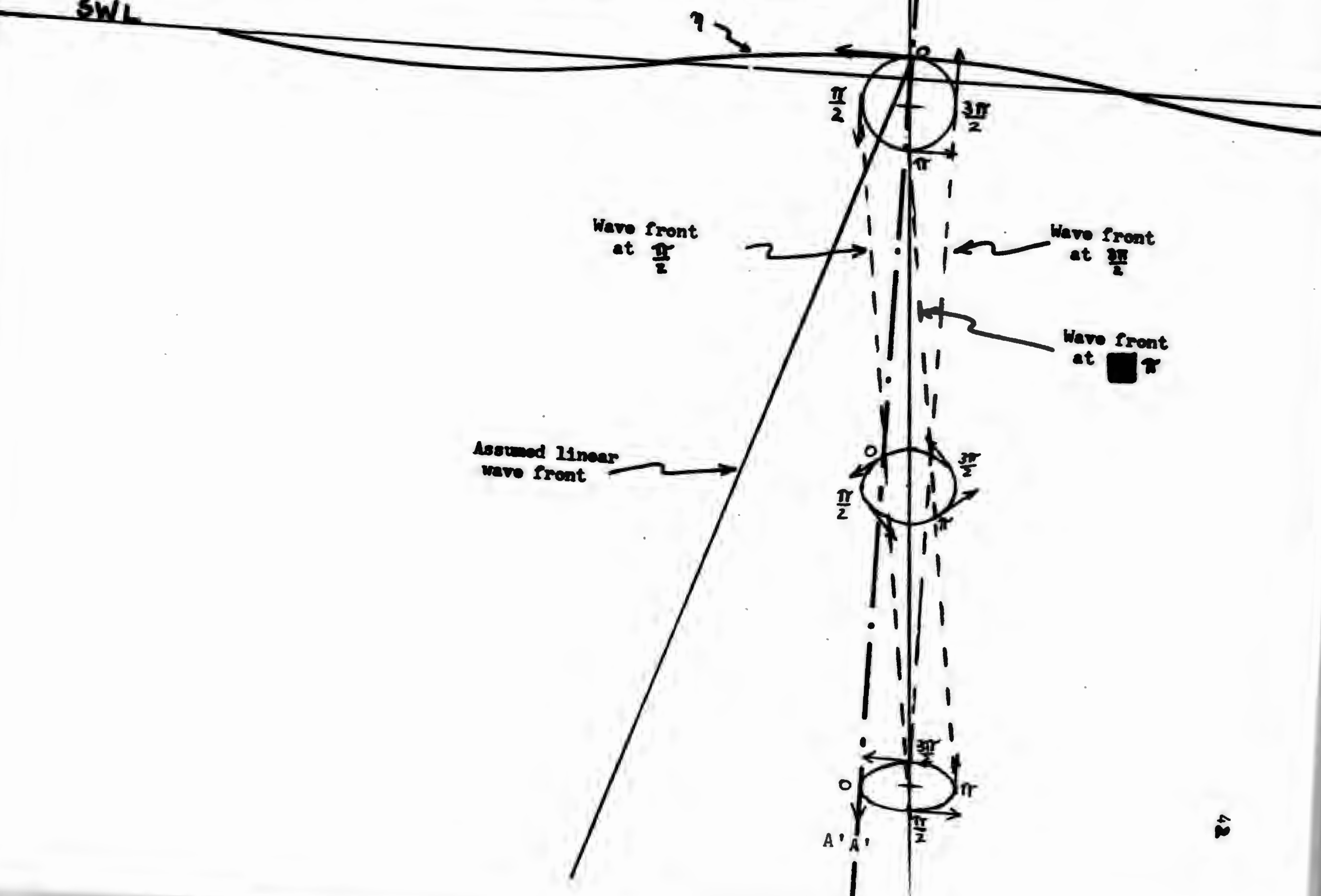

FIGURE (3)

TRIG FUNCTION RELATIONSHIPS

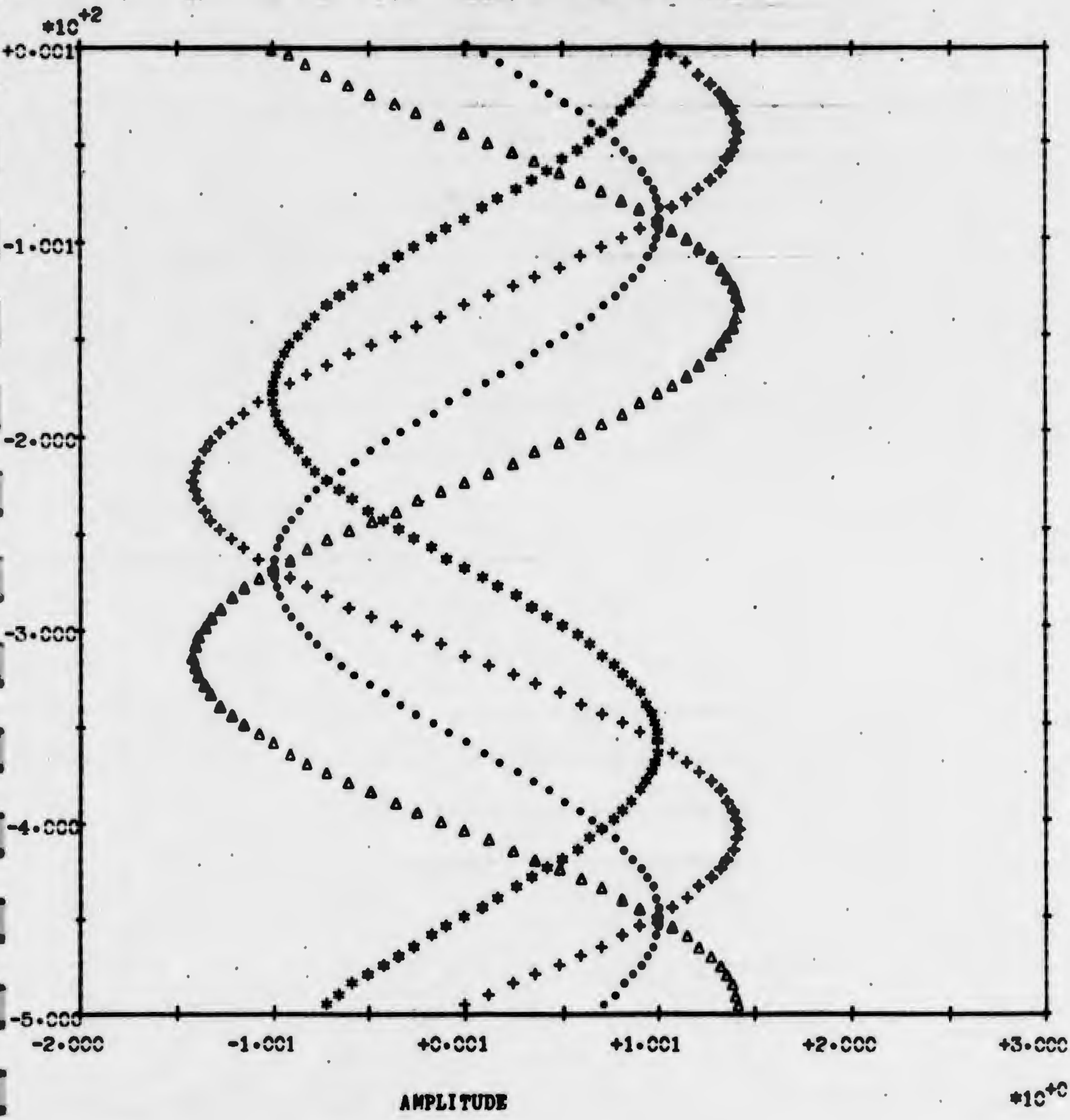

Symble	No Pts.	Legend
•	100	Sin(t)
*	100	Cos(t)
▲	100	Sin(t)-Cos(t)
+	100	Sin(t)+Cos(t)

FIGURE (4)

SHEAR-VELOCITY-PHASE RELATIONSHIP

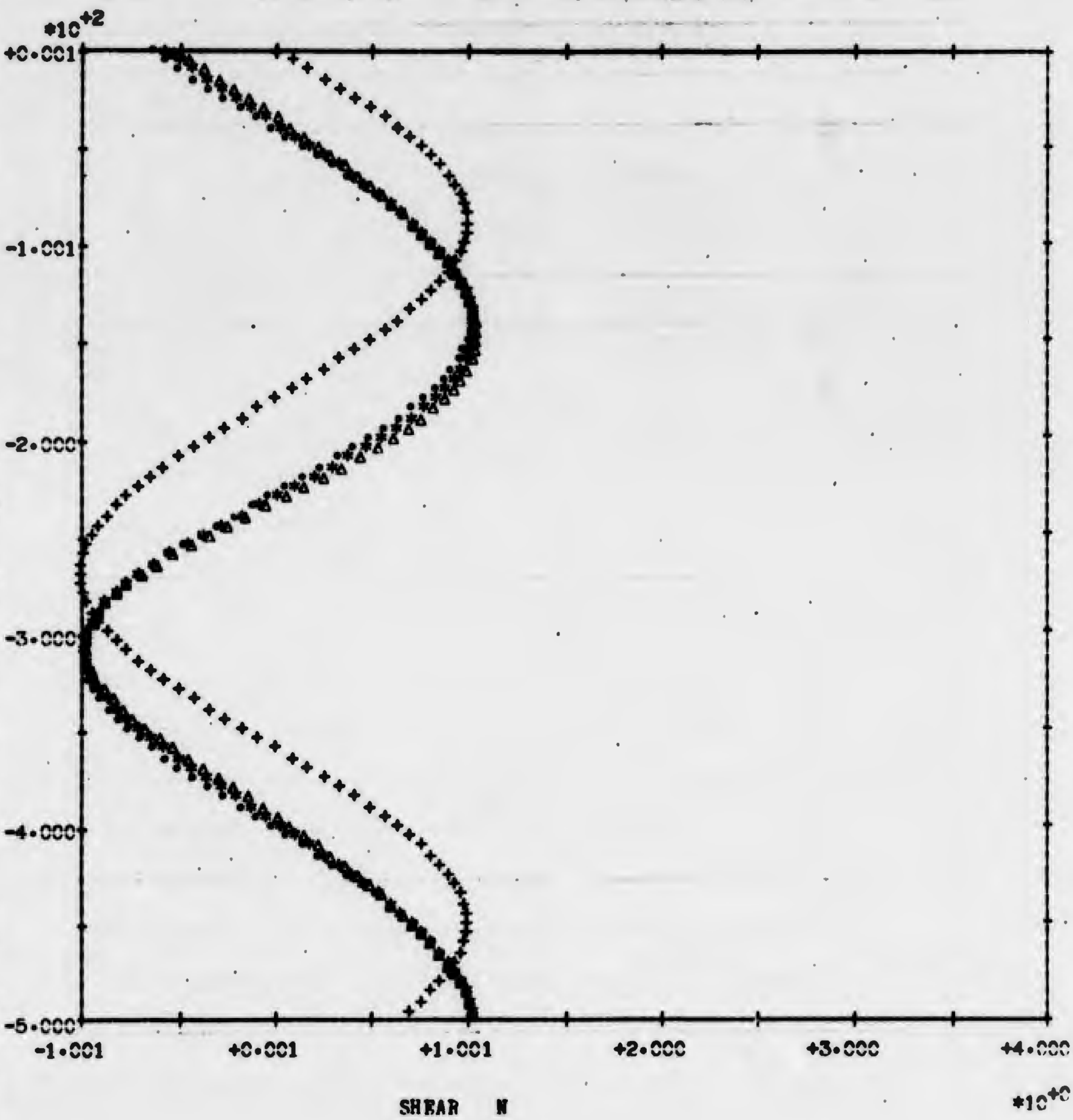

SYMBOL	NO.PTS.	LEGEND
•	100	-? 3' WAVE
*	100	-? 6' WAVE
Δ	100	-? 9' WAVE
+	100	-? SURFACE PROFILE

FIGURE (5)

RUN

WAVES 19 JAN 72 13:53

INPUT WATER DEPTH,IN FEET? 3.5

INPUT WAVELENGTHS: SHORTEST,LONGEST,INCREMENT? 5,11,.1

WAVELENGTH	CELERITY	PERIOD	FREQ	SQR(TANH)
5	5.0612	0.9879	1.0122	0.9998
5.1	5.1115	0.9978	1.0022	0.9998
5.2	5.1612	1.0075	0.9925	0.9998
5.3	5.2104	1.0172	0.9831	0.9998
5.4	5.2591	1.0268	0.9739	0.9997
5.5	5.3073	1.0363	0.965	0.9997
5.6	5.3551	1.0457	0.9563	0.9996
5.7	5.4023	1.0551	0.9478	0.9996
5.8	5.4492	1.0644	0.9395	0.9995
5.9	5.4956	1.0736	0.9315	0.9994
6.	5.5415	1.0827	0.9236	0.9993
6.1	5.587	1.0918	0.9159	0.9993
6.2	5.6321	1.1008	0.9084	0.9992
6.3	5.6768	1.1098	0.9011	0.9991
6.4	5.7211	1.1187	0.8939	0.999
6.5	5.7649	1.1275	0.8869	0.9988
6.6	5.8084	1.1363	0.8801	0.9987
6.7	5.8514	1.145	0.8734	0.9986
6.8	5.8941	1.1537	0.8668	0.9984
6.9	5.9364	1.1623	0.8603	0.9983
7.	5.9783	1.1709	0.854	0.9981
7.1	6.0198	1.1794	0.8479	0.998
7.2	6.0609	1.1879	0.8418	0.9978
7.3	6.1017	1.1964	0.8358	0.9976
7.4	6.1421	1.2048	0.83	0.9974
7.5	6.1821	1.2132	0.8243	0.9972
7.6	6.2218	1.2215	0.8187	0.9969
7.7	6.2611	1.2298	0.8131	0.9967
7.8	6.3	1.2381	0.8077	0.9964
7.9	6.3386	1.2463	0.8024	0.9962
8.	6.3768	1.2545	0.7971	0.9959
8.1	6.4147	1.2627	0.7919	0.9956
8.2	6.4522	1.2709	0.7869	0.9953
8.3	6.4894	1.279	0.7819	0.995
8.4	6.5263	1.2871	0.7769	0.9947
8.5	6.5628	1.2952	0.7721	0.9944
8.6	6.599	1.3032	0.7673	0.994
8.7	6.6348	1.3113	0.7626	0.9936
8.8	6.6703	1.3193	0.758	0.9933
8.9	6.7055	1.3273	0.7534	0.9929
9.	6.7404	1.3352	0.7489	0.9925
9.1	6.7749	1.3432	0.7445	0.9921
9.2	6.8091	1.3511	0.7401	0.9916
9.3	6.843	1.3591	0.7358	0.9912
9.4	6.8765	1.367	0.7315	0.9908
9.5	6.9097	1.3749	0.7273	0.9903
9.6	6.9427	1.3828	0.7232	0.9898
9.7	6.9753	1.3906	0.7191	0.9893
9.8	7.0076	1.3985	0.7151	0.9888
9.9	7.0396	1.4063	0.7111	0.9883
10.	7.0713	1.4142	0.7071	0.9878
10.1	7.1026	1.422	0.7032	0.9872
10.2	7.1337	1.4298	0.6994	0.9867
10.3	7.1645	1.4376	0.6956	0.9861
10.4	7.195	1.4455	0.6918	0.9855
10.5	7.2251	1.4533	0.6881	0.9849
10.6	7.255	1.4611	0.6844	0.9843
10.7	7.2846	1.4688	0.6808	0.9837
10.8	7.3139	1.4766	0.6772	0.9831
10.9	7.3429	1.4844	0.6737	0.9825
11.	7.3717	1.4922	0.6702	0.9818

0.915 SEC. 15 I/O

FIGURE 6)

INSTRUMENTATION SCHEMATIC

FOR VELOCITY PROFILE DETERMINATION

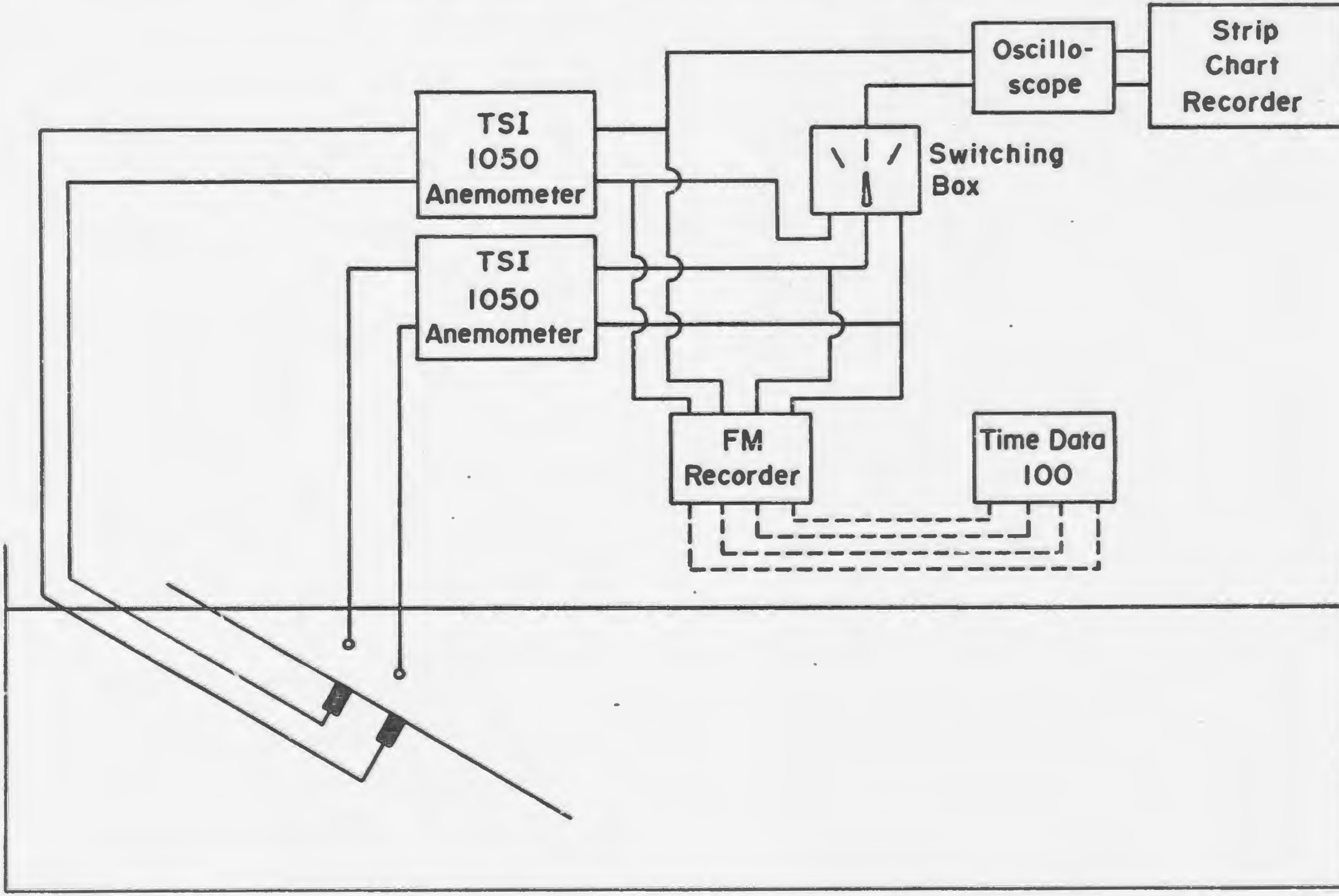

FIGURE (7)

TOW TANK AND INSTALLED BEACH SECTIONS
SCHEMATIC

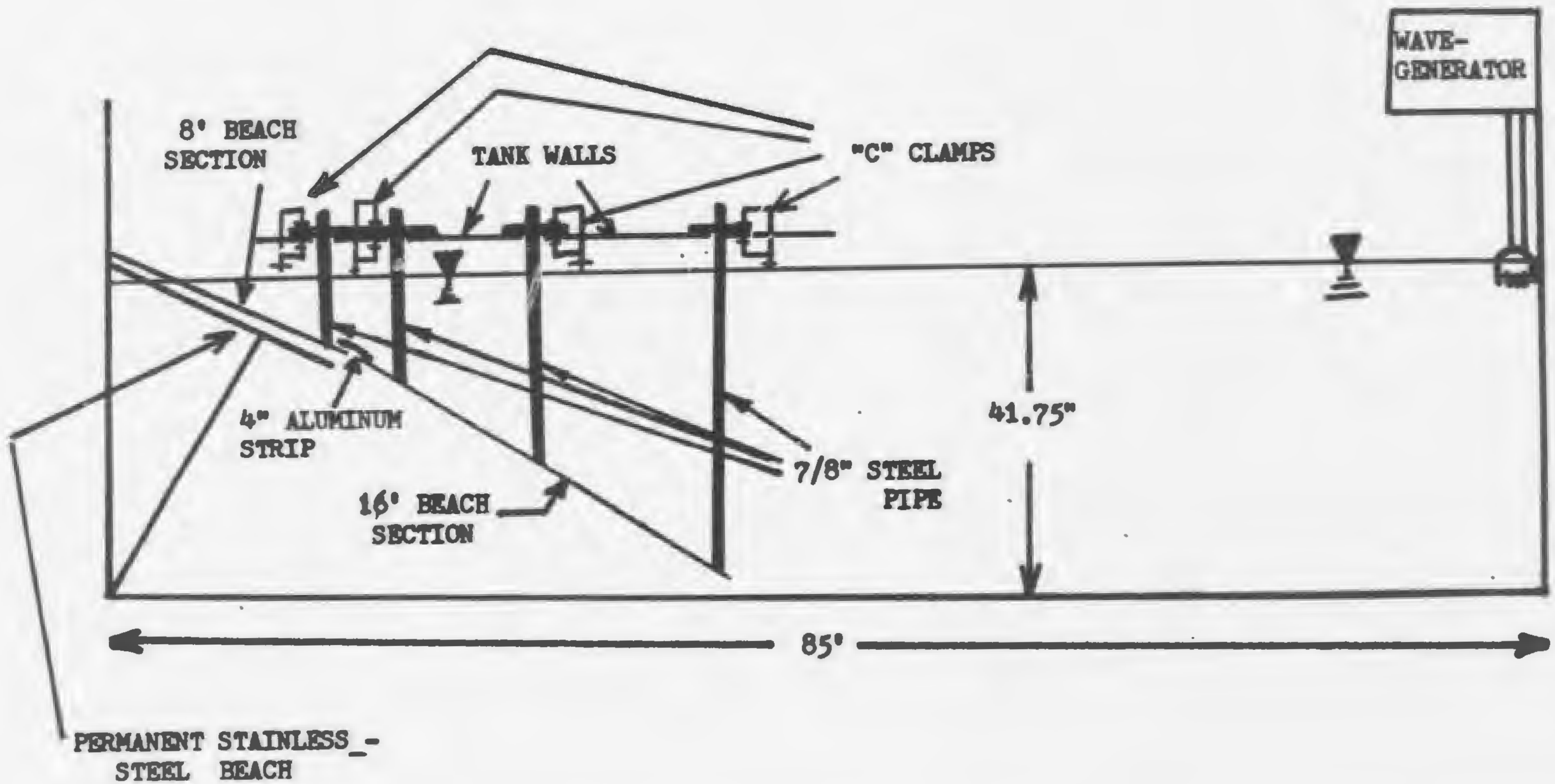

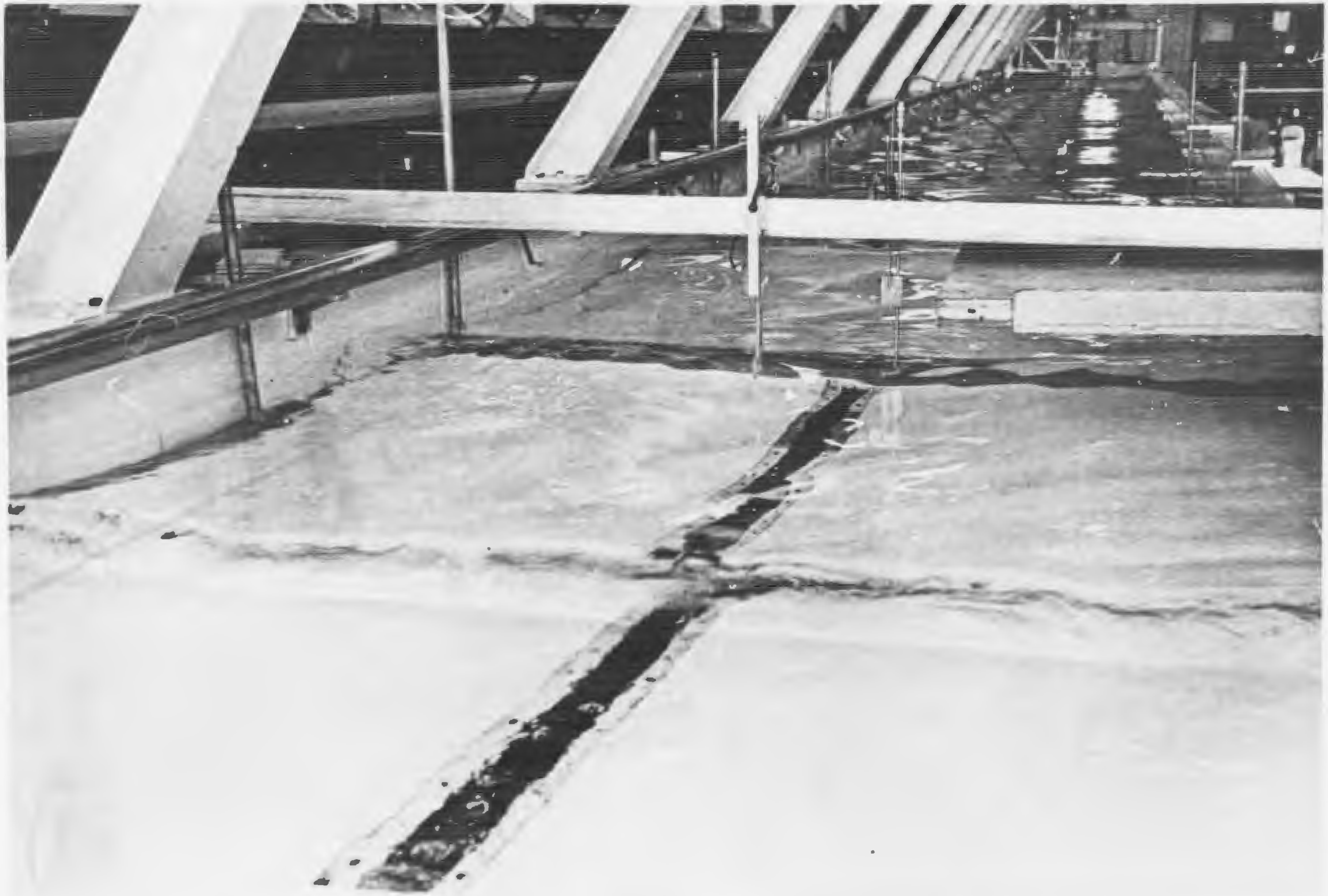

Naval Academy's 85' tow tank. 8' beach is in the foreground. Instrumentation console and wave generator are in the upper right-hand corner. Velocity probes are suspended from the aluminum angle across the tank. 16' beach is butt-joined and covered by 4" aluminum strip.

FIGURE(8)

4X

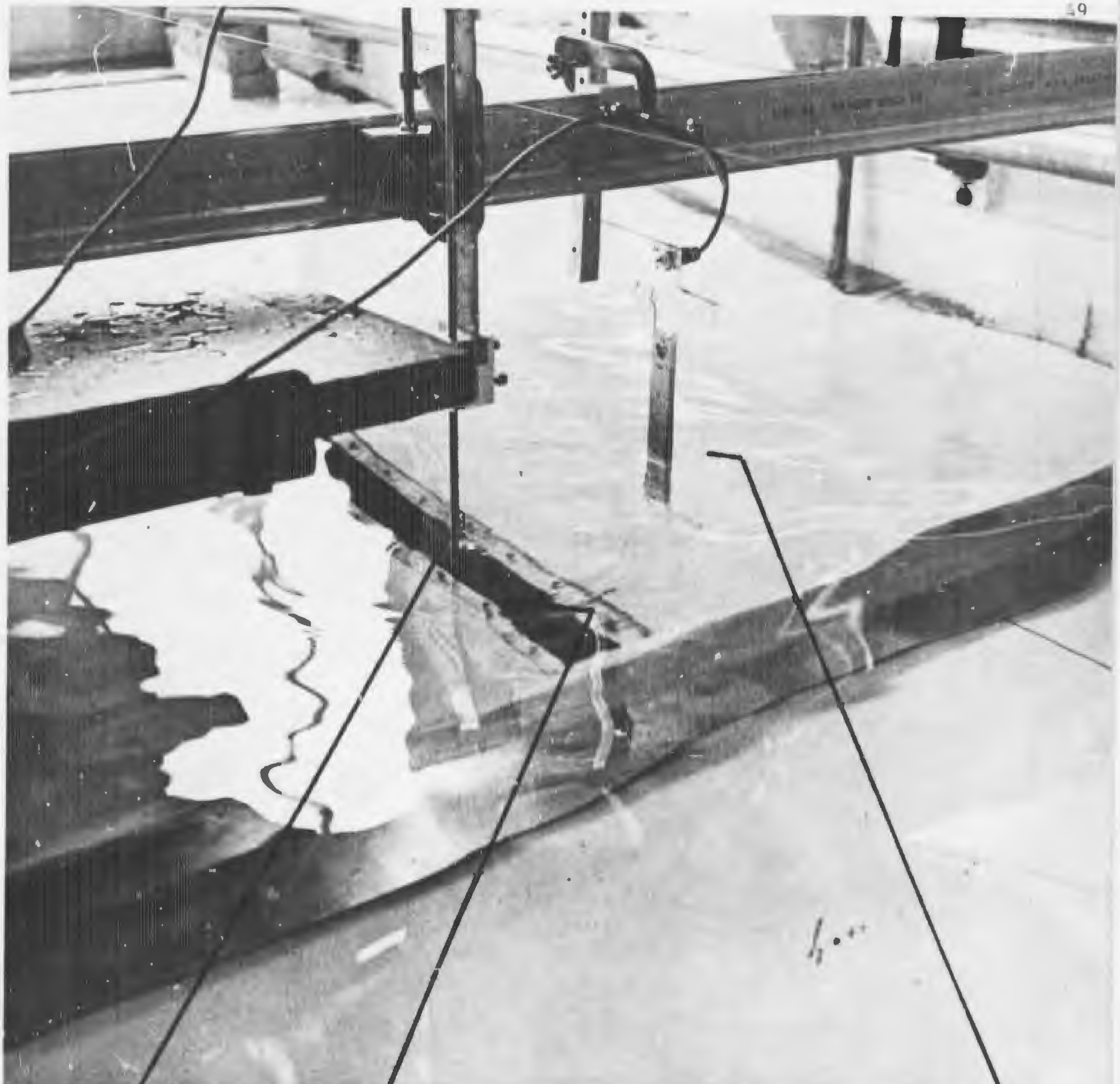
TSI 1211-20W
velocity probe
TSI 1237 Shear stress sensor
(flush mounted)
Wire resistance
wave gage

FIGURE ( )

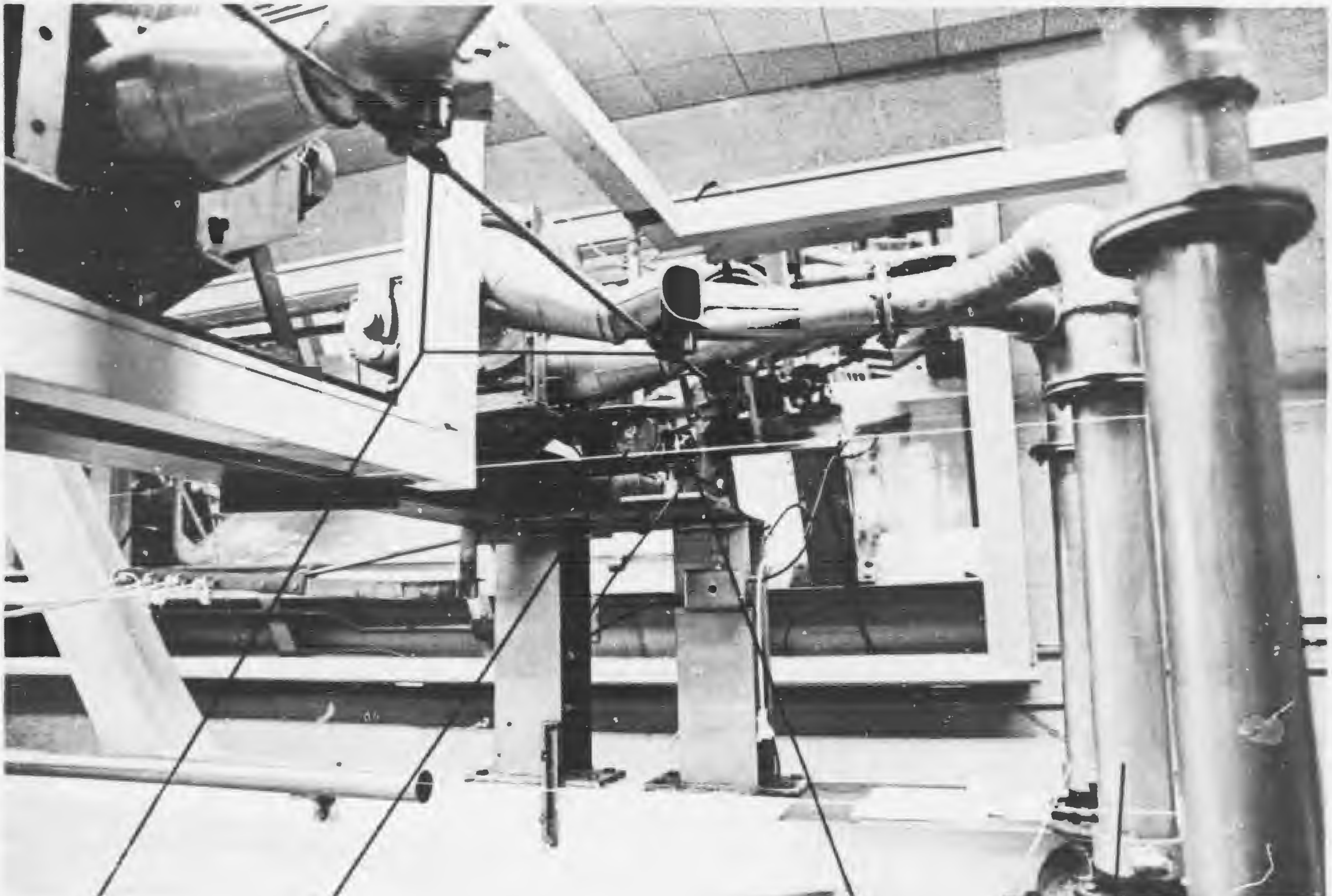
Flappers for modulating air flow to chamber
Rotating cam attached to D.C. motor
Photocell
Air pipes to generating chamber

FIGURE (10)

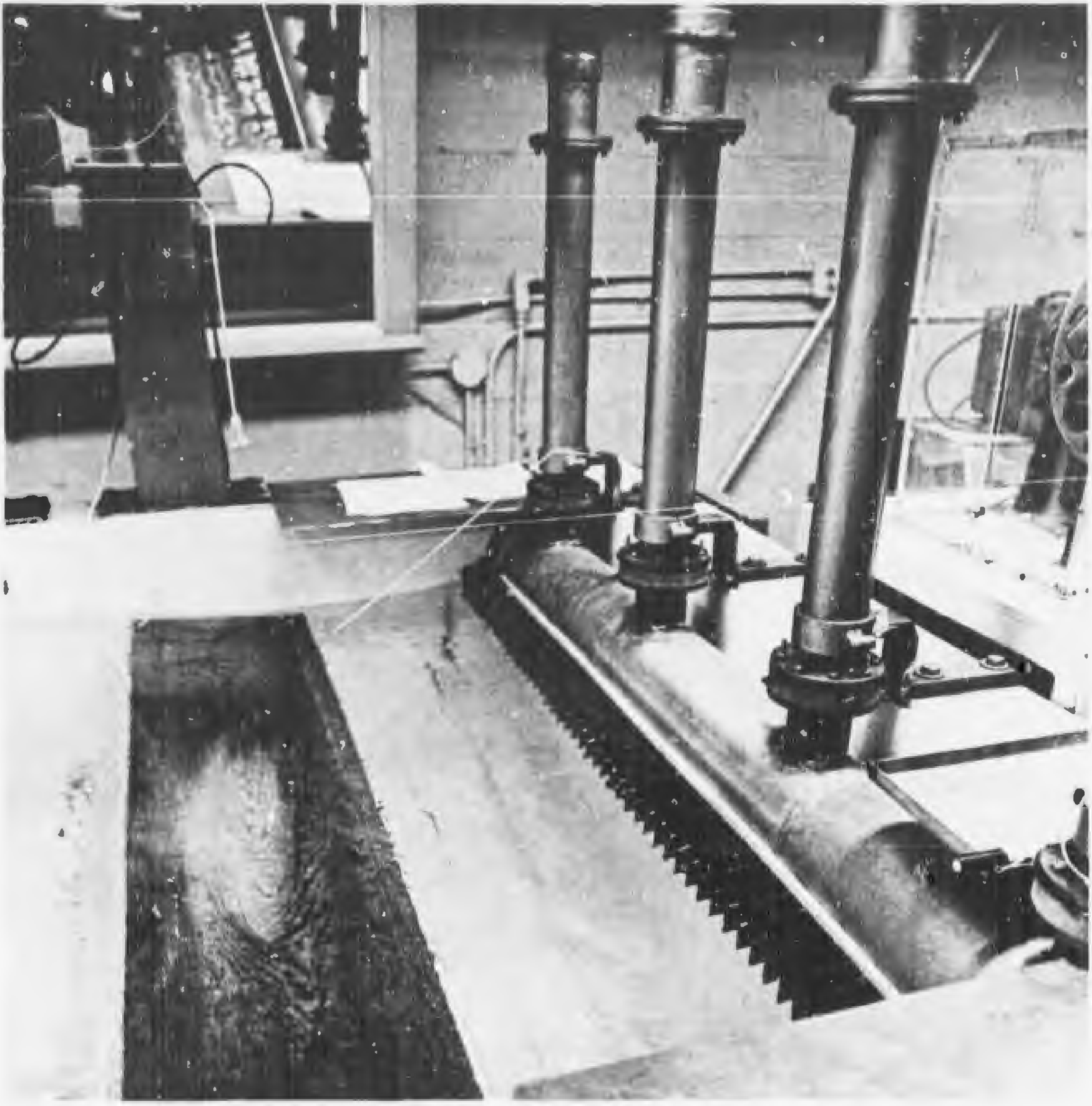

Wave generation air chamber. Floating board was tried as a means of smoothing out surface wavelets. The attempt failed and the board was removed prior to any recorded tests.

FIGURE ( )

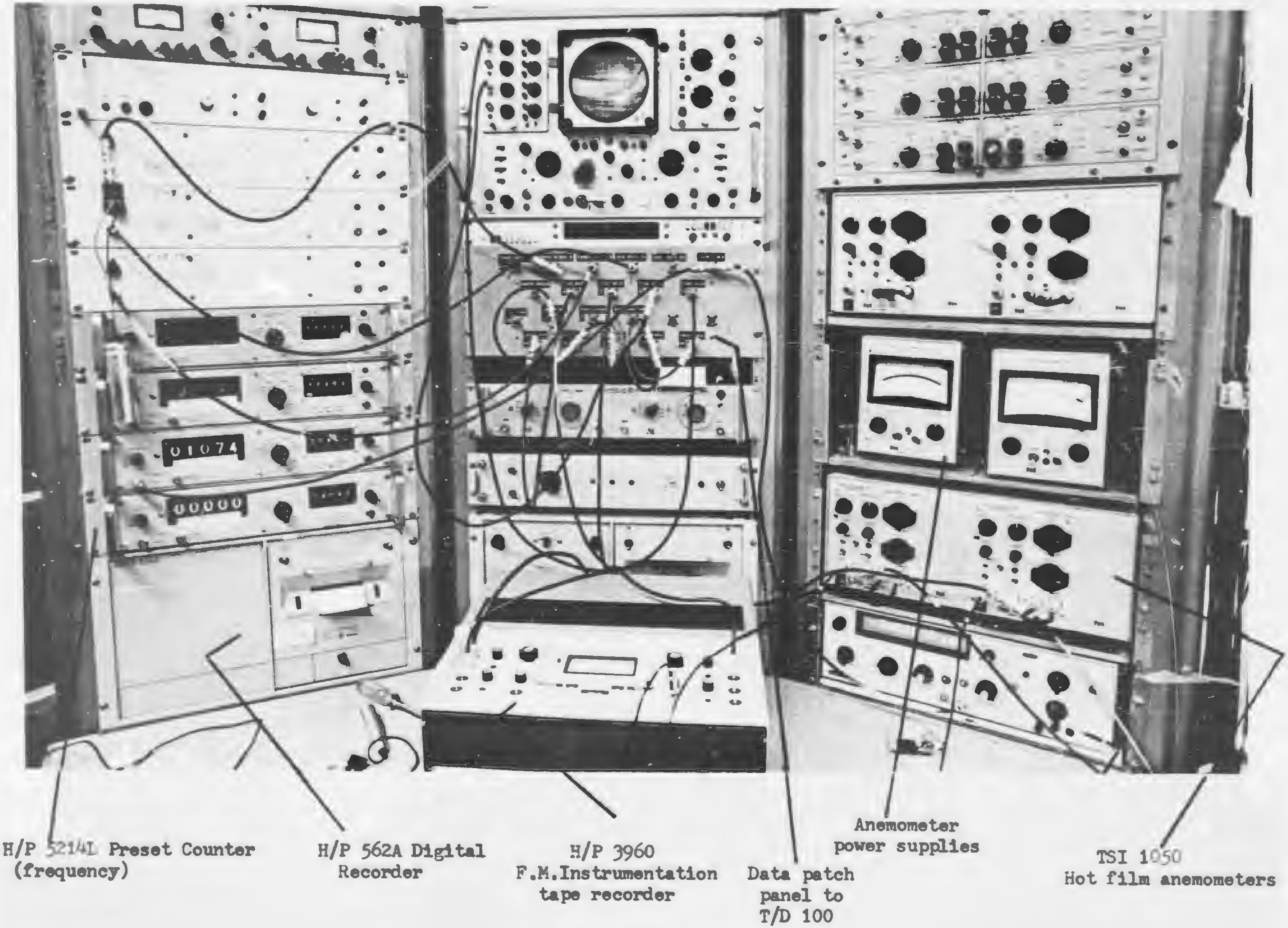
H/P 5214L Preset Counter
(frequency)
H/P 562A Digital
Recorder
H/P 3960
F.M.Instrumentation
tape recorder
Data patch
panel to
T/D 100
Anemometer
power supplies
TSI 1050
Hot film anemometers

FIGURE (12)

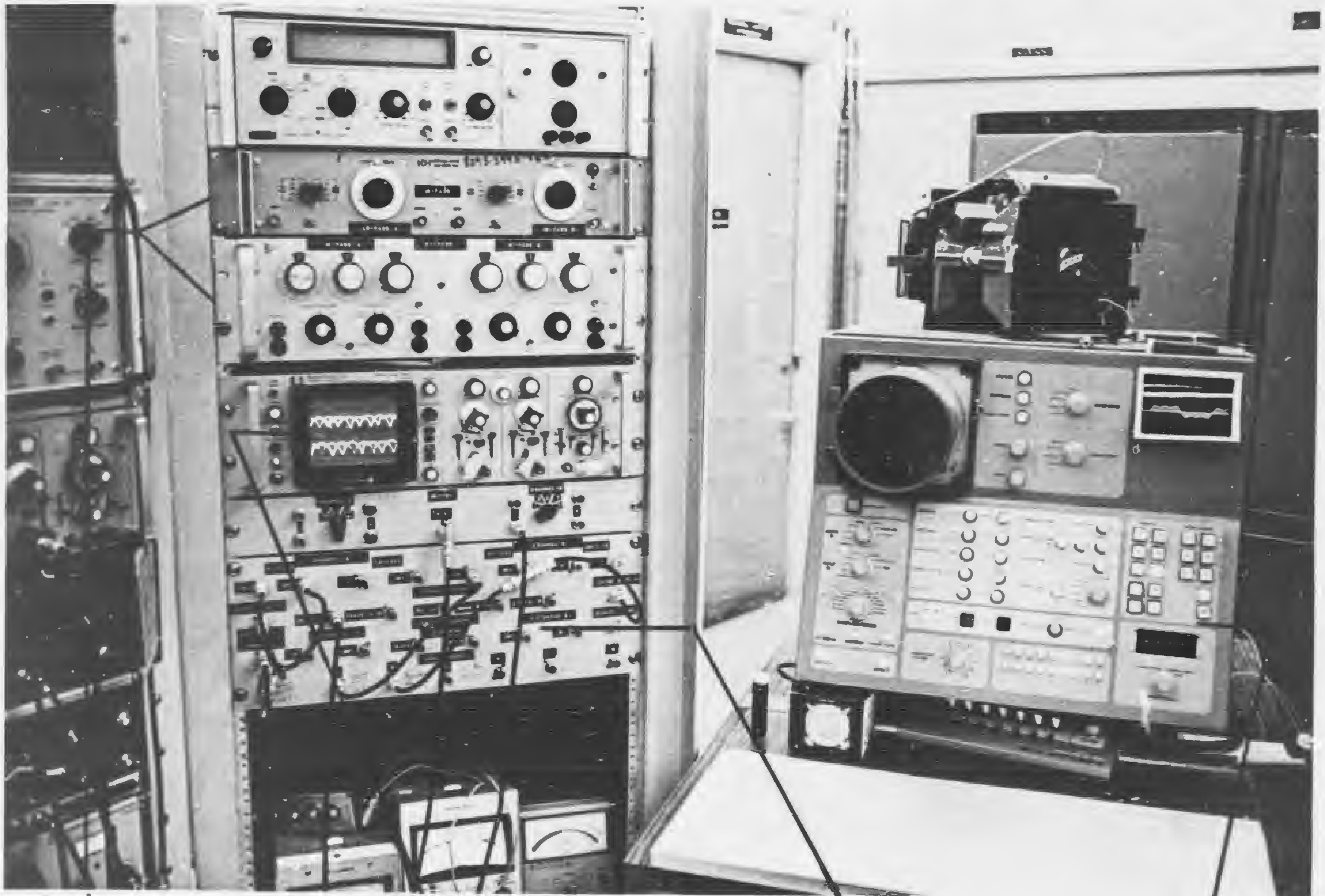
Low pass and
High pass
filters
H/P1201A
Variable persistance
oscilloscope
Data patch panel
from tow tank
T/D100 Control
Console

FIGURE (13)

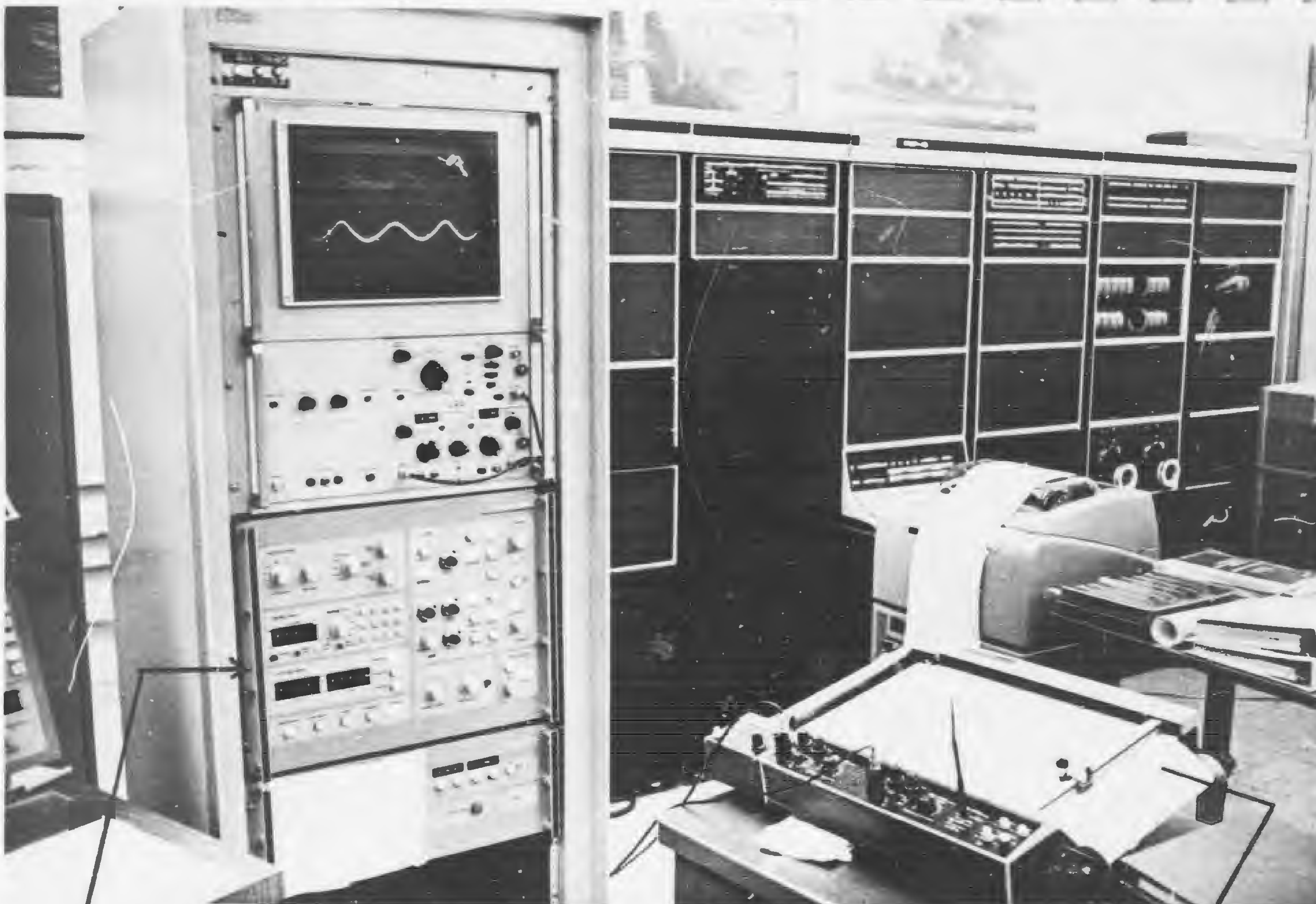

PC 102 Display Controller and Converter

H/P 70043 X-Y Recorder

FIGURE (14)

FIGURE 15

CELERITY STUDY COMPARISONS

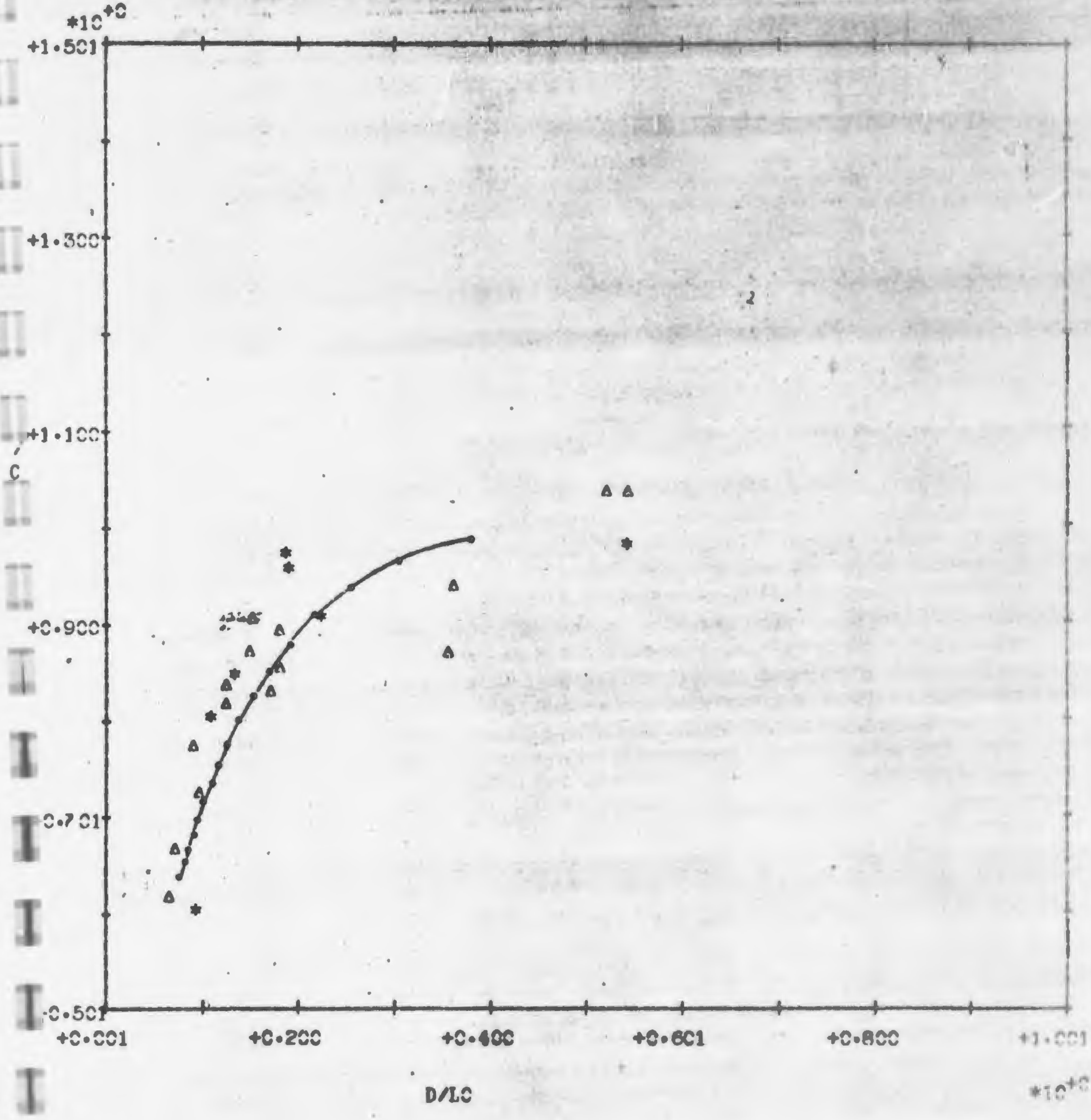

SYMBOL	NO.PTS.	LEGEND
•	17	-? LINEAR WAVE THEORY
*	7	-? DATA FROM 21 FEB 72 (QUESTIONABLE DATA REDUCTION METHODS)
Δ	15	-? DATA FROM 11-12 MAR 72

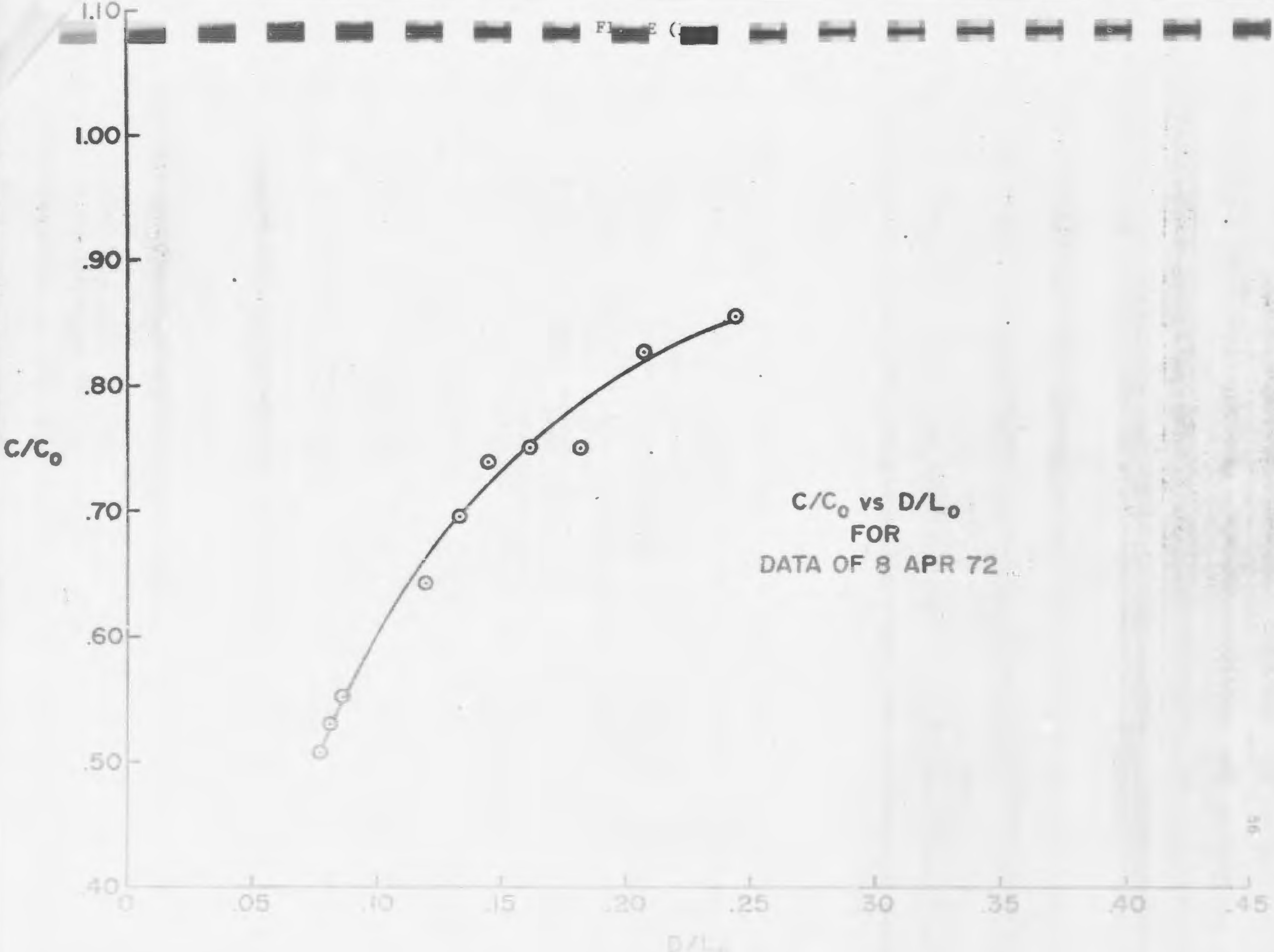
C/C0
1.10
1.00
.90
.80
.70
.60
.50
.40
0
.05
.10
.15
.20
.25
.30
.35
.40
.45
D/L0
C/C0 vs D/L0
FOR
DATA OF 8 APR 72

FIGURE (17)

CELERITY STUDY COMPARISONS

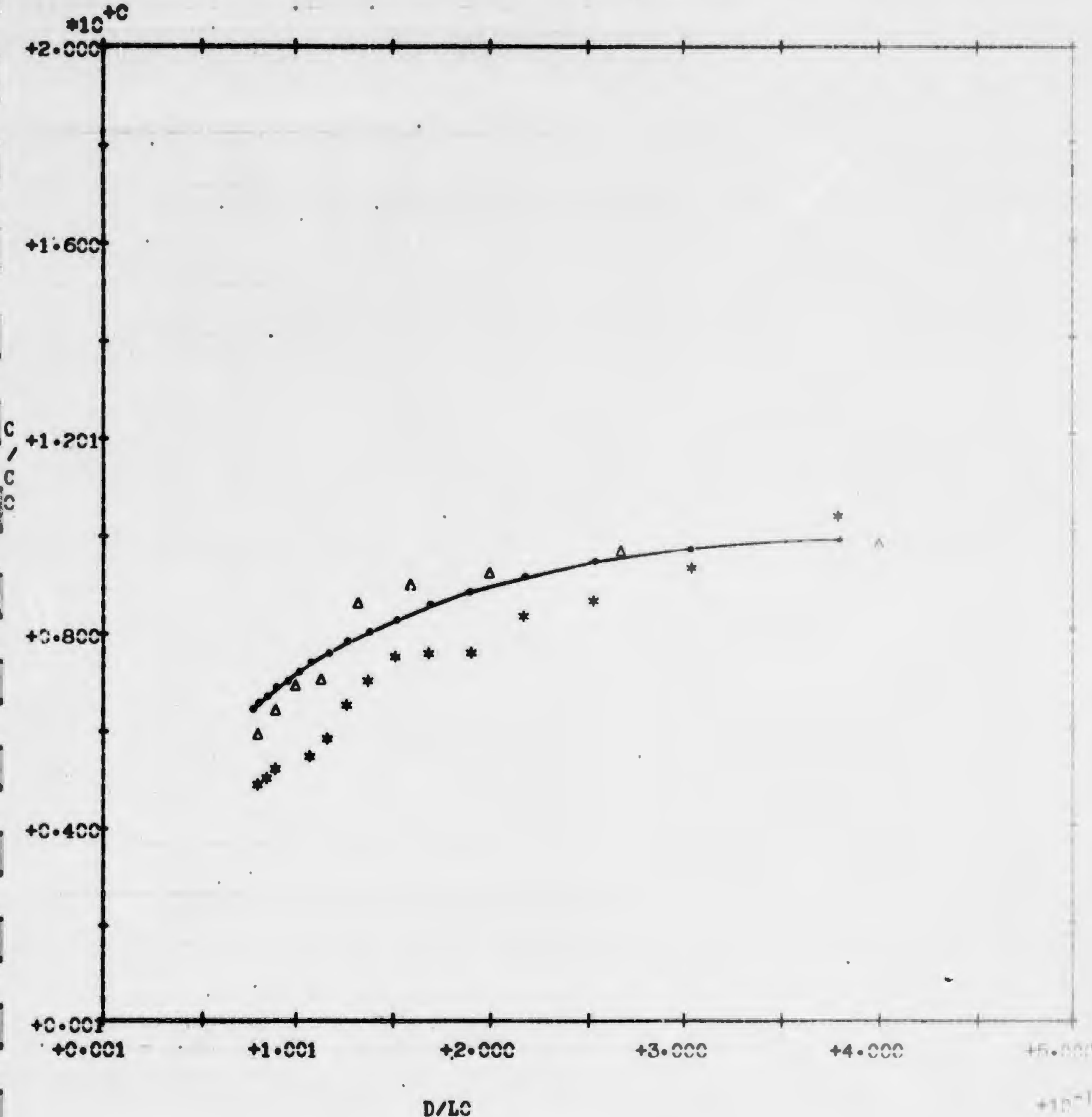

SYMBOL	NO.PTS.	LEGEND
•	17	-? LINEAR WAVE THEORY
*	14	-? SHEAR STRESS SENSORS (8APR72)
▲	9	-? VELOCITY PROBES (15APR72)

FIGURE (18)

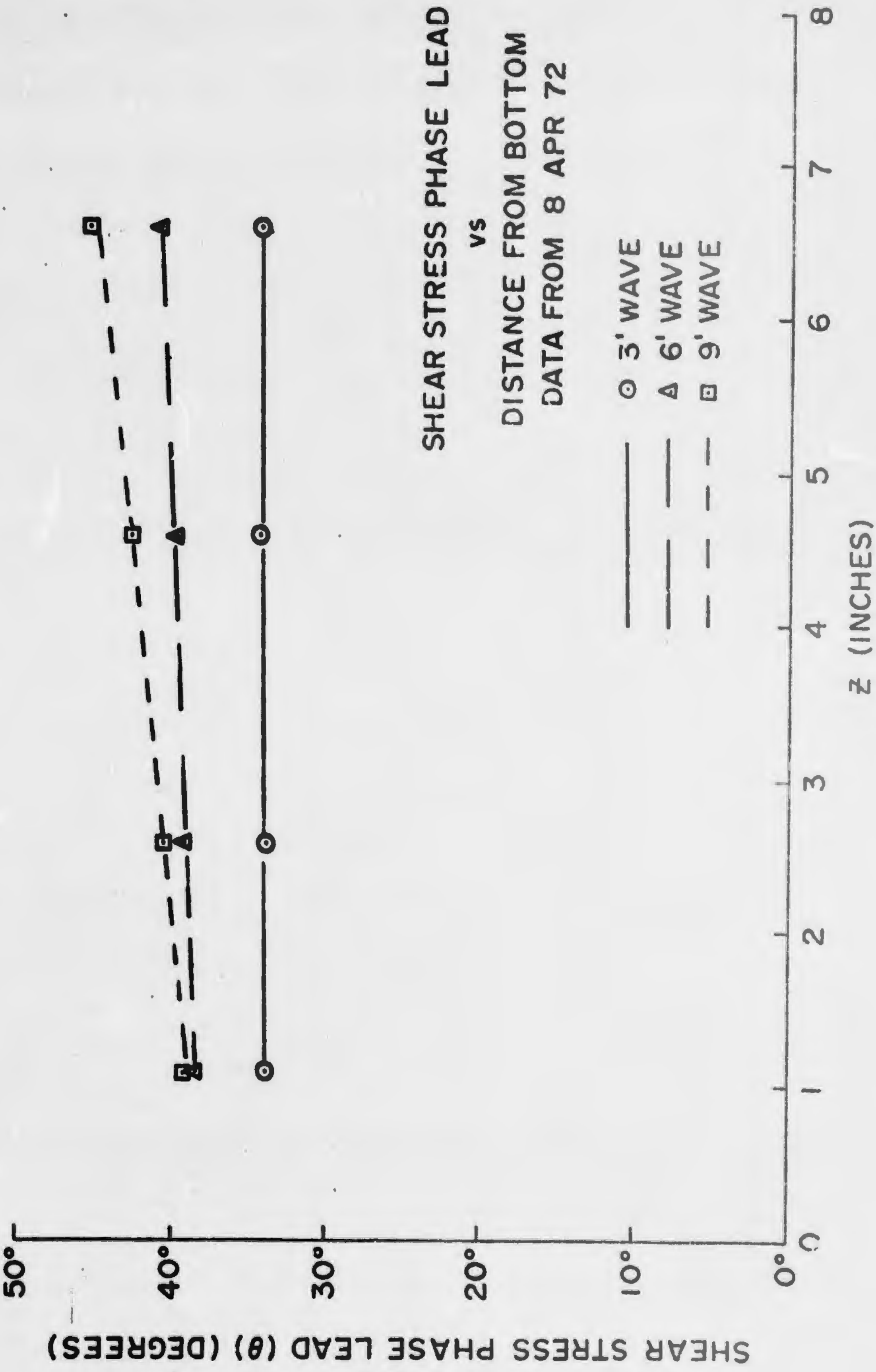
SHEAR STRESS PHASE LEAD
vs
DISTANCE FROM BOTTOM
DATA FROM 8 APR 72
3' WAVE
6' WAVE
9' WAVE
z (INCHES)
SHEAR STRESS PHASE LEAD (θ) (DEGREES)
0°
10°
20°
30°
40°
50°
0
1
2
3
4
5
6
7
8

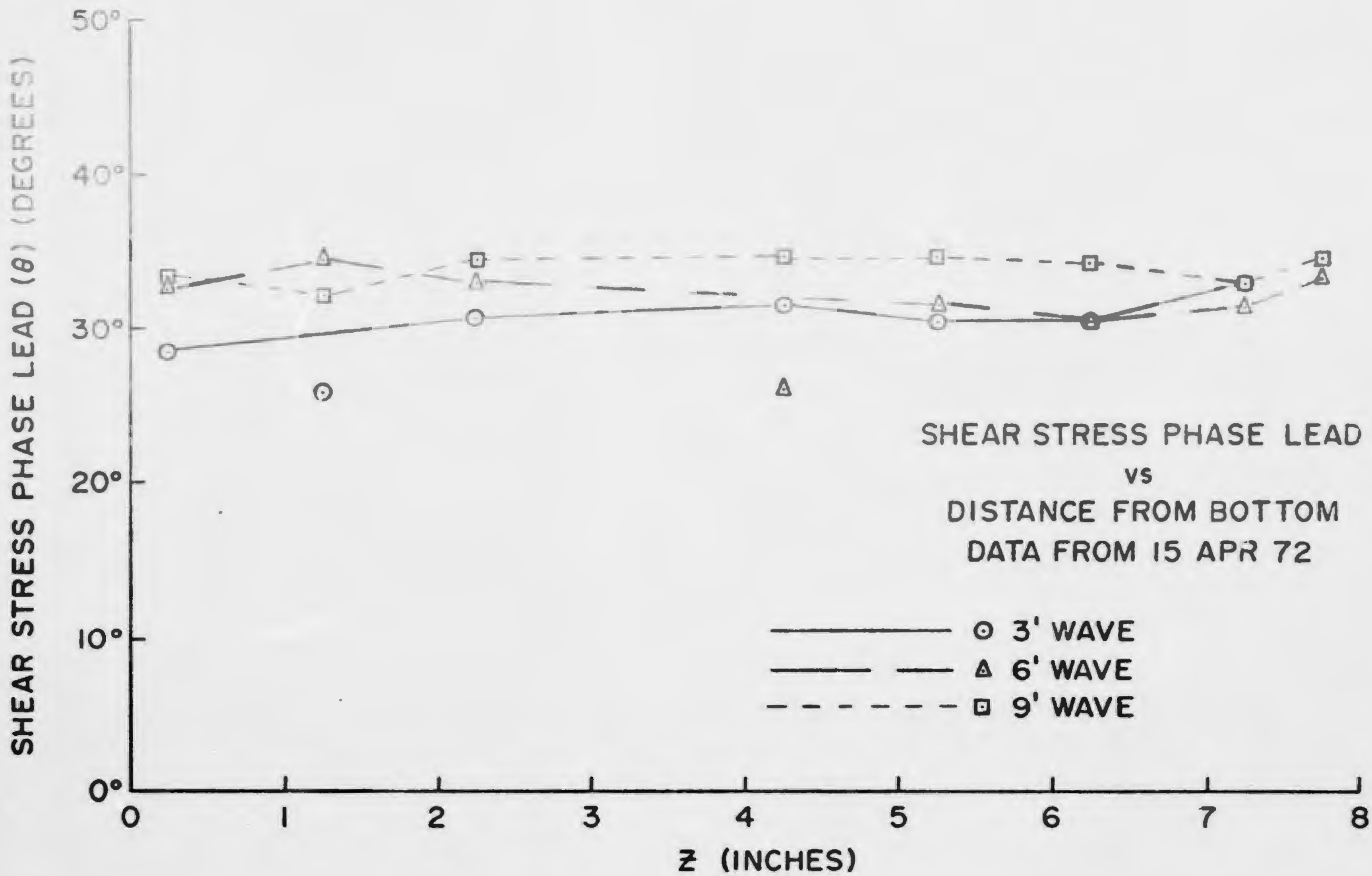
SHEAR STRESS PHASE LEAD
vs
DISTANCE FROM BOTTOM
DATA FROM 15 APR 72
3' WAVE
6' WAVE
9' WAVE
SHEAR STRESS PHASE LEAD (θ) (DEGREES)
50°
40°
30°
20°
10°
0°
0
1
2
3
4
5
6
7
8
Z (INCHES)

FIGURE (19)

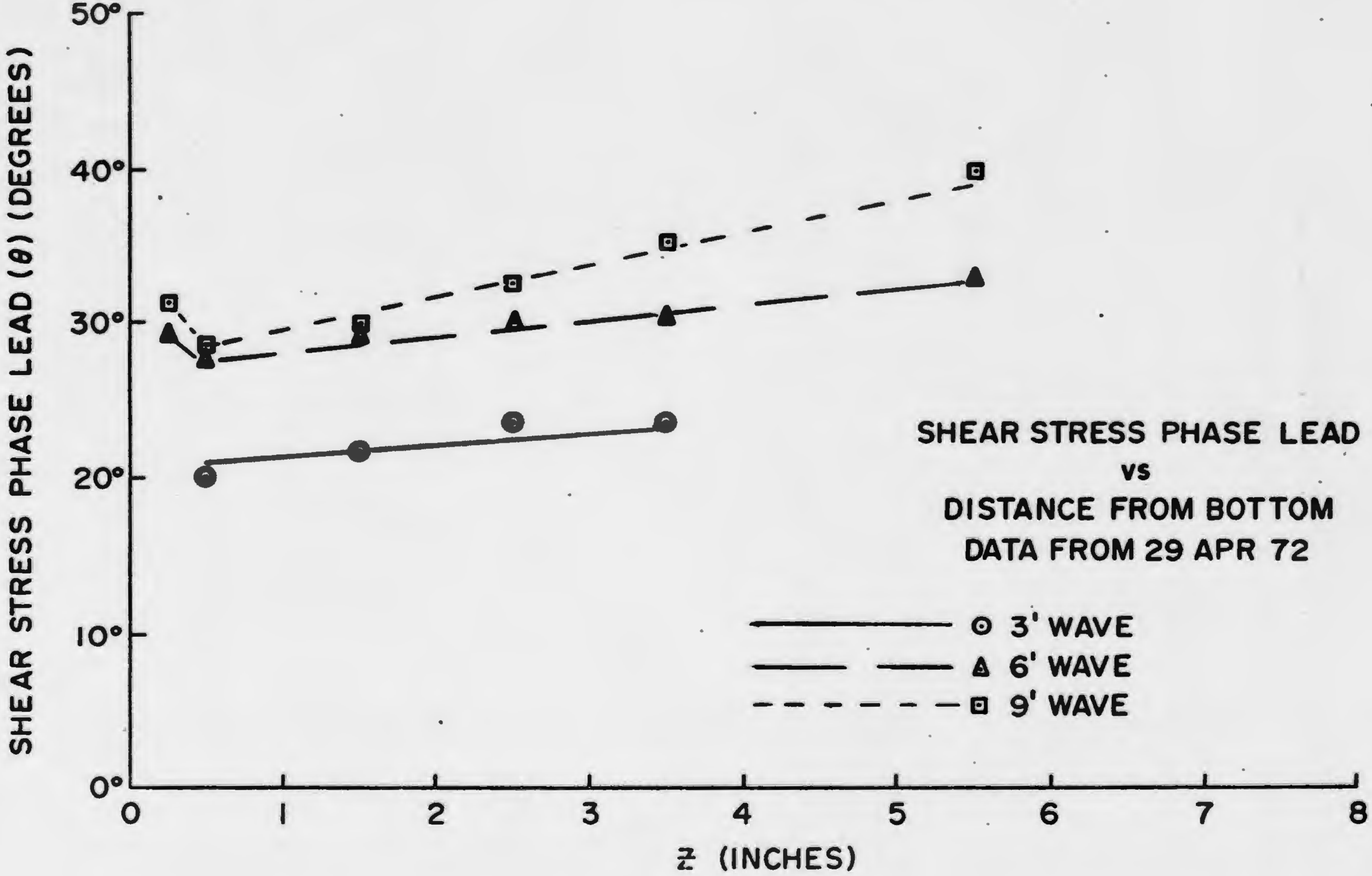
SHEAR STRESS PHASE LEAD (θ) (DEGREES)
50°
40°
30°
20°
10°
0°
0
1
2
3
4
5
6
7
8
z (INCHES)
SHEAR STRESS PHASE LEAD
vs
DISTANCE FROM BOTTOM
DATA FROM 29 APR 72
3' WAVE
6' WAVE
9' WAVE

FIGURE (21)

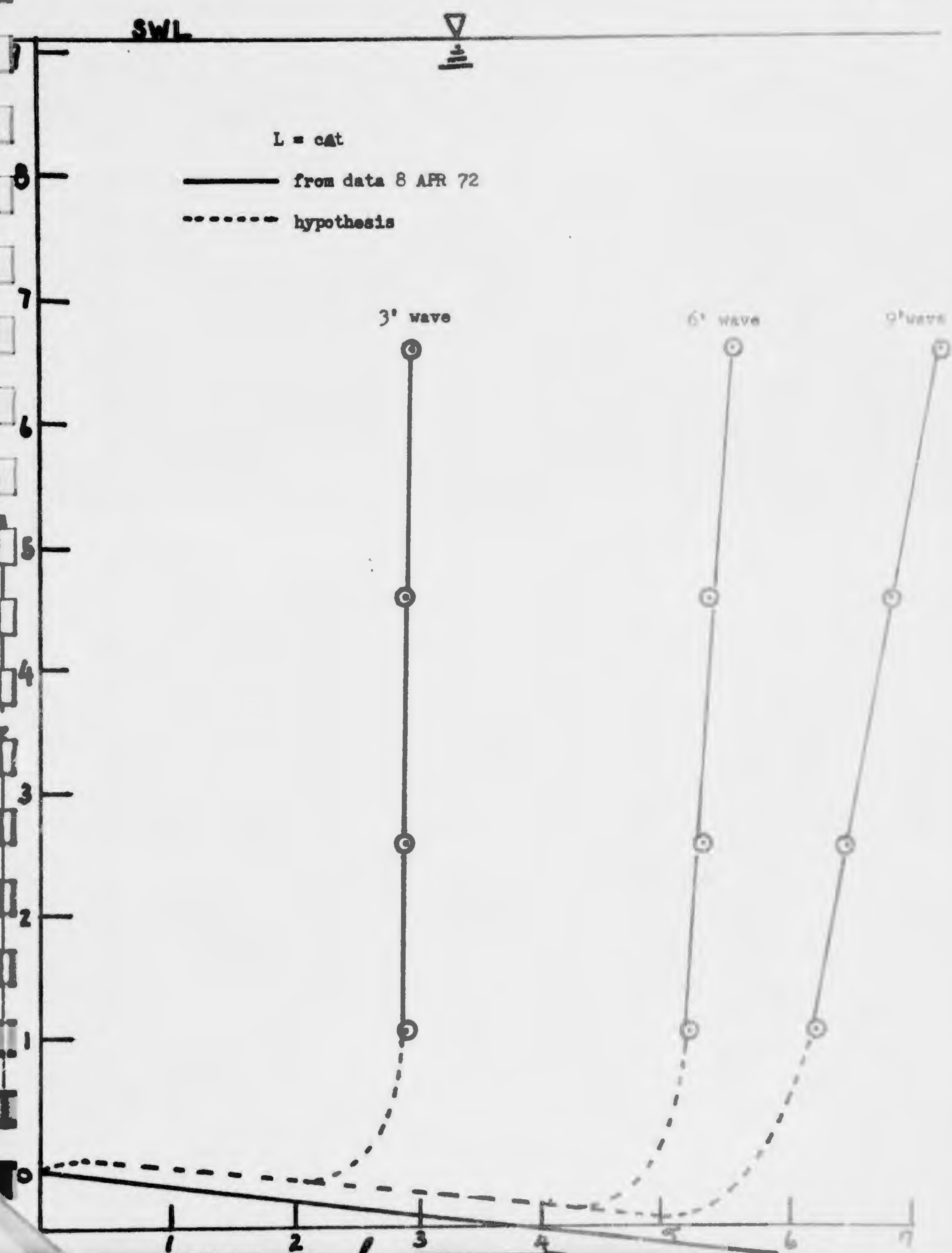
SWL
L = cat
from data 8 APR 72
hypothesis
3' wave
6' wave
9'wave
0
1
2
3
4
5
6
7
8

FI (2

BOUNDARY LAYER GROWTH

IN AN

ACCELERATING FLOW

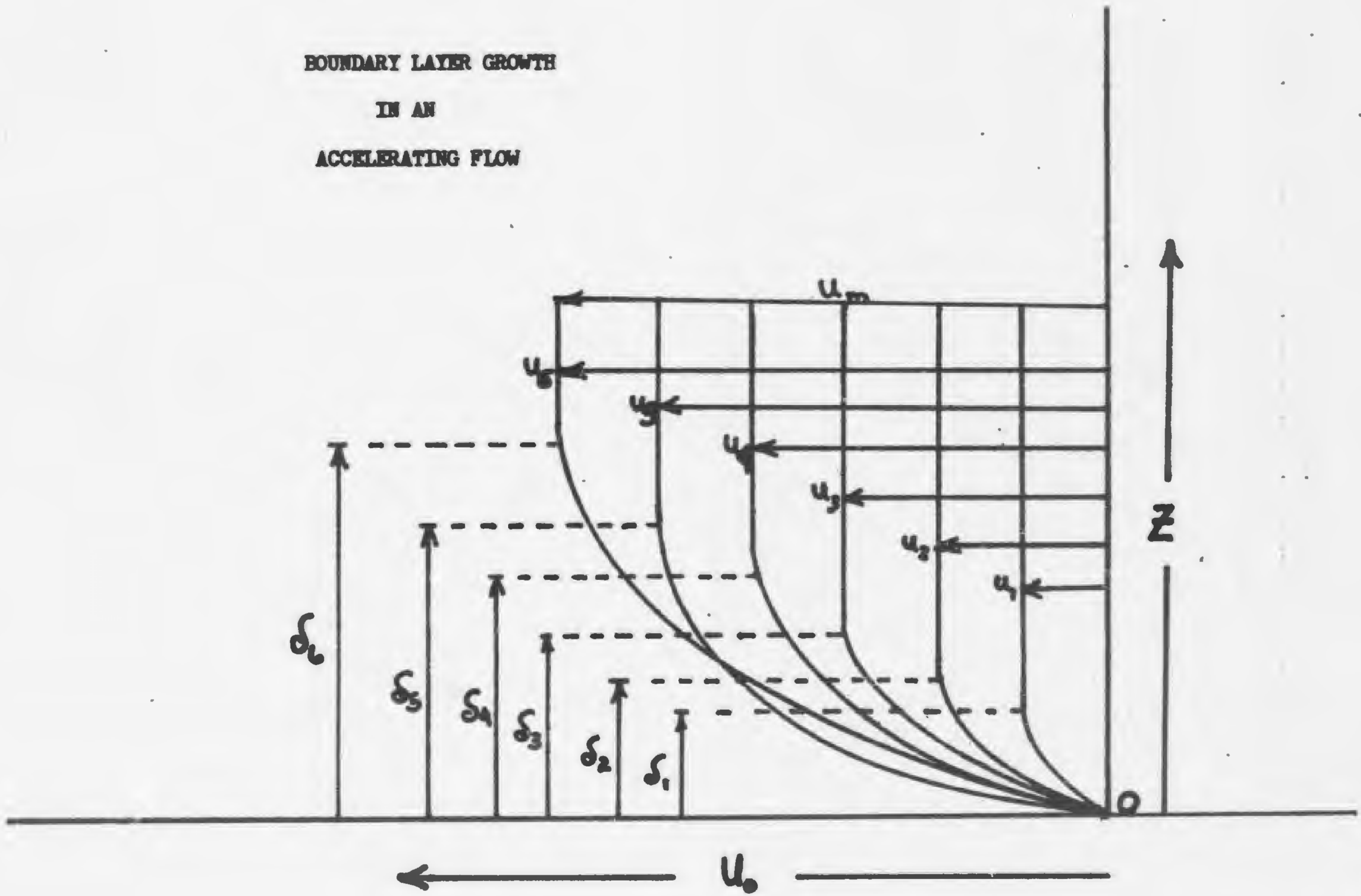

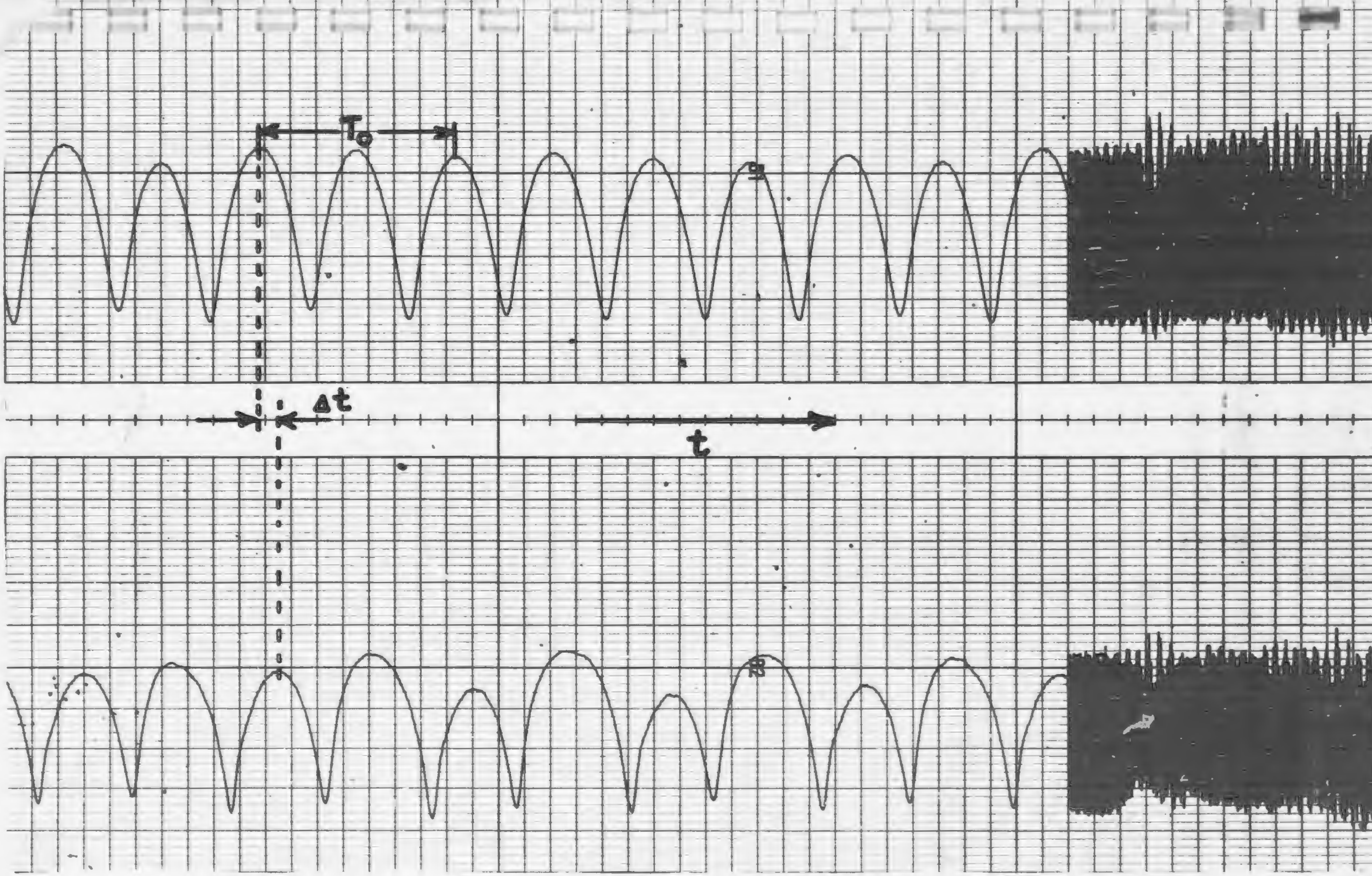

Clevite Mk. 280 strip chart recording of data from 8 APR 7 . Data is for a 3' wavelength. The velocity probe (bottom) is located 1" from the beach surface. There are two peaks per wave, one for the crest and one for the trough, since the probe senses only flow magnitude.

FIGURE (23)

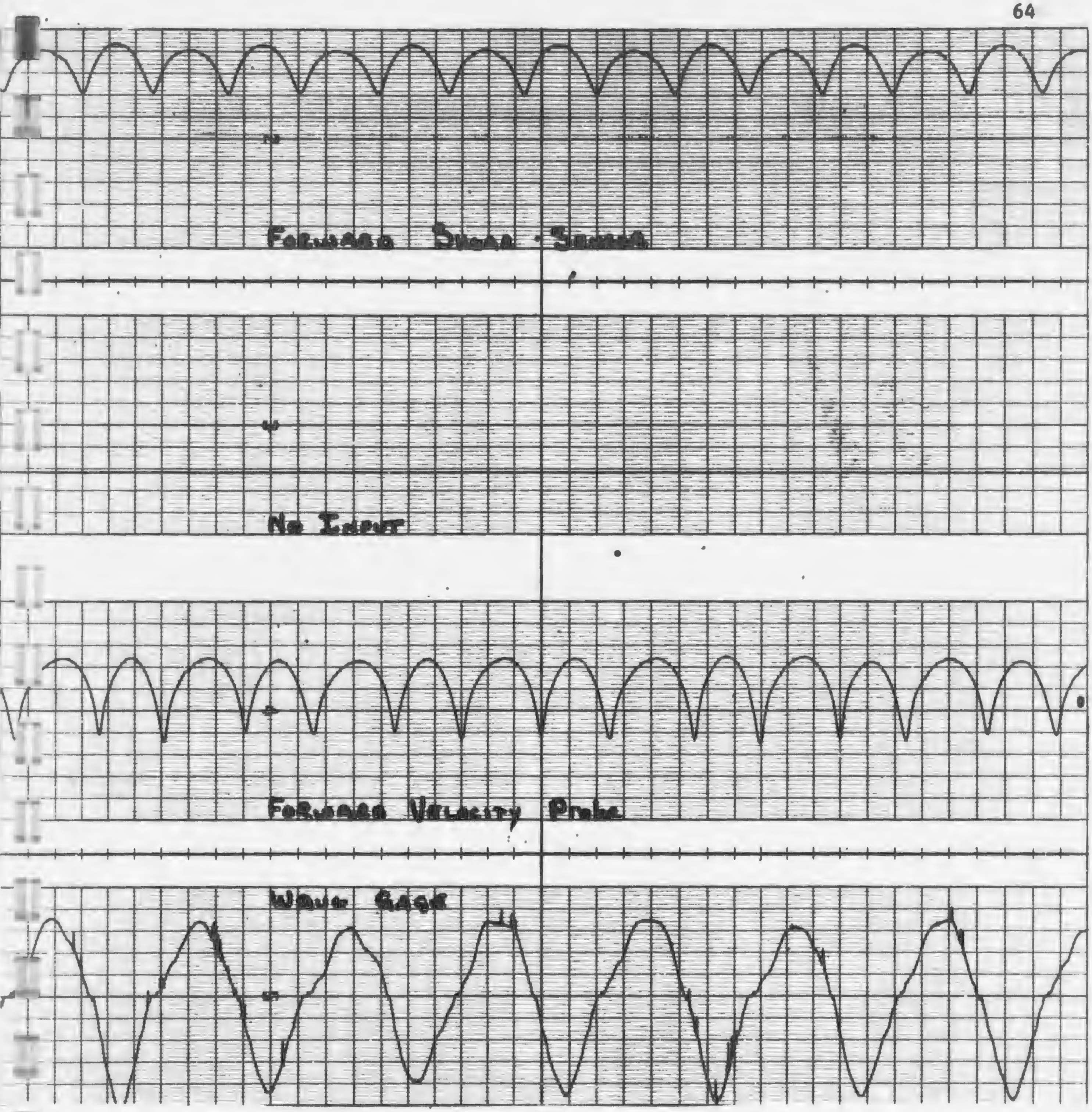

Clevite Mk 260 strip chart recording of data from 8 APR 72. The wave gage could not be linearized and was abandoned. The shear sensor was directly beneath the velocity probe, hence cross correlation provided phase lead/lag indication. There are two humps per wave .

FIGURE ([illegible])

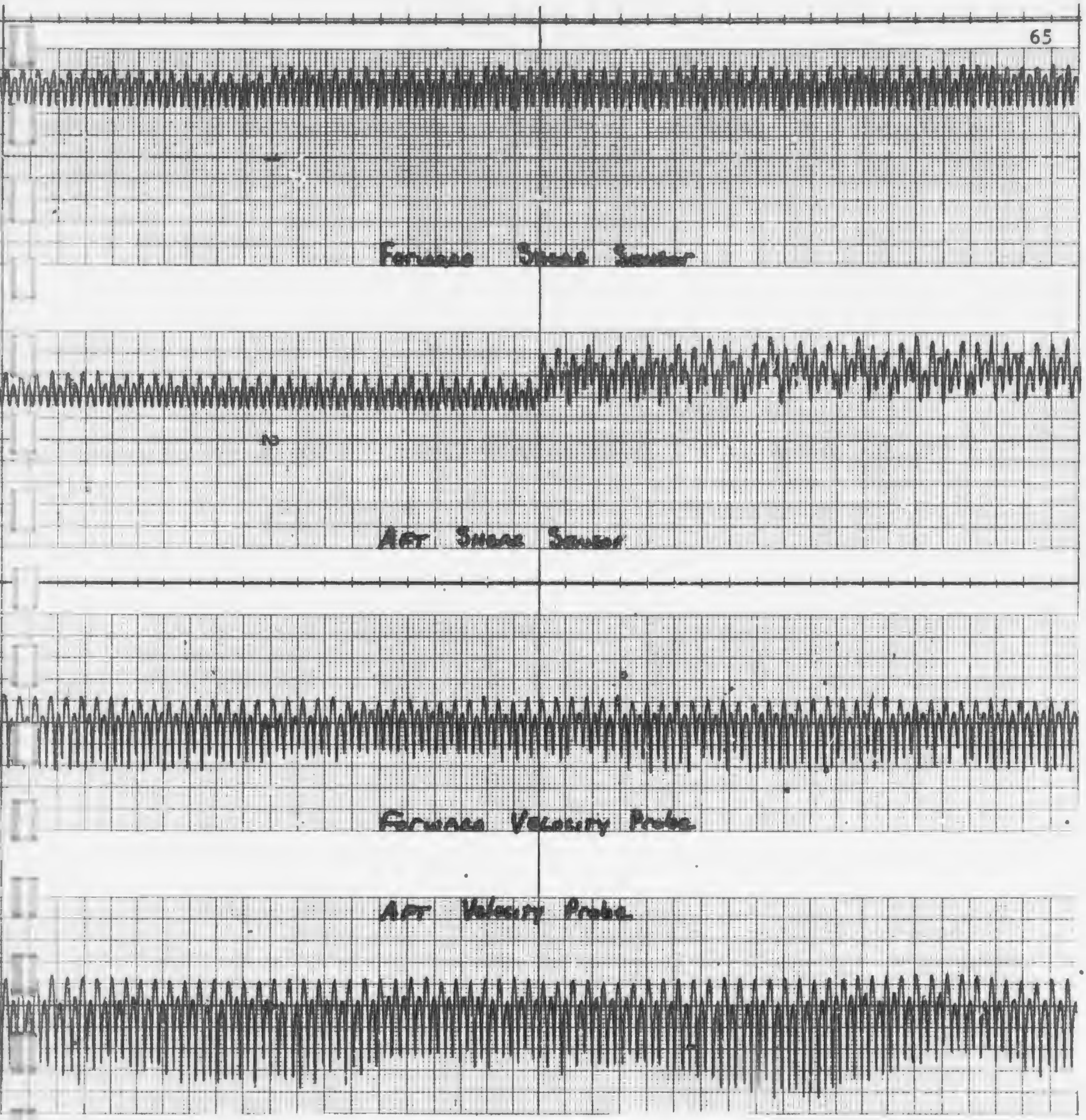

Apparent effect of bubble entrainment on the heat transfer characteristics of the after shear sensor. Note that only the after shear sensor is affected - there is no unusual [illegible] disturbance registered by the other shear sensor or by either of the velocity probes.

FIGURE ( )

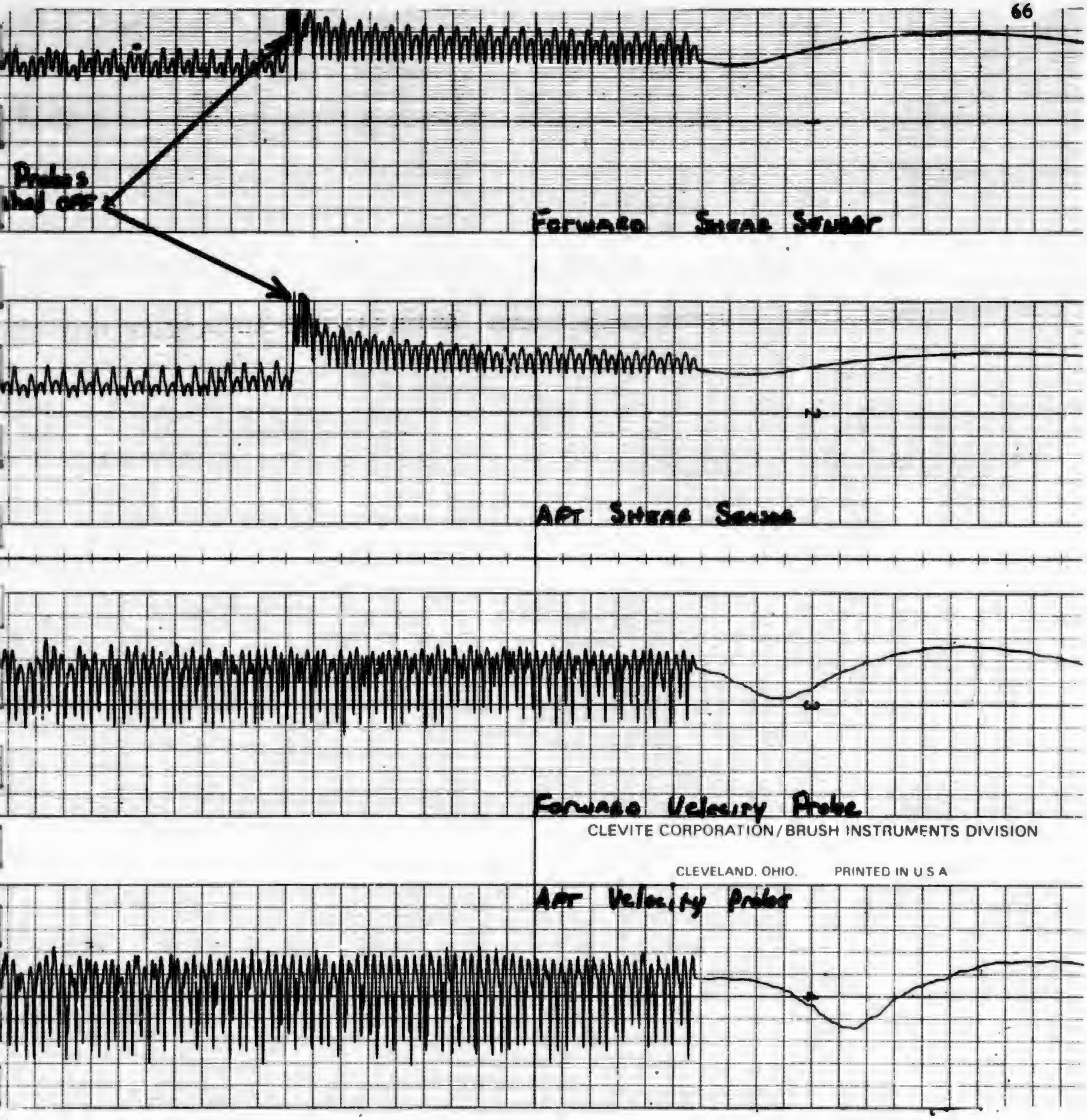

The effect of brushing the shear sensors lightly with the fingertips is clearly seen in this recording. Immediadely afterward, the the output increased, howver began a rapid decline, apparently as the flow disturbance caused by the fingers died away. The sensor surfaces also began attracting bubbles immediately, which decreased the output. By the end of the run (2 min. later) the output levels had returned to their original condition. Data from 15 APR 72

FIGURE (26)

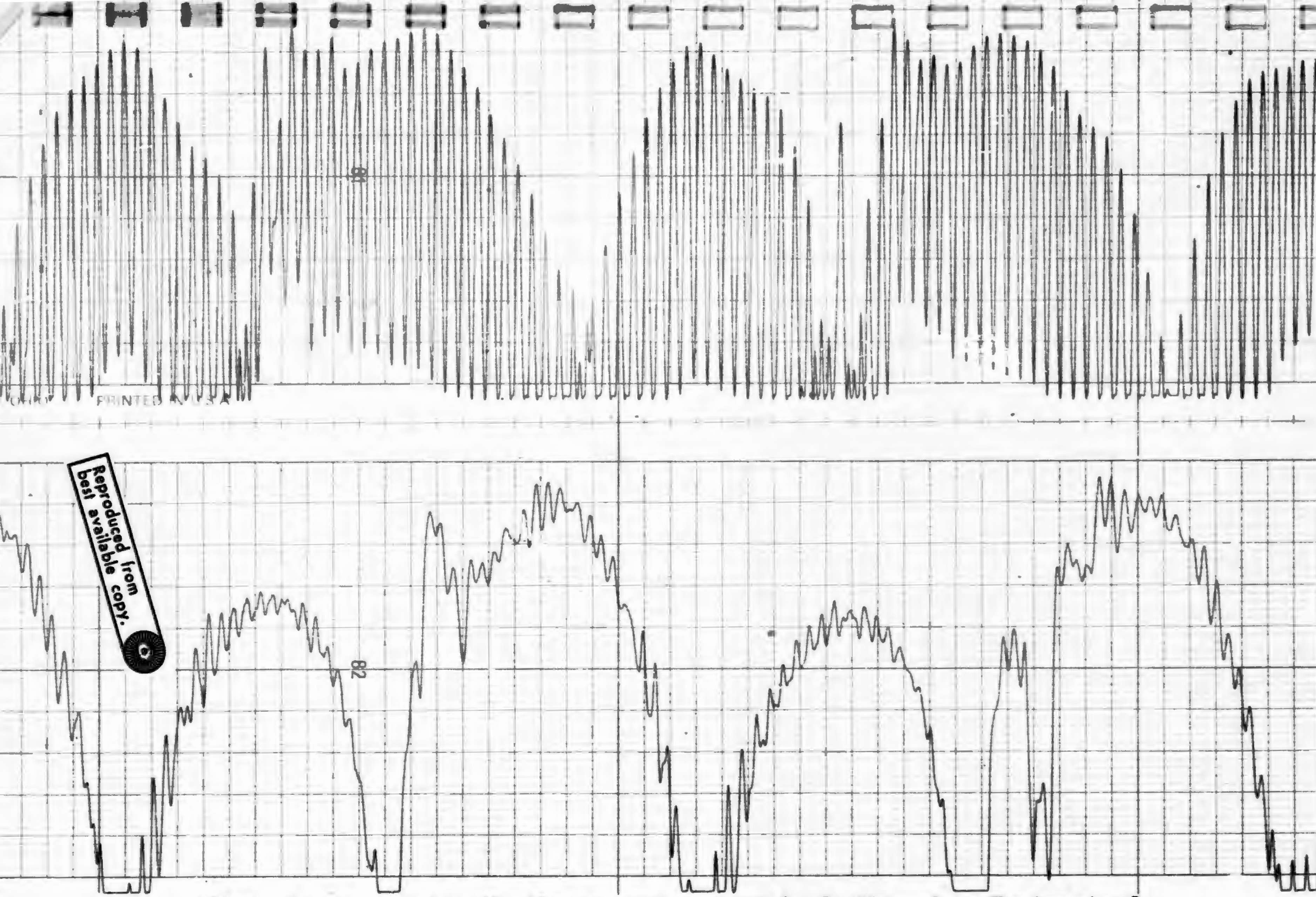

Effect of wave generator vibration on carriage-mounted velocity probes. The top signal is from a TSI 1211-20W horizontal probe, the bottom signal is from a TSI 1210-20W vertical velocity probe.

FIGURE (27)

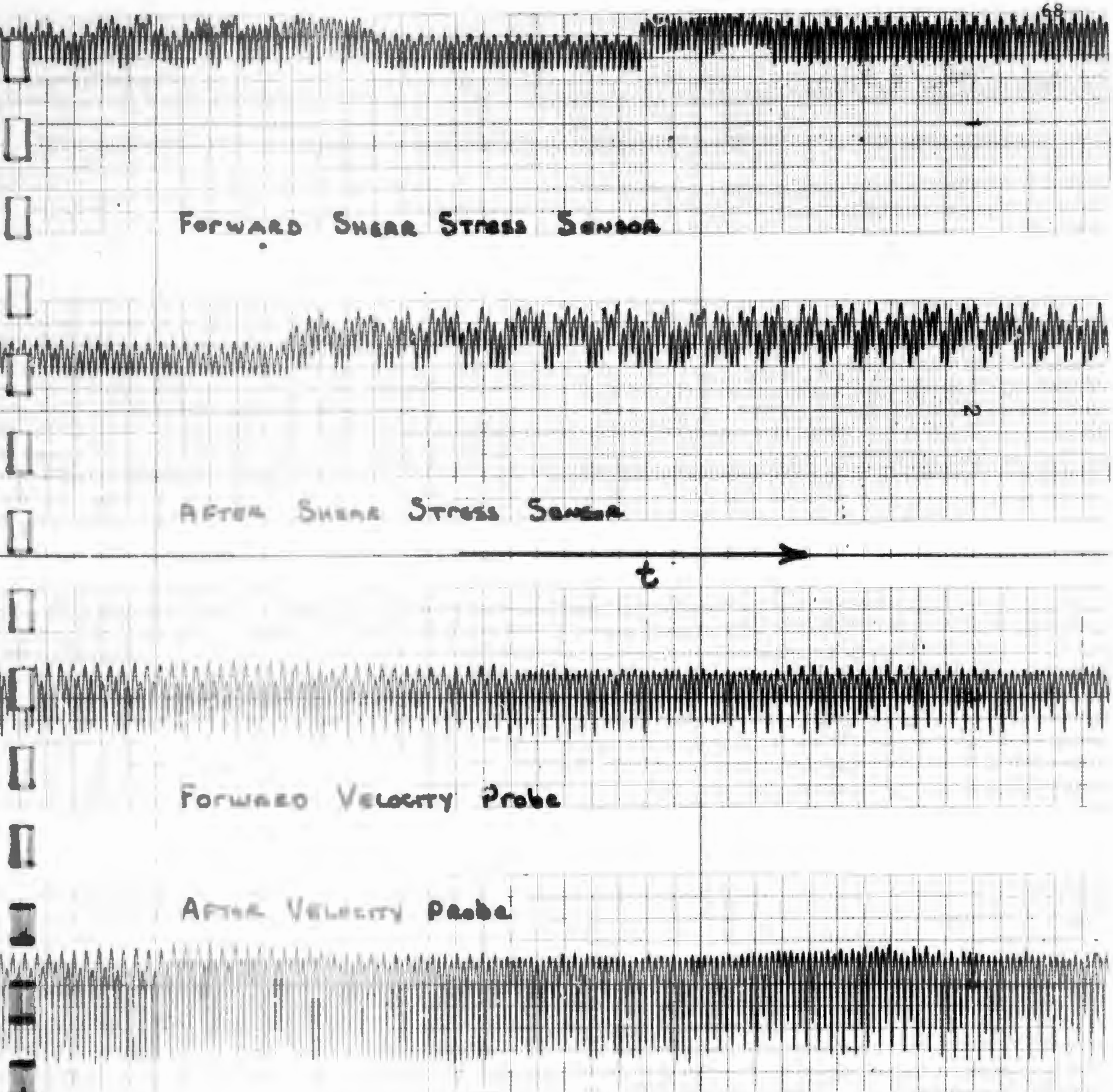

No explanation other than bubble effects is offered for the erratic behavior of the forward shear sensor. The aft shear sensor is apparently experiencing some periodic disturbance, although the velocity probes, 2.5" above, are not indicating any unusual flow. Note how sudden the transition was to this abnormal output. Such effects render calibration attempts useless.

FIGURE (28)

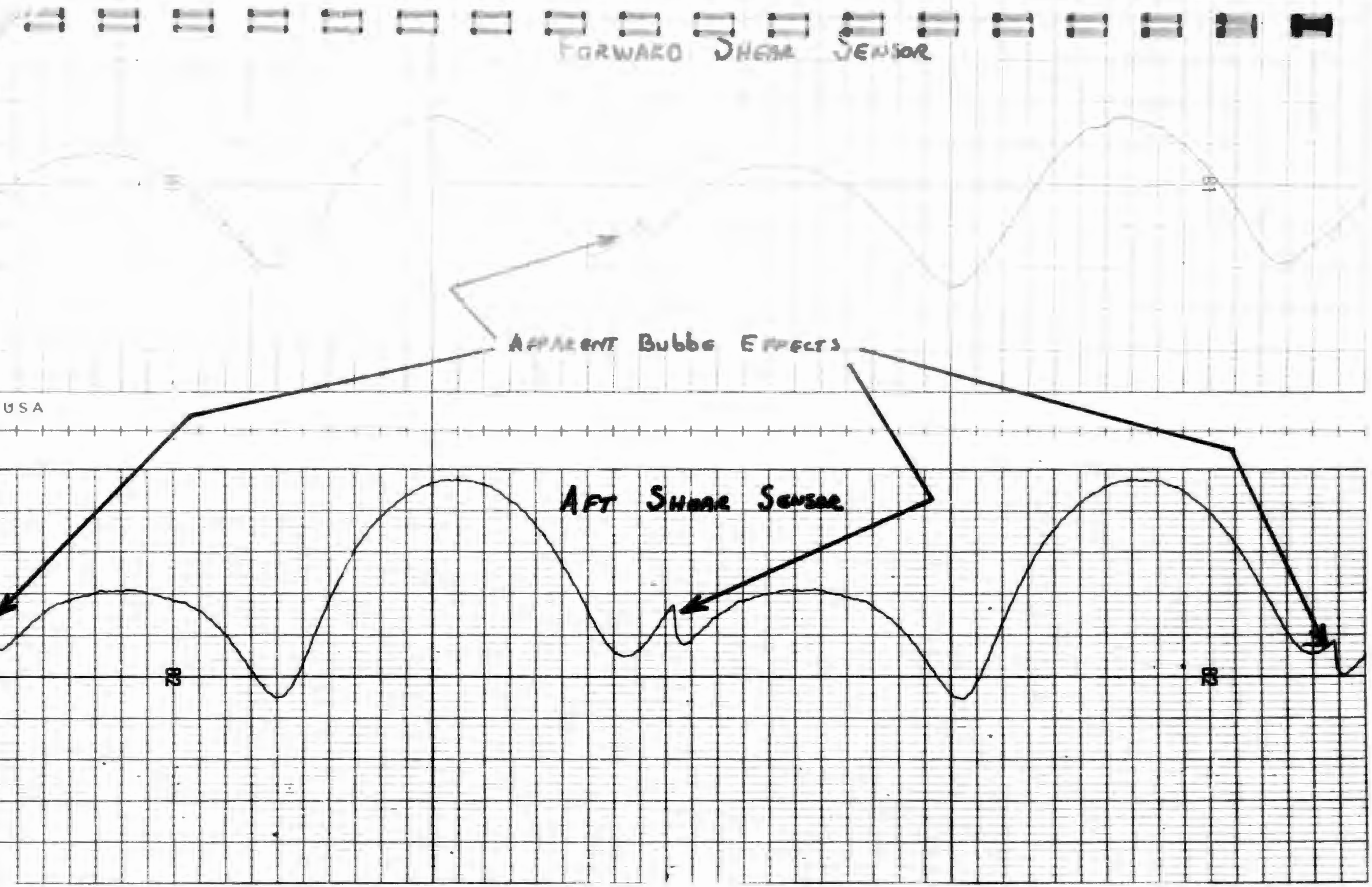

Abnormalities in the signal outputs of two shear sensors. This data is from 15 APR 72 and the vertical alignment of the sensor surfaces has been questioned. Thus, the discontinuities noted may be the result of flow disturbance rather than bubble effects.

FIGURE (29)

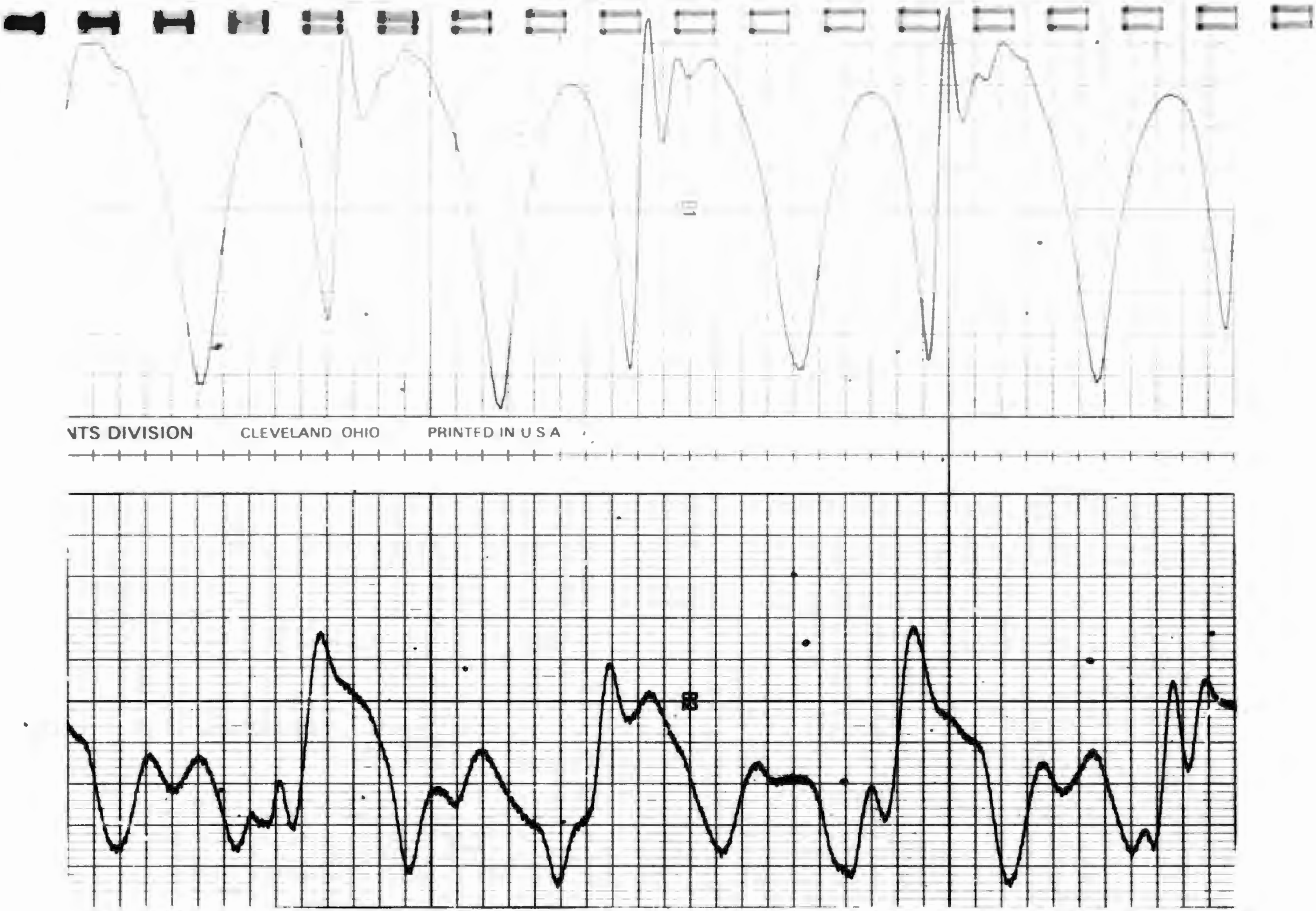

Effects of velocity probe misalignment with the incident flow. Both probes were misaligned approximately 5-7°. The top signal is from a TSI 1211-20W, the bottom signal from a TSI 1210-20W. Data from 11 MAR 72.

FIGURE (30)

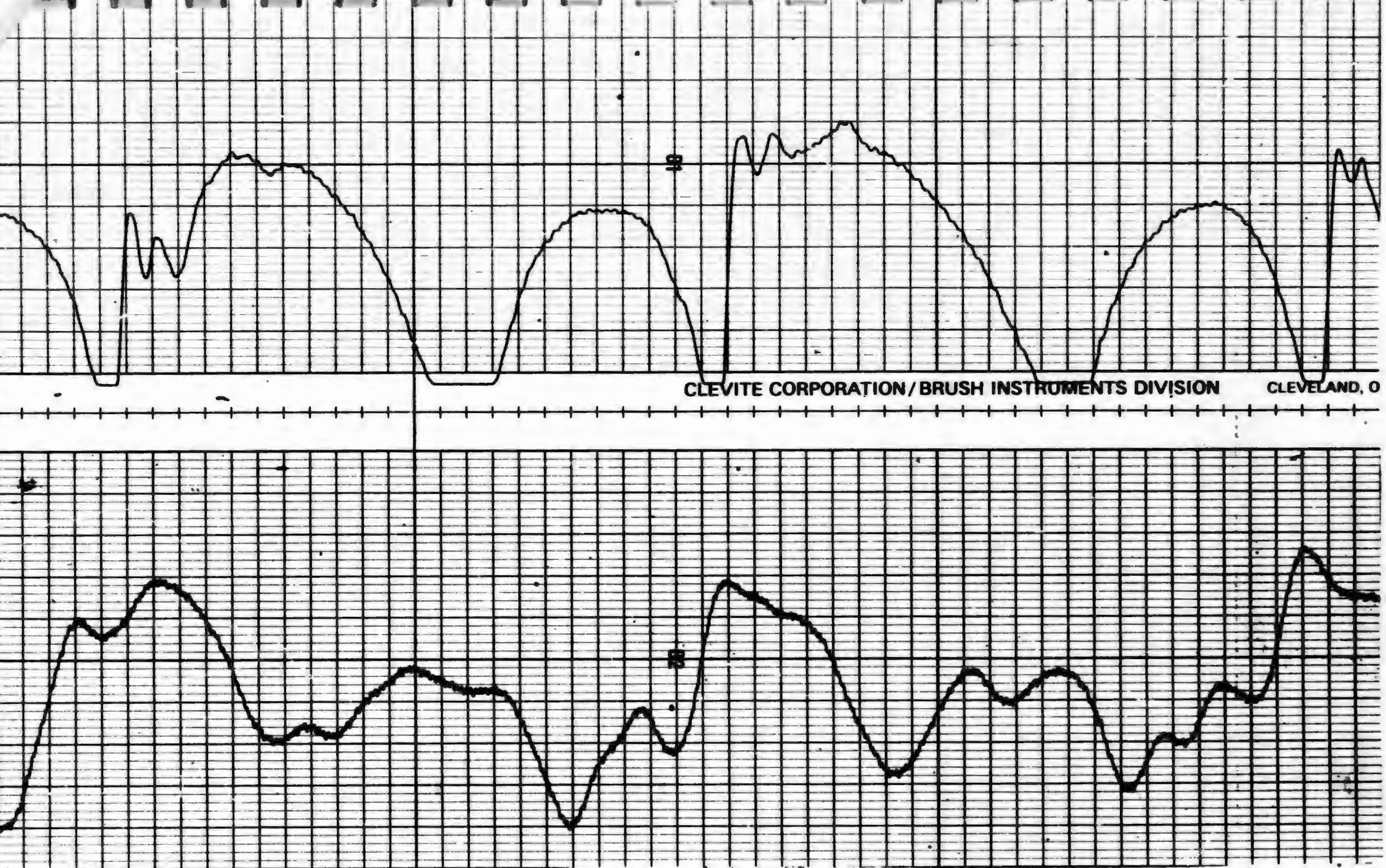

An increase in ϕ brings a dramatic increase in the signal distortion. Again, the top probe is a TSI 1211-20W and the bottom probe a 1210-20W. The value of ϕ was approximately $10\text{-}12^{\circ}$. Data from 11 MAR 72.

FIGURE (3[1])

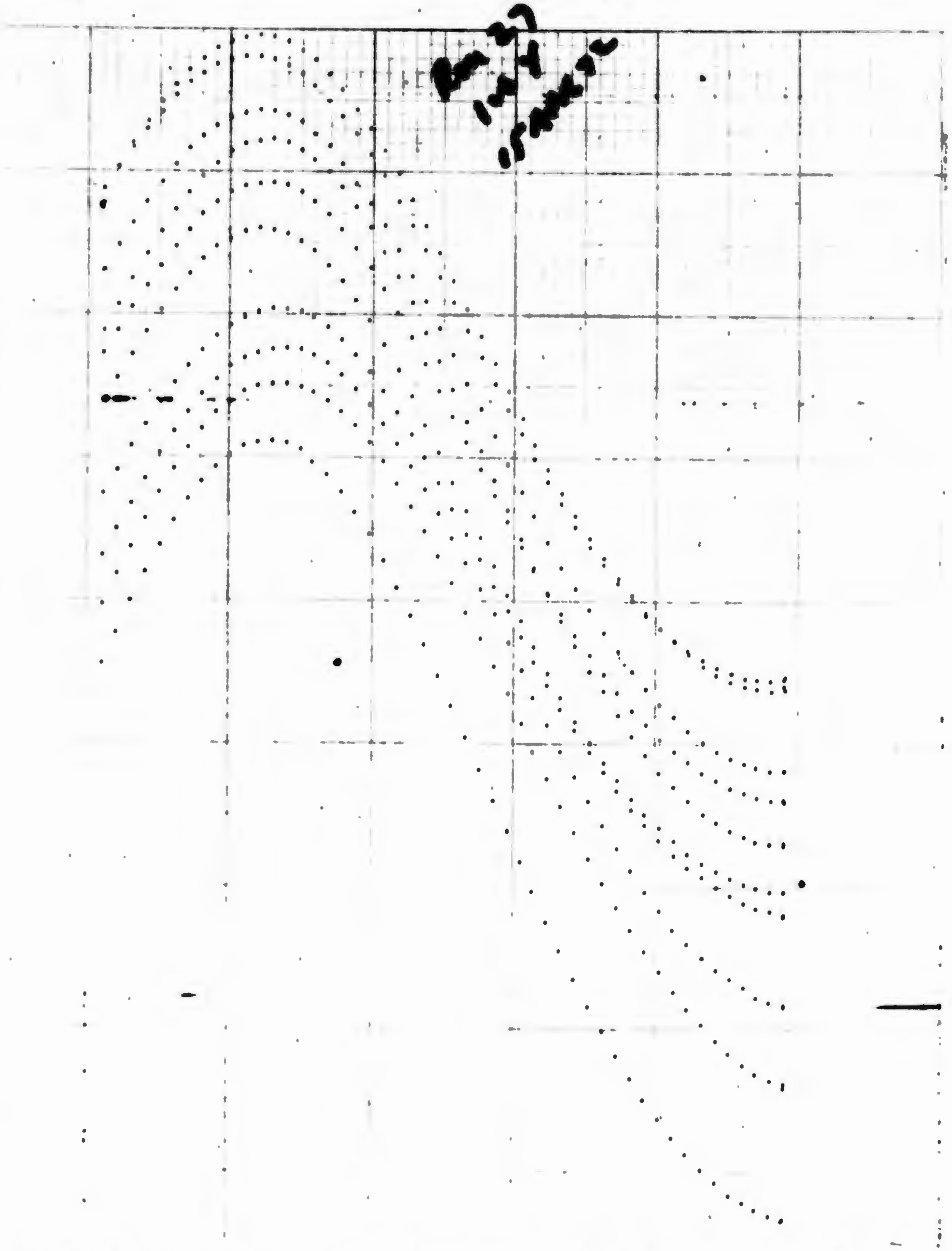

Sample plot of the cross correlation function for a shear sensor vs a velocity probe. The H/P 7004B X-Y Recorder which plotted it was calibrated in the X direction at 5msec/small div. Each curve represents a different cross correlation for a different set of data. Data is from 15 APR 72.

FIGURE (32)

FIGURE (33)

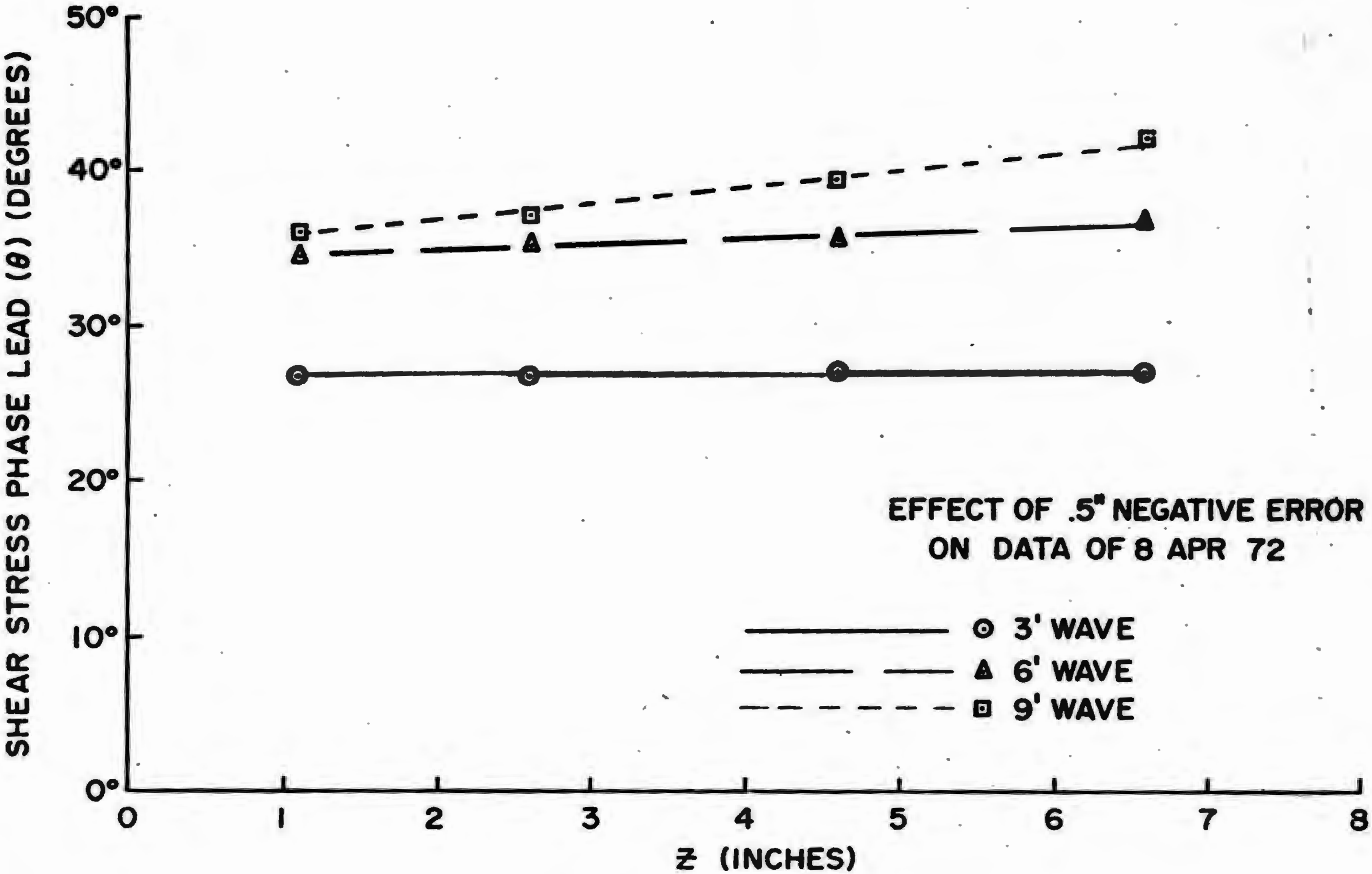

50°
40°
30°
20°
10°
0°
SHEAR STRESS PHASE LEAD (θ) (DEGREES)
0
1
2
3
4
5
6
7
8
Z (INCHES)
EFFECT OF .5" NEGATIVE ERROR
ON DATA OF 8 APR 72
3' WAVE
6' WAVE
9' WAVE

FIGURE (34)

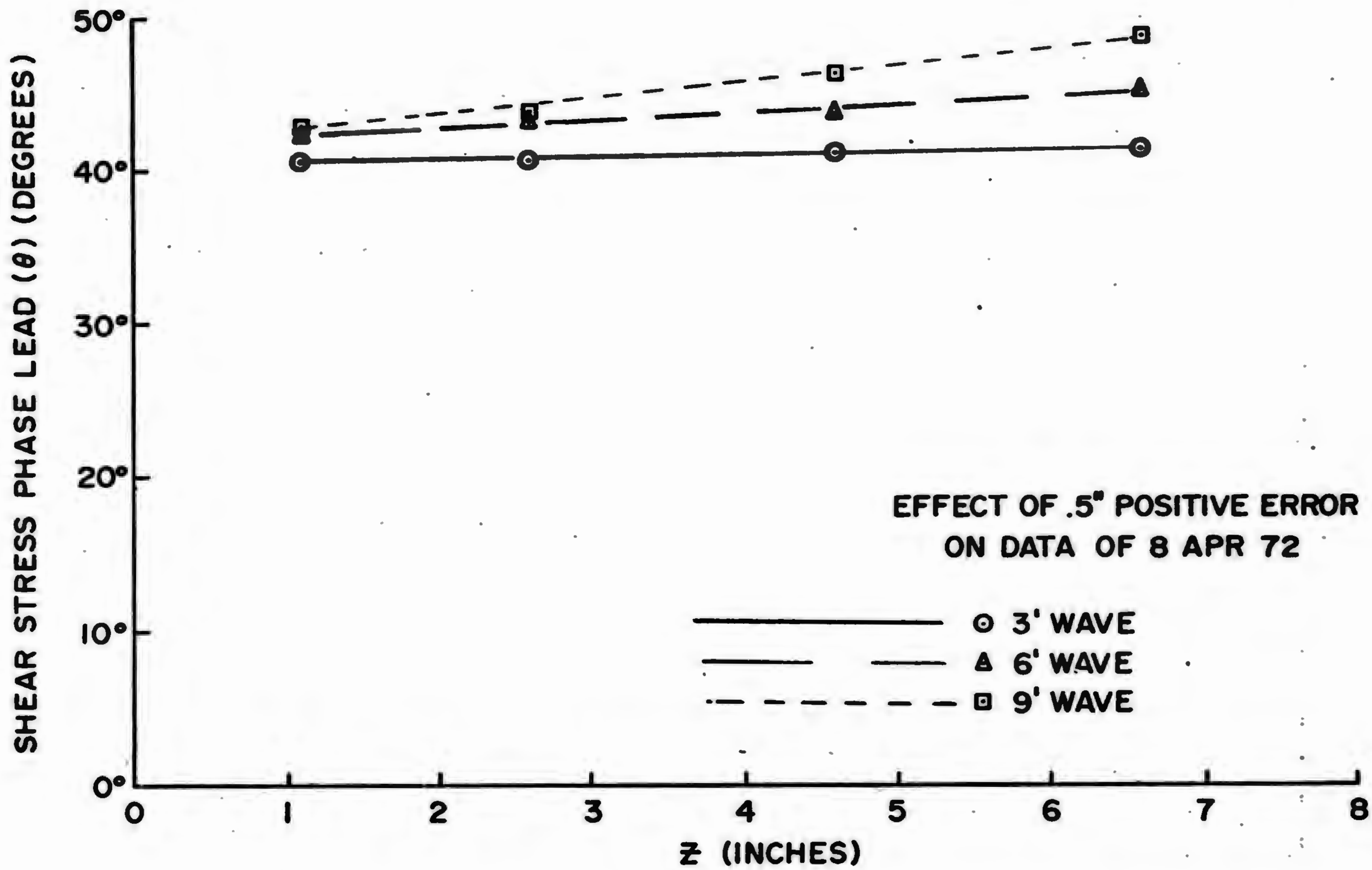

SHEAR STRESS PHASE LEAD (θ) (DEGREES)
50°
40°
30°
20°
10°
0°
0
1
2
3
4
5
6
7
8
Z (INCHES)
EFFECT OF .5" POSITIVE ERROR
ON DATA OF 8 APR 72
3' WAVE
6' WAVE
9' WAVE

REFERENCES

Dreyer, F. F., "Calibration of Hot Film Sensors in a Towing Tank and Application to Quantitative Turbulence Measurements," Engineering Department Report, U. S. Naval Academy, 1967.

Galvin, Cyril J., "Breaker Travel and Choice of Design Wave Height," ASCE, Journal of the Waterways and Harbors Division, May 1969 WW2 pp. 175-200.

Geremia, J. O., "An Experimental Investigation of Turbulence Effects at the Solid Boundary Using Flush-Mounted Hot Film Sensors," Engineering Department Report 70-2, U. S. Naval Academy, 1970.

Grosch, C. E., "Laminar Boundary Layer Under a Wave," Physics of Fluids Vol. 5 #10, 1962, pp. 1163-1167.

Huang, T. T., "Techniques for Ship Frictional Resistance Measurements," NSRDC Report 3307.

Iwagaki, Y., and Tsuchito, Y., "Laminar Damping of Oscillatory Waves Due to Bottom Friction," Proceedings 10th Conference on Coastal Engineering, Tokyo, 1966, pp. 149-174.

Iwagaki, Y., Yoshito Tsuchiya and H. Chen, "On the Mechanism of Laminar Damping Oscillatory Waves Due to Bottom Friction," Bulletin of Disaster Prevention Research Institute Kyoto University, Vol. 16 Part 3, March 1967.

Iwagaki, Y. and Tetsuo Sakai, "Horizontal Water Particle Velocity of Finite Amplitude Waves," Proceedings 12th Conference on Coastal Engineering, Washington, D.C., 1970, pp. 309-325.

Johnson, B. and R. H. Barchi, "Effect of Drag Reducing Additives on Boundary-Layer Turbulences," Journal of Hydronautics, Vol.2 No.3, pp. 168-175.

Jonsson, Ivar G., "Measurements in the Turbulent Wave Boundary Layer," I.A.H.R. Congress, London, 1963, pp. 85-92.

Jonsson, Ivar G., "Friction Factor Diagrams for Oscillatory Boundary Layers," Basic Research - Progress Report #10, Technical University of Denmark, Dec. 1965.

Lamb, Horace, "Hydrodynamics," Cambridge University Press, 1945, 6th Ed.

Le Me'haute', Bernard, David Divoky and Albert Lin, "Shallow Water Waves: A comparison of Theories and Experiments," Proceedings 11th Conference on Coastal Engineering, London, 1968, pp. 86-109.

Liepmann, H. W. and G. T. Skinner, "Shearing Stress Measurements by use of a Heated Element," NACA Technical Memorandum 3268.

Ludwieg, H., "Instrument for measuring the wave shearing stress of Turbulant Boundary Layers," NACA, Technical Memorandum 1288.

McCormick, M. E. and S. S. Saslaw, "An Analysis of the Shoaling of Traveling Waves on a Beach of Arbitrary Slope," Unpublished paper, Engineering Department, U. S. Naval Academy, 1971.

McCormick, M. E., Bruce Johnson and William Lee, "Effects of a Flexible Surface on Surface Shear Stress Fluctuations Beneath a Turbulent Boundary Layer," Journal of Hydronautics, Vol.6, No.1, Jan 1972, pp. 62-64.

Mies, Richard W., "The Development of Calibration Techniques for a Flush-Mounted Hot Film Anemometer in the Study of Turbulent Boundary Layers," Trident Scholar Theses, U. S. Naval Academy, 1967.

National Committee for Fluid Mechanics Films, "Boundary Layer Formation," experiments conducted at M.I.T.

Thermo Systems, Inc., "1050 Series Constant Temperature Anemometers and Accessories," Bulletin #1050.

Thermo Systems, Inc., "Hot Film and Hot Wire Anemometry Theory and Application," Bulletin TB5.

Time/Data Corporation, Time/Data 100 Digital Analyzer Tech Manual, Time/Data Corporation, Palo Alto, California (c) 1967.

Time/Data Corporation, "A Simple Discussion of Time-Series Analysis," Ed. Leo J. Chamberlain, Nov. 1970.

Schlichting, H., "Boundary Layer Theory," Trans. by J. Kestin, McGraw-Hill, Series in Mechanical Engineering (c) 1960, pp. 75-78.

Wiegal, Robert L., Oceanographical Engineering, Prentice-Hall, Englewood Cliffs, N.J. (c) 1964.

APPENDIX A.

HOT FILM ANEMOMETERS

A central facet of this project was the application and evaluation of hot film sensors in shoaling wave studies. To evaluate their utility, it is first necessary to have some understanding of what a hot film anemometer is and how it operates.

There are two basic parts to any hot film system: the sensor probe, and the anemometer. The sensor probe is essentially a 4th leg of a whetstone bridge in the feedback loop of the anemometer. Physically, the probe takes many forms--cylindrical, conical, flat, paradolic, etc. The three probe types used in this project are illustrated in Fig.(35-36). All have one thing in common--they all have sensor surfaces consisting of a thin quartz-coated platinum film fused to a supporting glass form. The electrical resistance in the film causes it to heat when a voltage supplied by the anemometer is applied across it. The film assumes a higher temperature than the surrounding water and a heat transfer occurs. The rate of heat transfer is proportional to the velocity or velocity gradient of the fluid flow normal to the film surface. As the film loses heat due to the cooling effect of the fluid flow, its resistance decreases. This results in a voltage decrease, thus changing the input to the anemometer amplifier. The construction of the amplifier is such that this decrease in input voltage results in an increase in the amplifier output current to the sensor. Thus, any resistance change in the sensor film is immediately corrected for by a countering change in the sensor current. This is known as a constant temperature anemometer.

The heat transfer rate between the film and the fluid is related by King's formula, which is, in terms of the bridge voltage:

$$KE_b^{\,2} = (A + BU^n)\ \Delta t \tag{1}$$

where

E_b = bridge output

K and B = constants of probe geometry and heat transfer characteristics of fluid

U = mean fluid velocity

n = probe constant (1/2 for conical & parabolic sensors, fy cylindrical)

Δt = temperature differential between the fluid and sensor

The constants A and B can absorb K:

$$A_1 = A/K \qquad B_1 = B/K$$

Thus,

$$E_b = (A_1 + B_1 U^n)\ \Delta t\ . \tag{1A}$$

Differentiating (1A),

$$2\ E_b\ d(E_b) = n\ B_1\ \Delta t\ U^{n-1}\ dU \tag{2}$$

and summing with (1A),

$$\frac{2\ E_b\ d(E_b)}{E_b^{\,2} - E_{bo}^2} = n\ \frac{dU}{U} \tag{3}$$

where $E_{bo} = A_1 \Delta t$ (since the tank is essentially a constant temperature system, Δt will remain approximately constant)

[1]The higher order terms are generally neglected.

From this expression it is evident that there is no simple expression to relate the bridge output of the anemometer with the fluid velocity flowing past the probe. The simplest method of relating the two is to determine the constants A_1 and B_1 and put them into a linearizer which will then produce a straight line voltage-velocity approximation curve. The accuracy of the approximation varies with the design, however Dreyer (1967) found it to be quite good for TSI's conical sensor.

For lack of a linearizer, an alternative point-for-point calibration was made. The method described by Dreyer was used, with the exclusion of the linearizer. The bridge output was passed through a vidar model 240 voltage to frequency converter and recorded on an H/P 651 digital recorder with carriage velocity, integrated over a set 15 sec. period. The Naval Academy's IRA designed data acquisition system was also used, with the output of bridge voltage, carriage velocity and time printed on computer tape for direct feed into the GE-635 computer. The computer program on page 95 was used to compute mean bridge output and carriage velocity and print them on a data file for plotting by a typagraph terminal using the BASGRAF*** program.

Velocity was incremented at .2 FPS intervals between 0 and 3 FPS. The resultant calibration curves were plotted on both linear (Fig.) and logarithmic scales. The tremendous sensitivity of the cylindrical sensor is quite in the linear scale plot. A voltage gradient on the order of 1.8-1.9 volts/FPS is not uncommon for the low velocity region.

The towing carriage system as currently designed is not capable of operating at velocities between 0 and .2 FPS, hence experimental data in this critical region was not taken. The curve was interpolated using a complete calibration curve for a similar probe supplied by Mr. R. Sathyakumar of Thermo Systems, Inc.

FIGURE (35)

Vertical Velocity sensor

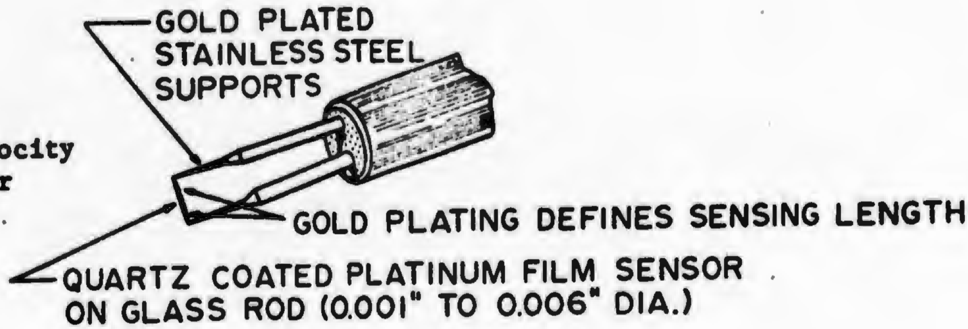

CYLINDRICAL HOT FILM

Shear Stress sensor

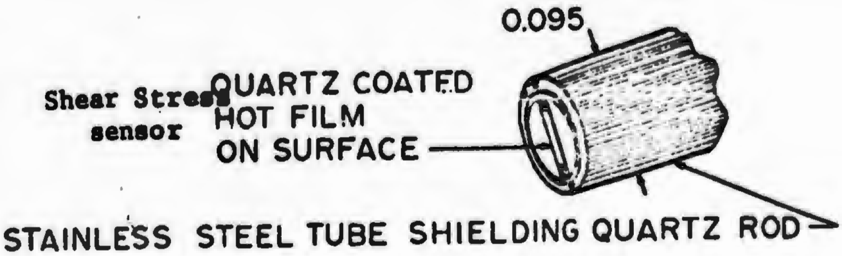

FLAT SURFACE HOT FILM

Horizontal Velocity sensor

SENSOR MOUNTED PARALLEL TO THE PROBE.

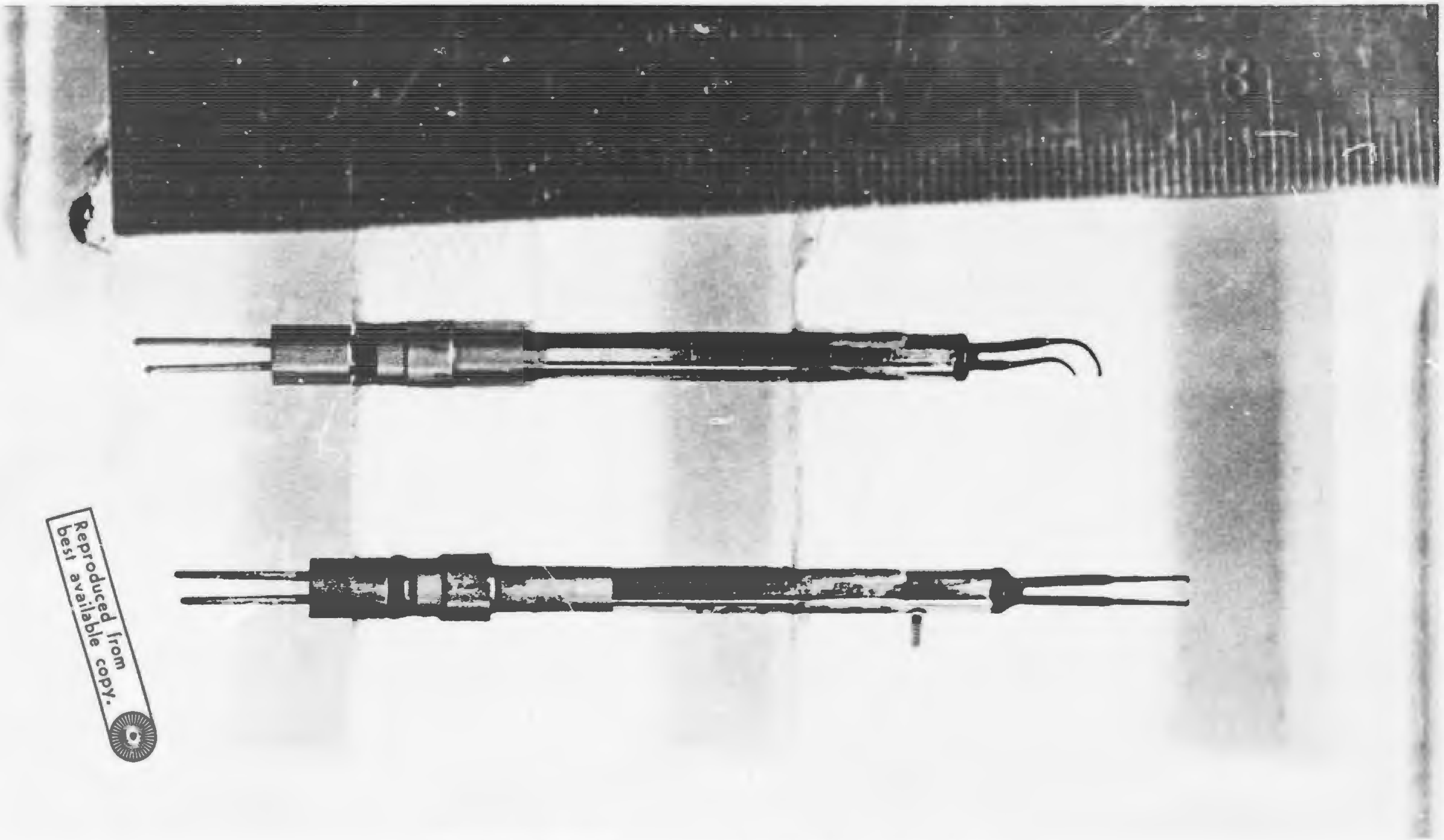

TSI 1211-20W horizontal velocity probe (top)
and
TSI 1210-20W vertical velocity probe (bottom)
Scale across the top is ruled in inches.

FIGURE (3 6)

FIGURE (37)

HOT FILM ANEMOMETER
SCHEMATIC

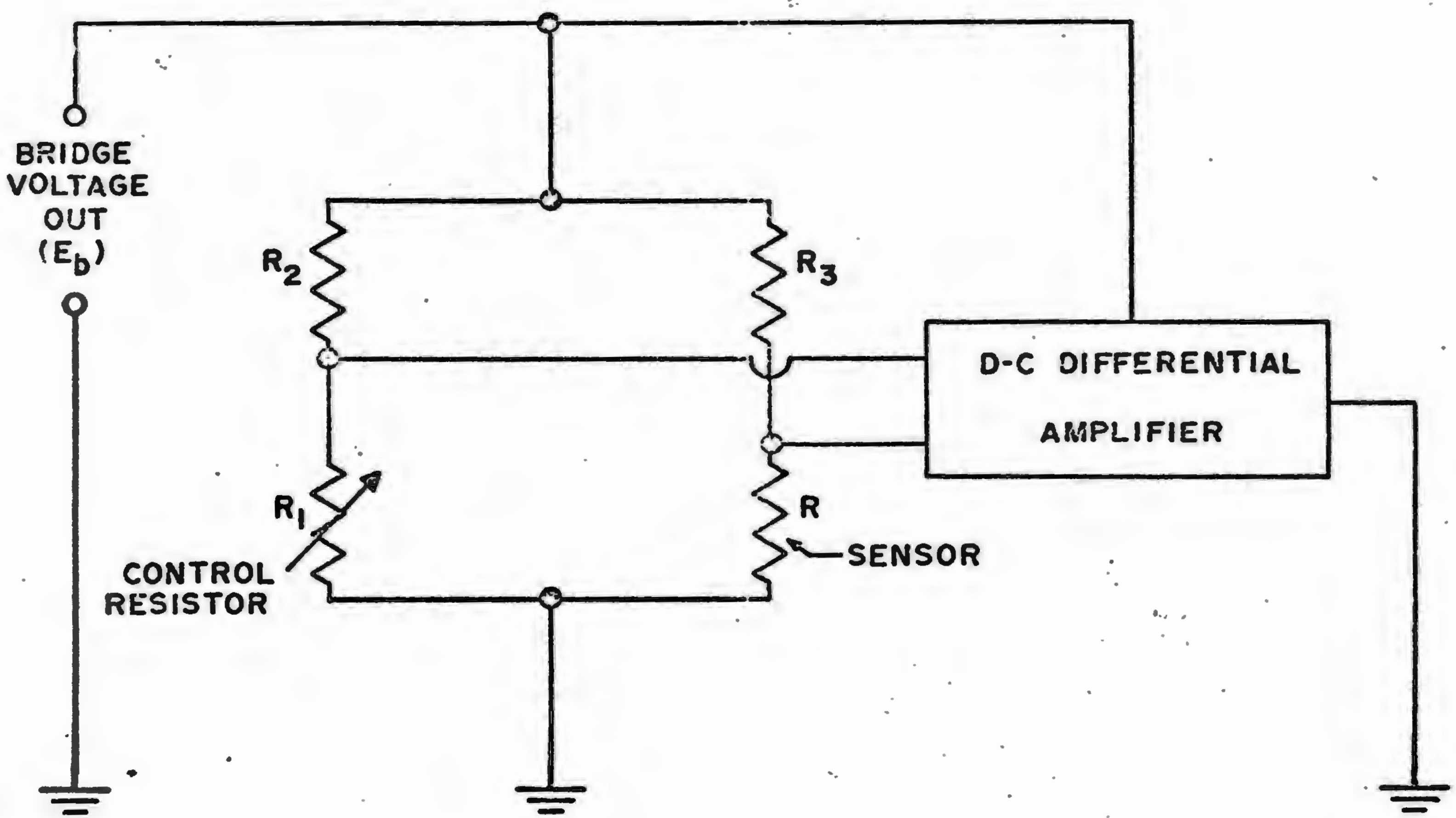

APPENDIX B

CROSS CORRELATION

The cross correlation algorithm was computed on the Time/Data 100 to determine time variation between sequentially occuring events in the time history of two hot film sensors. The cross correlation is a measure of the similarity of two wave forms as a function of the time shift between them. Given two sample wave forms A(t) and B(t) in Fig. (38), their cross correlation may be expressed by the relation

$$R_{AB}(\tau) = \int_{-T}^{T} A(t)\, A(t-\tau)\, dt \qquad \ldots\ldots\ldots\ldots\ldots \qquad (B-1)$$

In practice, the first sample point is defined as zero time reference and dt is replaced with the finite sample period at Δt where $\Delta t = T_s/2000$ (T_s being the total sample period). Equation (B-1) then becomes

$$R_{AB}(m\tau) = \sum_{n=0}^{1000} A_n \cdot B_{n+m} \qquad \ldots\ldots\ldots\ldots\ldots \qquad (B-2)$$

where successive values of A_n and B_n are separated by Δt seconds.

Physically speaking, the two waveforms are multiplied, point for point, and the products summed. Thus summation represents the first point in the cross-correlation. The second function (B(t)) is then time shifted Δt seconds to the right and the two wave forms again multiplied point for point and summed. After 1001 time shifts the two sample wave forms have been completely shifted relative to one another and a 1001 point cross correlation has been computed (Fig. 39).

This process may be better understood by looking at the mathematical formulation for the process just described for the positive lags (B shifted while A held constant).

$$R_{AB}(0) = A_oB_o + A_1B_1 + \ldots + A_{1000}B_{1000}$$
$$R_{AB}(1\tau_o) = A_oB_1 + A_1B_2 + \ldots + A_{1000}B_{1001}$$
$$R_{AB}(12\tau_o) = A_oB_{12} + A_1B_{13} + \ldots + A_{1000}B_{1012}$$
$$R_{AB}(1000\tau_o) = A_oB_{1000} + A_1B_{1001} + \ldots + A_{1000}B_{2000}$$

Similarly, the cross correlation of B against a time shifting A may be thought of as a negative lag and computed as

$$R_{AB} = (-m\tau_o) = \sum_{n=0}^{100} A_{n+m} \cdot B_n$$

Again, the formulations are

$$R_{BA}(o) = R_{AB}(-o) = B_oA_o + B_1A_1 + \ldots + B_{1000}A_{1000}$$
$$R_{BA}(1\tau) = R_{AB}(-1\tau_o) = B_oA_1 + B_1A_2 + \ldots + B_{1000}A_{1001}$$
$$R_{BA}(1000\tau_o) = R_{AB}(-100\tau_o) = B_oA_{1000} + B_1A_{1001} + \ldots + B_{1000}A_{2000}$$

The cross correlation $R_{AB}(\tau)$ is described in Fig.(38-c). Note that while A(t) and B(t) are functions of time, $R_{AB}(\tau)$ is a function of the relative time shift. The first peak in the correlation indicates that A(t) leads B(t) by a time shift at 2 τ_o. The period of A(t) and B(t) may be determined as the time separation between corresponding peaks of equal size. No interpretation is associated with the magnitude of the correlation, except as peaks and troughs are sized relative to one another for any one correlation.

FIGURE (38)

Cross correlation imputs (a) and (b) add the resultant cross correltaion (c)

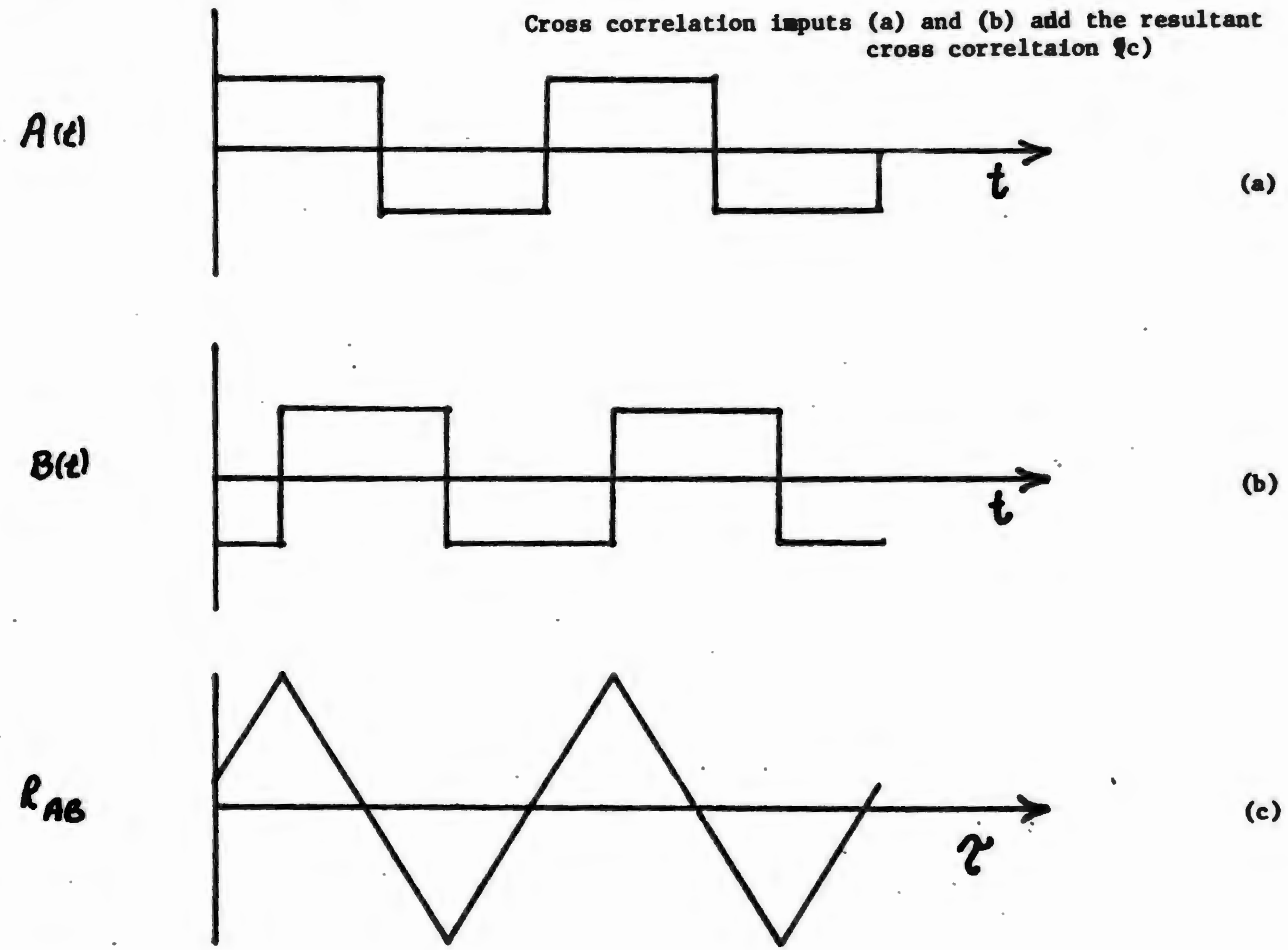

Figure (39)

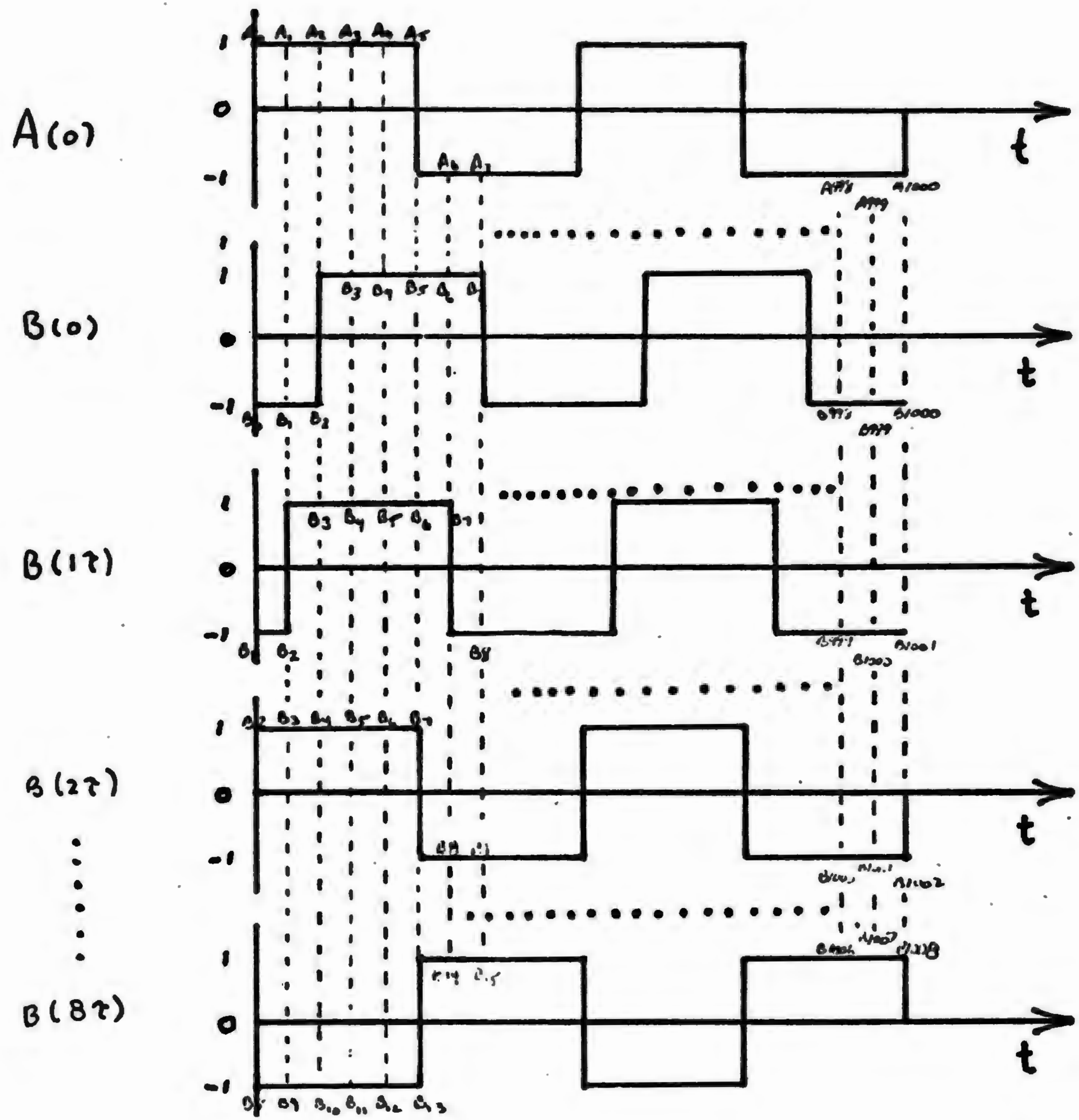

APPENDIX C

The Naval Academy's GE-635 time-sharing computer system was used extensively in this project as both a data reduction tool and an investigative aid. The language used was edition 6 BASIC, although some of the earlier programs may use edition 5. The programs are included as the best explanation for what processes were used to determine the various calculated parameters used in the study. The graphical outputs were obtained using a typagraph terminal and the BASIC program BASGRAF*** stored in the Academy's disk file program library.

The first program, WAVES, was originally suggested by Dr. Bruce Johnson as a course requirement. It employs linear wave theory to calculate the frequency and celerity of an incremented set of desired wavelengths. The output from this program (Fig.(5)) was used to set the wave generator for the desired wavelengths. A later version employed a FILE output at d/L_0 and c/L_0 and was used to plot Fig.(40).

The second program, SHOL3, utilizes an iterative process with a cascading incrementation to calculate various inshore parameters for an incremented deep water wave length passing a depth of .75883 feet. The iterative loop is contained in statements 200-290 and solves the equation:

$$L = gT^2/2\pi \tanh 2\pi d/L$$

Again, the calculated parameters were stored on files and used in conjunction with BASGRAF*** to plot the various linear wave theory plots in the text.

GOUGE2, the third program presented, is simply a solution of Iwagaki's equation for the time dependent shear stress (equation (6)) for τ = 0 to 500 degrees (0 to 2.77π). The same iterative loop used in SHOL3 may be recognized in statements 140-230. Here it was used to compute the linear theory wavelength of the three deep water waves at a depth of .75833 feet. Thus, the parameter ϵ represents the linear theory approximation of the project conditions. The free surface profile η is plotted for reference and phase comparisons.

The fourth program, BRIDGE2, represents an abortive attempt at calibrating the particle velocity probes. The data statements were fed in by a paper tape which was punched by the IRA data acquisition system. When the system was working, it worked fine, however, it has been plagued by severe trouble throughout the year. The probes were calibrated by towing them in the carriage sub-assembly in Fig.(43) and 1000 count/sec values of velocity, time and probe voltage output (converted to frequency by a Vidar 240 V to F converter). BRIDGE2 reduces these outputs to velocity and voltage and stores them on file for plotting.

Attempts at probe calibration were suspended until 29 April 1972 due to problems with the data acquisition system. At this time the H/P 52142 preset counters and 562A digital recorder were substituted and a calibration attempted. A malfunction in the anemometer amplifier burned out the velocity probe, however, and the calibration attempt was aborted.

```
WAVES     05 MAY 72  11:39

10 DEF FNR(Y)=INT(Y*1E4+0.5)/1E4
20 PRINT "INPUT WATER DEPTH,IN FEET";
25 INPUT D
27 PRINT
30 PRINT"INPUT WAVELENGTHS: SHORTEST,LONGEST,INCREMENT";
35 INPUT M,N,K
40 PRINT
50 PRINT "WAVELENGTH","CELERITY","PERIOD","FREQ","D/(T*T)"
90 LET P=2*3.14159
100 FOR L=M TO N STEP K
110 LET X=P*D/L
120 LET A=EXP(X)
130 LET B=EXP(-X)
140 LET J=(A-B)/(A+B)
150 LET R=32.2*L/P
160 LET S=SQR(R)
170 LET U=SQR(J)
180 LET C=S*U
190 LET T=L/C
200 LET G=1/T
210 LET H=12*L/(10*P)
220 LET E=D/(T*T)
250 PRINT L,FNR(C),FNR(T),FNR(G),FNR(E)
280 NEXT L
300 END
READY
```

```
SHOL3     05 MAY 72  11:34

10 FILE #1:"CVSD"
20 FILE #2:"HVSD"
30 FILE #3:"COVSDLO"
40 SCRATCH #1
50 SCRATCH #2
60 SCRATCH #3
70 DEF FNZ(X)=(EXP(X)-EXP(-X))/(EXP(X)+EXP(-X))
80 DEF FNR(Y)=INT(Y*1E5+0.5)/1E5
90 PRINT "  L0","  D/L0","   C0","   C","C/C0"
100 PRINT
110 LET G=32.2
120 LET Y=3.14159
130 LET H0=.75833
140 FOR Q8=2 TO 10 STEP .5
150 LET L=100
160 LET L0=L
170 LET H= H0*L0/Q8
180 LET T=L/(SQR(G*L/(2*Y)))
190 LET L1=1
200 LET X=(2*Y*H)/L
210 LET Z=FNZ(X)
220 LET L2=(G*T↑2*Z)/(2*Y)
230 IF ABS(L2-L)<.001 THEN 300
240 IF L2-L>.001 THEN 270
250 LET L=L-L1
260 GO TO 200
270 LET L=L+L1
280 LET L1=L1/10
290 GO TO 250
300 LET N=1+(4*X)/(EXP(2*X)-EXP(-2*X))
310 LET H5=H/L2
320 LET L2=L2/100
330 LET A2=SQR(1/(N*L2))
340 LET H2=A2*4
350 LET H4=H/100
360 LET L9=H0/H4
370 LET X0=2*Y*41.5/(12*L9)
380 LET C0=((G*L9*FNZ(X0))/(2*Y))↑.5
390 LET C=C0*L2
400 LET N2=1/N
410 PRINT L9,H4,FNR(C0),FNR(C),FNR(L2)
420 PRINT #1:H4;",";FNR(C)
430 PRINT #2:H4;",";FNR(A2)
440 PRINT #3:H4;",";FNR(L2)
450 NEXT Q8
460 PRINT #3:"1.0E37,1.0E37"
470
480 READ Q8,E1
490 IF Q8=1E37 THEN 560
500 LET H4=9.12/(12*Q8)
510 PRINT #3:H4;",";E1
520 GO TO 480
530 DATA2,1.04,2.5,.928,3,.855,3.5,.828,4,.75,4.5,.75,5,.741,5.5,.693,6,.641
540 DATA6.5,.578,7,.537,8.5,.515,9,.494,9.5,.482
550  DATA 1E37,1E37
560 END
READY
```

```
GOUGE2     12 MAY 72  21:11

10 FILE #1:"GOUGEDAT"
20 SCRATCH #1
30 DEF FNS(X)=EXP(X)-EXP(-X)
40 DEF FNC(X)=EXP(X)+EXP(-X)
50 DEF FNT(X)=FNS(X)/FNC(X)
60 LET G=32.2
70 LET Y=3.14159
80 LET H0=.75833
90 FOR 08=3 TO 9 STEP 3
100 LET L=100
110 LET H=H0*100/08
120 LET T=L/(SQR(G*L/(2*Y)))
130 LET L1=1
140 LET X=(2*Y*H
150 LET Z=FNT(X)
160 LET L2=(G*T↑2*Z)/(2*Y)
170 IF ABS(L2-L)<.001 THEN 240
180 IF L2-L>.001 THEN 210
190 LET L=L-L1
200 GO TO 140
210 LET L=L+L1
220 LET L1=L1/10
230 GO TO 190
240 LET E=Y*1.875/(12*FNS(X))
250 FOR T=0 TO 2.77*Y STEP Y/36
260 LET 01=1/(2↑1.5)+(11/18-5*2↑.5/18)*SIN(2*T)
270 LET 02=SIN(T-Y/4)
280 LET 03=(11/18-4*2↑.5/18)*COS(2*T)
290 LET T0=02+(01+03)*E
300 LET R=-T*(180/Y)
310 PRINT #1:T0;",";R
320 NEXT T
330 PRINT #1:"1.0E37,1.0E37"
340 NEXT 08
350 FOR T=0 TO 2.77*Y STEP Y/36
360 LET N=SIN(T)
370 LET R=-T*(180/Y)
380 PRINT #1:N;",";R
390 NEXT T
400 END
READY
```

Data reduction program for velocity calibration. Data in statements 170-310 is from 6DEC71 and plotted in Figs. (4) and (5)

```
5 DIMS(100), F(100)
10 FILES *
15 LET N=0
20 FILE #1:"PLANE"
25 LET B$="1.0E37,1.0E37"
45 SCRATCH #1
50 READ T
80 IF T=1E37 THEN 500
85 LET N=N+1
90 READ S,A2,E1,F2
100 LET S=S*1.689/(T*1000)
105 LET S(N)=S
110 LET E1=E1/(T*1000)
120 LET F(N)=F2/(T*1000)
130 PRINT #1,S;",";E1
150 GO TO 50
170 DATA 030.152,003991,000000,298528,300866
180 DATA 029.883,007879,000000,330677,330295
190 DATA 030.209,011928,000000,355094,353157
200 DATA 029.849,015683,000000,365787,362160
210 DATA 029.726,019461,000000,376985,373185
220 DATA 030.240,023751,000000,395012,390365
230 DATA 030.057,027559,000000,403067,398055
240 DATA 026.554,027841,000000,364271,359326
250 DATA 023.949,028188,000000,335517,331140
260 DATA 021.268,027845,000000,304599,300381
270 DATA 018.611,026839,000000,271397,267427
280 DATA 017.064,026828,000000,252598,248714
290 DATA 015.901,027037,000000,238578,234734
300 DATA 014.961,027357,000000,227250,223327
310 DATA 013.821,027057,000000,212037,208430
330 DATA1E37
500 PRINT #1,B$
510 FOR X=1 TO N
520 PRINT #1,S(X);",";F(X)
530 NEXT X
540 PRINT #1,B$
600 END

READY
```

Figure (40)

C/CO VS D/LO CONSTANT DEPTH

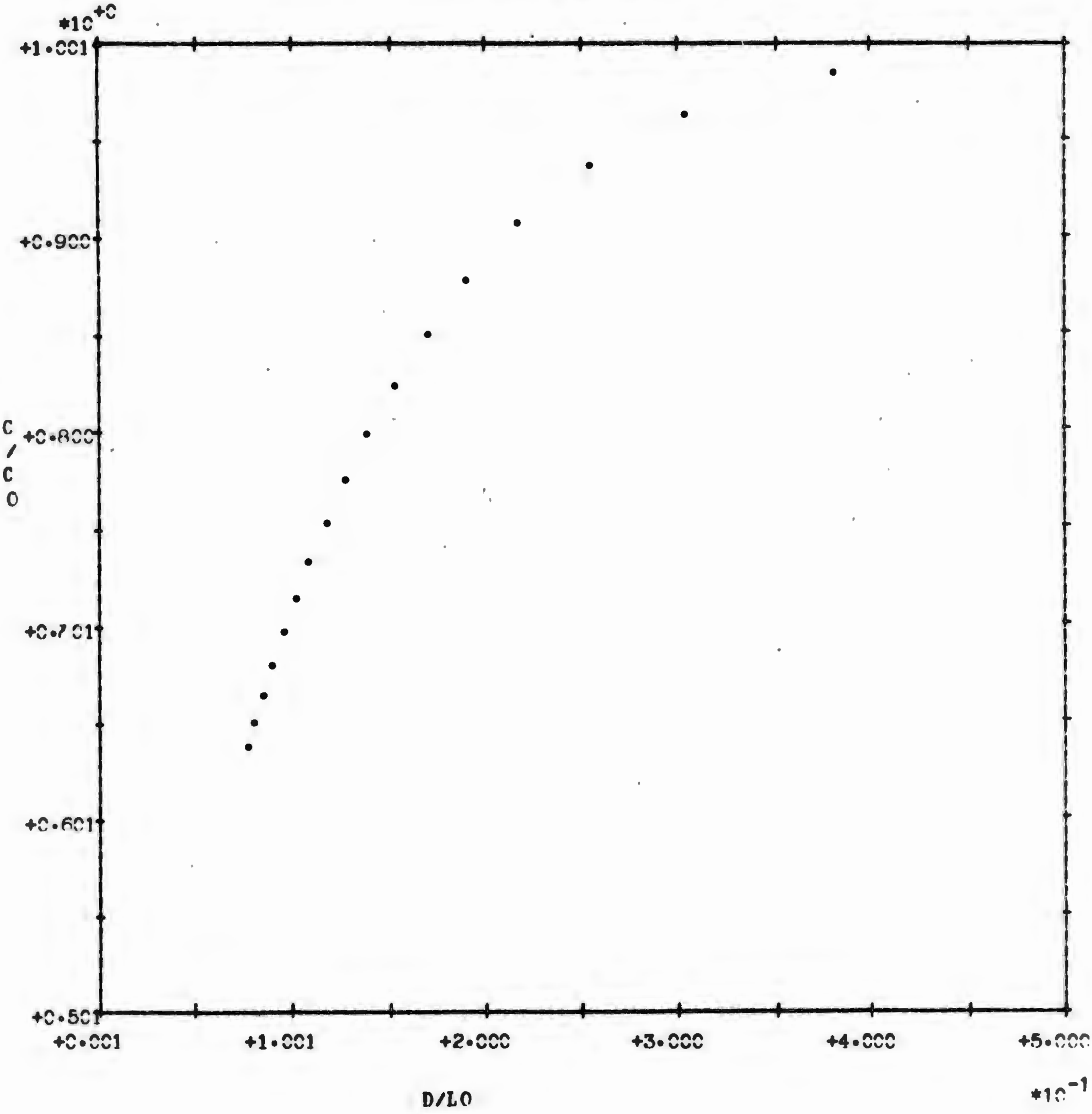

SYMBOL NO.PTS. LEGEND
• 17 -? VARIABLE WAVELENGTN 2 ' TO 10' .5' INCREMENTS

FIGURE (41)

H/HO VS D/LO CONSTANT WAVELENGTH

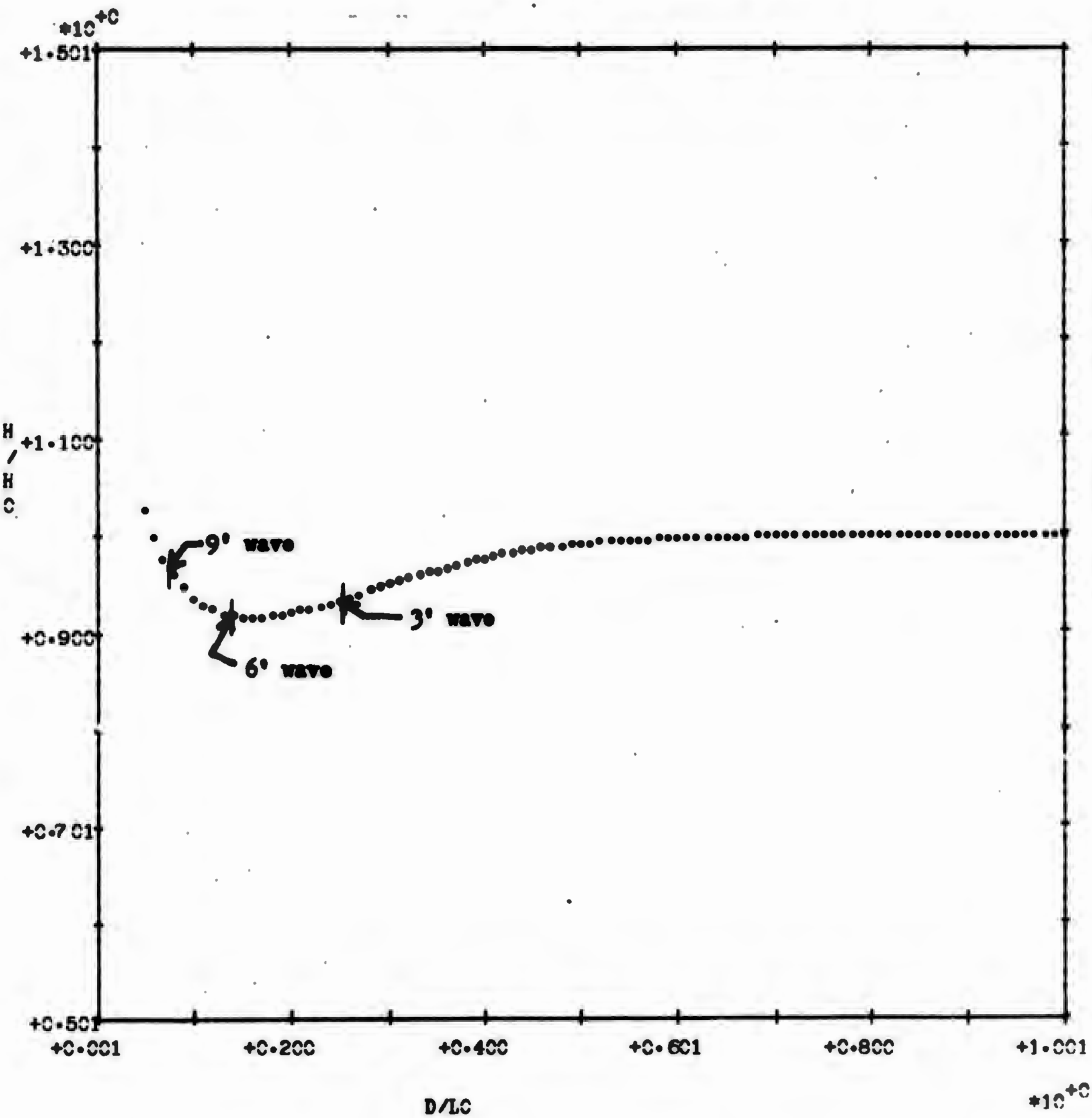

SYMBOL NO.PTS. LEGEND
• 96 -? WAVELENGTH 100 FT. (DEEP WATER)

CHANGE FOR NEXT RUN = ? ALL

SH CL3 02 MAY 72 11:00

LC	D/LC	CC	C	C/CC
2	0.379165	3.2015	3.1513	0.98432
2.5	0.303332	3.57939	3.44546	0.96258
3	0.252777	3.92101	3.66691	0.93519
3.5	0.216666	4.23516	3.83581	0.90571
4	0.189583	4.52751	3.96724	0.87625
4.5	0.168518	4.80193	4.07168	0.84792
5	0.151666	5.06116	4.15614	0.82118
5.5	0.137878	5.30711	4.22541	0.79618
6	0.126388	5.54119	4.28274	0.77289
6.5	0.116666	5.76438	4.33039	0.75123
7.	0.108333	5.97742	4.36999	0.73108
7.5	0.101111	6.18083	4.4027	0.71232
8	9.47913 E-2	6.37506	4.42946	0.69481
8.5	8.92153 E-2	6.56046	4.45091	0.67845
9	8.42589 E-2	6.73732	4.46767	0.66312
9.5	7.98242 E-2	6.90594	4.48013	0.64874
10	0.075833	7.06659	4.48876	0.63521

2.590 SEC. 33 I/O
READY

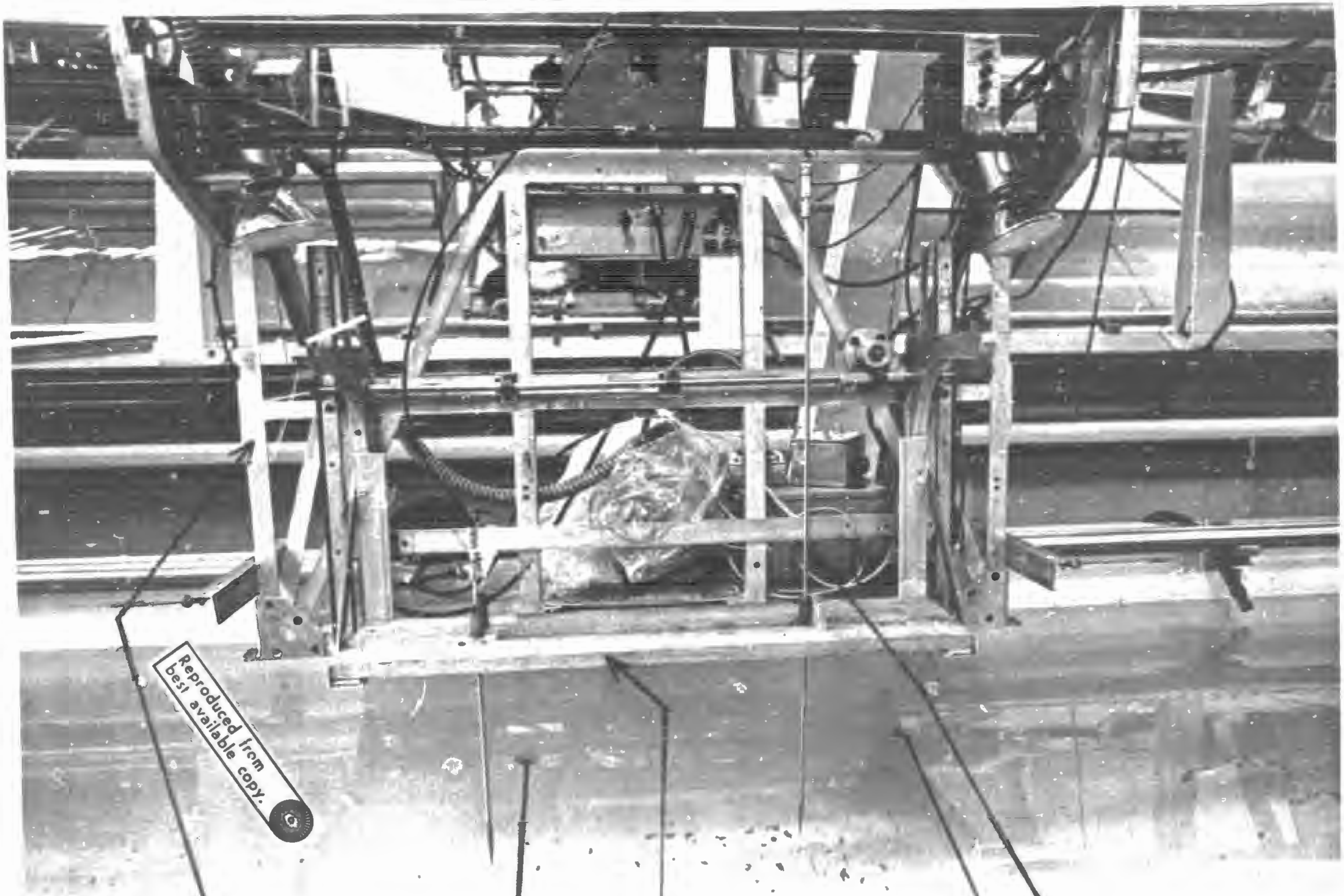

Model towing carriage

Velocity probe calibration carriage sub-assembly

TSI 1211-20W probe mounted in a steel protective shield.

FIGURE (43)

FIGURE (44)

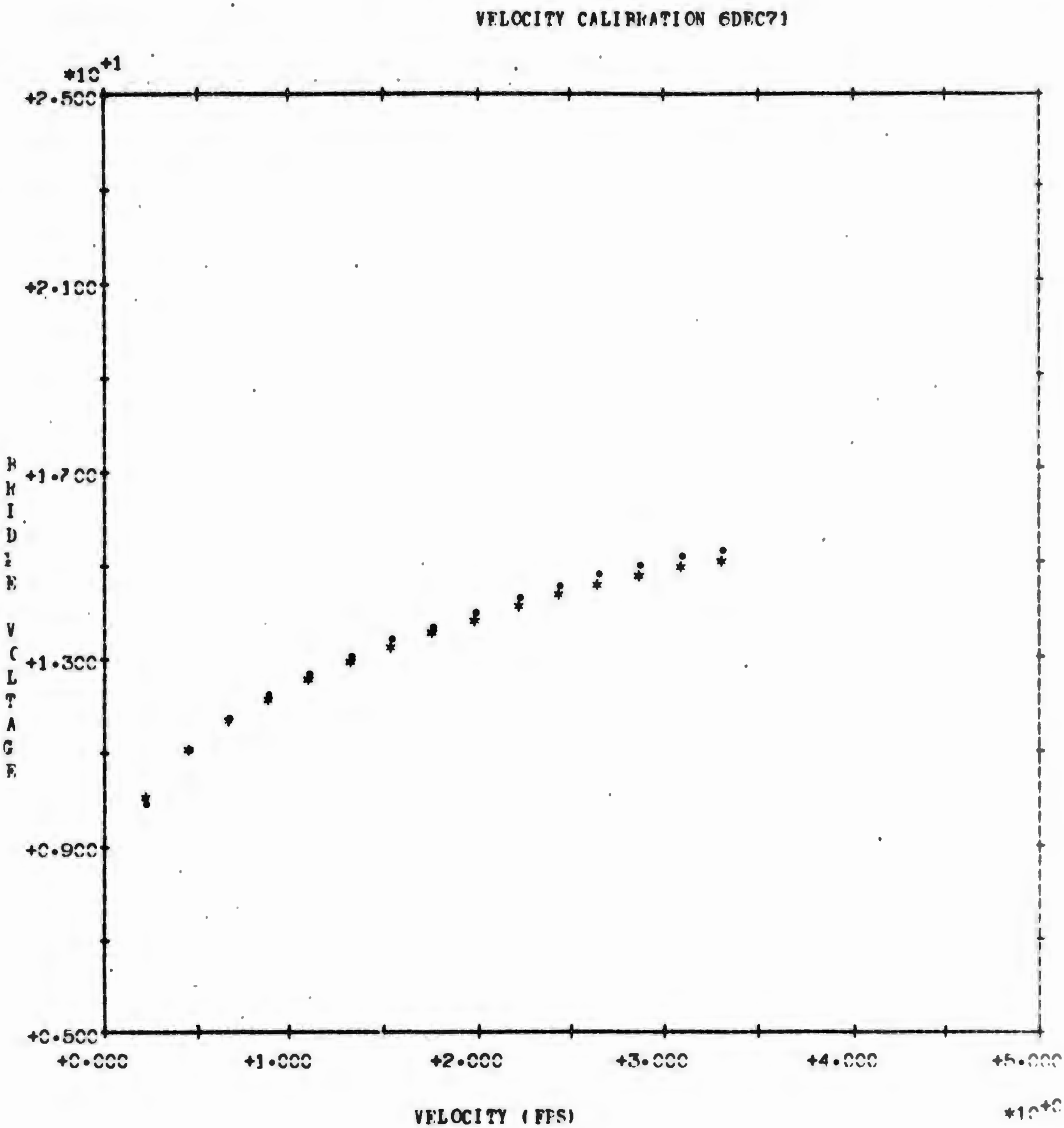

SYMBOL	NO.PTS.	LEGEND
•	15	-? PROBE 1
*	15	-? PROBE 2

FIGURE (45)

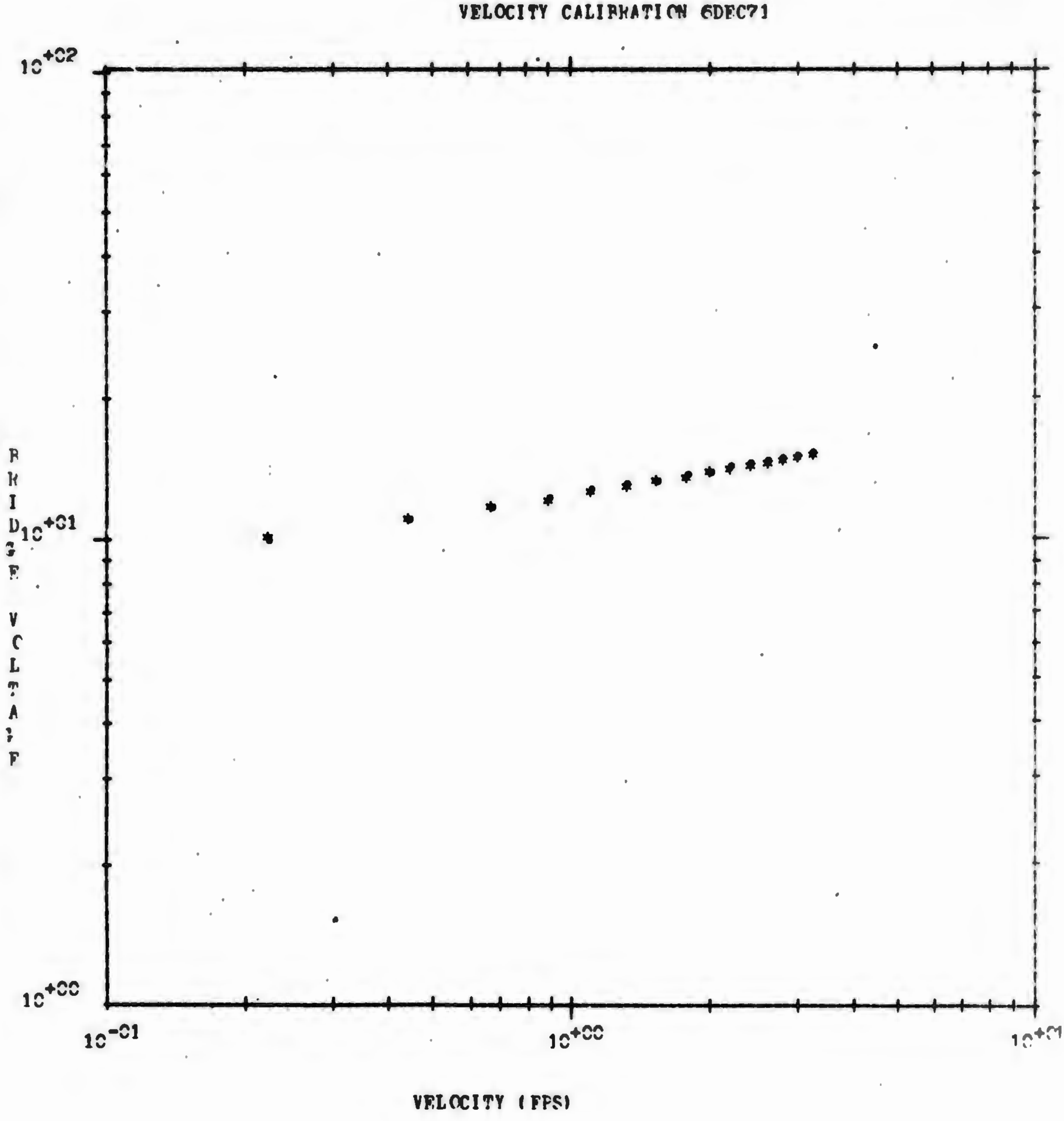

SYMBOL	NO.PTS.	LEGEND
•	15	-? PROBE 1
*	15	-? PROBE 2